MEASUREMENT OF THE KERR ELECTRO-OPTIC EFFECT BY INDUCED BIREFRINGENCE

BY

ANN SINGH

B Sc Hons (Natal)

Submitted in partial fulfilment of the
requirements for the degree of
Master of Science
in the School of Physics
University of KwaZulu-Natal

Pietermaritzburg

January 2005

DEDICATED TO MY PARENTS

RAMNANDAN AND SARITA DEVI SINGH

ACKNOWLEDGEMENTS

A rainbow remains one of the simplest optical phenomena to be marveled at by the masses. A breathtaking sight it certainly is but as most gasp at this extraordinary picture I must count myself as fortunate to be able to appreciate both its aesthetic and scientific value. And for my wonderful experience with optics many names need to be mentioned.

In order of equal priority my thanks and appreciation go out to my supervisor Dr V W Couling for bearing with my inadequacies and for the support, guidance and encouragement. Also to Prof C Graham and Mr T J Sono for introducing many basic yet important aspects of optics to me.

People involved in experimental work will testify to needing more than a pair of hands and a head and so heartfelt appreciation and gratitude goes out to the individuals from the University's Mechanical Instrument Workshop and the Electronics Centre, in particular to Mr A Cullis and Mr G Dewar. Included in this list are Mr Sewrathan and Mr Penzhorn of the Physics Technical Staff for all their help at various stages of the project. These certainly were the correct doctors for any job.

Financially the Cannon Collins Educational Trust of South Africa must be thanked for being a regular sponsor of my studies. The National Laser Centre (NLC) awarded me an M Sc Scholarship, and provided various pieces of equipment, including the lock in amplifier, which were used in the experiment. The NLC staff were both very interested in and encouraging of my work so to them a very sincere thank you.

God has been a force that gave me an opportunity I least expected and in the same breath, my parents Mr and Mrs R Singh have been a constant source of support, encouragement, understanding and countless sacrifices. To Ajith, Nirana, Shaur, Shikaar, my aunt and all of my friends it is a small thank you for a huge effort. Some of these acts would include carrying dewars of liquid nitrogen, help with relearning Mathematica and loan of a digital camera. A further note of thanks to the entire School of Physics, in particular to the

various individuals who have along the way either encouraged or helped me learn about life. Each in some way certainly contributed to my temperament and understanding of the project.

I could write a thesis on acknowledgements but I believe a true appreciation of these individuals will be best expressed by presenting the work each has in some way contributed to.

DECLARATION

This thesis describes the work carried out at the School of Physics, University of KwaZulu-Natal (Pietermaritzburg), under the supervision of Dr V W Couling between January 2003 and January 2005.

I declare the work reported in this dissertation to be my own research, unless specifically indicated to the contrary in the text. This thesis has not been submitted in any form for any degree or examination to any other university.

Signed :  Dated : 15 March 2006

I hereby certify that this statement is correct

V. W. Couling

Dr V W Couling

(SUPERVISOR)

ABSTRACT

During the period January 2001 to January 2003, M Sc student Mr Tleyane Jonas Sono developed an apparatus to measure the pressure- and temperature-dependence of the electro-optic Kerr effect (electric-field-induced birefringence) in gases. Mr Sono presented experimental results for dimethyl ether at a wavelength of 632.8 nm, extracting polarizability tensor components, first and second Kerr hyperpolarizabilities, and second Kerr-effect virial coefficients for this molecular species.

This thesis has been primarily concerned with a thorough re-investigation of the Kerr effect for the dimethyl ether molecule. Of primary concern is the reproducibility of the measured data, which depend upon precise and accurate knowledge of various experimental parameters. These include calibrations of the high-voltage power supply which is used to establish the electric field across the medium, the pressure transducer, the platinum thermistors, as well as the Faraday cell which forms the heart of the compensator. There is also a possibility of the 316-stainless-steel electrodes buckling and warping as they are cycled over ±200°C, leading to variations in the applied field and a consequent hysteresis in the results.

In essence, we have been loath to publish our Kerr-effect investigation of dimethyl ether before making a thorough investigation of the reproducibility of our measured data. Here we present our investigations, and compare our new Kerr virial coefficients and the molecular (hyper)polarizability data extracted from them against the previous work of Sono. It will become apparent agreement is excellent, and that the findings for dimethyl ether are now ready for publication.

The molecular-tensor theory of the Kerr-effect; including the second Kerr-effect virial coefficient B_K, which describes the effects of intermolecular collisions on the molecular Kerr constant; is reviewed. The computed data is compared with the experimental data, yielding good agreement over the full experimental temperature range of 280 to 450 K.

Attempts to obtain measured data at 260 K proved fruitless in the present study, though efforts are underway to complete this task.

CONTENTS ***PAGE***

Chapter 4: Results and Discussion

Appendices

CHAPTER 1: INTRODUCTION

1.1 INTRODUCTION

In 1875, the Reverend John Kerr discovered the first nonlinear electro-optic effect when he found that glass placed in a strong electric field becomes birefringent.[1,2] Kerr's initial experiment showed that when glass was placed in an electric field it behaved as if placed under mechanical tension in a direction parallel to the lines of force[3]. A birefringent medium is optically anisotropic, having different refractive indices $n_{//}$ and $n_{\perp}$ for light polarized parallel and perpendicular respectively to the applied electric field. The effect has come to be known as the Kerr electro-optic effect, and arises because the applied electric field (whether static or alternating) tends to orient the dipoles in the medium.

Measurement of the electro-optic Kerr effect has become a primary tool in deducing the fundamental electric properties of a molecule, such as the polarizability and hyperpolarizability tensors.

The molecular-tensor theory of the Kerr effect, which relates the macroscopic observables to the molecular property tensors, will be reviewed. A review of the dipole-induced-dipole (DID) model of Silberstein will allow for description of molecular-interaction effects in the long-range model of intermolecular forces, against which our Kerr-effect measurements shall be compared.

Since the discovery of the Kerr-effect phenomenon, various research groups have investigated the Kerr effect for molecules of spherical,[5,6] linear[7-11] and non-linear[12,13] symmetry, achieving accuracies of 5-10%. The greatest accuracy was claimed by Shelton to be ±1.5%, although he later retracted his claim.[14]

The work described in this thesis was undertaken on the new Kerr-effect apparatus built during the M Sc project of Mr Tleyane Jonas Sono.[4] Our aim has been to verify reproducibility of the measurements on dimethyl ether reported in Sono's thesis. Only

once reproducibility has been established would we be confident to move on to studies of new molecular species.

Our initial measurements were discrepant when compared with those of Sono. This was thought to be due perhaps to changes in the calibration constants of any one or more of the high-voltage supply, the pressure transducer, the platinum thermistors or the Faraday cell. As a consequence of this, measurements of the molar Kerr constant of dimethyl ether were performed over the entire accessible temperature range. These results are presented in due course, and serve to show that the discrepancy arose not because of the calibration changes, but rather due to changes in the method of temperature control used in the experiment. This part of the investigation took a significant amount of time, but the results were crucial to establishing the reproducibility of gathered data.

We turn now to a review of the molecular-tensor theory of the Kerr effect.

1.2 REFERENCES

1. A. Isaacs, *Oxford Dictionary of Physics*, Oxford Paperback Reference, 4th edition, Oxford Press, pg 200
2. K. D. Moller, *Optics*, New Jersey, University Science Books, 1998
3. J. W. Beams, *Reviews Of Modern Physics*, **5**, 1932,149-160
4. T. J. Sono, M Sc thesis, University of Natal, 2003
5. A. D. Buckingham and D. A. Dunmur, *Trans Faraday Soc.*, 1968, **64**, 1776
6. D. A. Dunmur, D.C. Hunt and N. E. Jessup, *Molec. Phys.*, 1979, **37**, 713
7. A. D. Buckingham and B. J. Orr, *Trans Faraday Soc.*, 1969, **65**, 673
8. A. D. Buckingham, M. P. Bogaard, D. A. Dunmur, C. P. Hobbs and B. J. Orr, *Trans Faraday Soc.*, 1970, **66**, 1548
9. D. W. Schaeffer, R. E. Sears and J. S. Waugh, *J. Chem. Phys.*, 1970, **53**, 1976
10. A. D. Buckingham and H. Sutter, *J. Chem. Phys.*, 1976, **64**, 364
11. I. R. Gentle, D. R. Laver and G. L. D. Ritchie, *J. Phys. Chem.*, 1989, **93**, 3035
12. I. R Gentle, D. R. Laver and G. L. D. Ritchie, *J. Phys. Chem.*, 1990, **94**, 3434
13. R. Tammer and W. Huttner, *Mol. Phys.*, 1994, **83**, 579
14. D. P. Shelton, *Rev. Sci. Instrum.* 1993, **64**, 917

CHAPTER 2: THEORY

2.1 INTRODUCTION

The theory reproduced here should not be seen in isolation since it provides one with the means for experimental determination of the Kerr effect in gases, as well as the means for analyzing the experimental data to extract fundamental molecular properties such as the (hyper)polarizabilities. This theoretical review is based on Buckingham and Pople's modification of the Langevin-Born theory.[1]

This chapter is divided into two subsections, the first dealing with the simpler case of gases at low pressure with non-interacting molecules, and the second outlining the more complex case of gases at relatively high pressure where intermolecular interactions become significant.

2.2 LOW-PRESSURE : NON-INTERACTING MOLECULES

The Kerr effect is an induced-birefringence optical effect, which means that on application of an electric field to the medium under study, the medium becomes birefringent. This is a consequence of the induced anisotropy in the refractive index due to the permanent and induced multipole moments of the molecules in the sample aligning themselves so as to minimize the forces acting on them.[2] A consequence of this birefringent behaviour is that linearly polarized light which passes through the medium becomes elliptically polarized as a result of the phase difference induced between the coherent resolved components of the incident beam linearly polarized parallel and perpendicular to the direction of the applied field. When the azimuth angle of the linearly-polarized incident beam is at 45° relative to the applied field the phase difference δ is a maximum, given by

$$\delta = \frac{2\pi\ell}{\lambda}\left(n_{\parallel} - n_{\perp}\right) \qquad (1)$$

where ℓ is the path-length of the birefringent medium, $n_{\parallel} - n_{\perp}$ is the difference between the refractive indices parallel and perpendicular to the applied field, and λ is the wavelength of the incident beam. This δ is in turn related to the Kerr effect by

$$\delta = 2\pi B \ell E^2 \qquad (2)$$

where B is the Kerr constant which is substance, temperature and wavelength specific, and E is the applied electrostatic field.

Experimentally one measures the molar Kerr constant ${}_mK$ defined by [1,3]

$${}_mK = \frac{18nV_m}{3(n^2+2)^2(\varepsilon_r+2)^2}\lim_{E\to 0}\left[\frac{n_{\parallel}-n_{\perp}}{E^2}\right] \qquad (3)$$

where n and ε_r are the refractive index and relative permittivity of the medium in the absence of the field. V_m is the molar volume of the medium, and is obtainable (provided the pressure P and temperature T are known) from the virial expression

$$\frac{PV_m}{RT} = 1 + \frac{B}{V_m} + \frac{C}{V_m^2}. \qquad (4)$$

Here B and C are to the second and third pressure virial coeffifients. The molar Kerr constant in equation (3) can also be expressed as a virial expansion

$${}_mK = A_k + \frac{B_k}{V_m} + \frac{C_k}{V_m^2} + \ldots \qquad (5)$$

where A_k, B_k, C_k ... are the 1st, 2nd, 3rd ... Kerr-effect virial coefficients with the 2nd, 3rd ... coefficients describing deviations from the zero-density molar Kerr constant A_k due to pair, triplet, ... molecular interactions.

For dilute fluids ${}_mK$ has been shown to reduce to[3]

$$ {}_mK = \lim_{V_m \to \infty} \left[\frac{2(n_{\parallel} - n_{\perp})V_m}{27(4\pi\varepsilon_o)E^2} \right]_{E \to 0} . \qquad (6) $$

Now consider a system of space-fixed axes $O(x,y,z)$ as being fixed in a Kerr cell such that x and y are respectively parallel and perpendicular to the direction of the applied field while z is in the direction of the propagating beam. Application of an electric field to the electrodes results in a difference in the refractive indexes parallel and perpendicular to the applied field, this difference being proportional to the induced phase difference δ. This birefringent behavior can then be related to the molecular-property tensors of the fluid's individual molecules.

In the case of dilute fluids with negligible molecular interactions the oscillating electric field ξ_{0j} is solely responsible for inducing the dipole moment $\mu_i^{(p)}$ in molecule p. Applying a strong static electric field E_i to the fluid changes the optical-frequency polarizability α_{ij} to a new effective polarizability π_{ij}, which is physically interpreted as the increase in moment per unit increase in field [1], and is mathematically defined as

$$ \pi_{ij} = \frac{\partial \mu_i}{\partial \xi_{0j}} = \alpha_{ij} + \beta_{ijk} E_k + \tfrac{1}{2} \gamma_{ijkl} E_k E_l + \ldots \qquad (7) $$

where the first and second hyperpolarizability tensors, β_{ijk} and γ_{ijkl} respectively, describe the distorting effect the applied field has on the polarizability. This new effective polarizability has components parallel and perpendicular to the biasing field given by

$$\pi_{xx} = l_i^x l_j^x \pi_{ij}$$
$$\pi_{yy} = l_i^y l_j^y \pi_{ij} \qquad (8)$$

where l_i^x is the direction cosine between the x space-fixed and the i molecule-fixed axis and l_j^y is the direction cosine between the y space-fixed and the j molecule-fixed axis. When a molecule is held in a fixed configuration τ, the differential polarizability in the presence of the biasing field is

$$\begin{aligned}\pi(\tau,E) &= \pi_{ij}\left(l_i^x l_j^x - l_i^y l_j^y\right) \\ &= \left(\alpha_{ij} + \beta_{ijk} E l_k^x + \tfrac{1}{2}\gamma_{ijkl} E^2 l_k^x l_l^x + \ldots\right)\left(l_i^x l_j^x - l_i^y l_j^y\right).\end{aligned} \qquad (9)$$

Since this molecule is tumbling in space the above quantity has to be averaged over all configurations in the presence of the biasing influence of the applied field E_i. To achieve this the Boltzmann-type distribution function is used:

$$\bar{\pi} = \frac{\int \pi(\tau,E) e^{-U(\tau,E)/k_B T} d\tau}{\int e^{-U(\tau,E)/k_B T} d\tau} \qquad (10)$$

where $U(\tau,E)$ is the potential energy of the molecule in the presence of the biasing field, written as

$$\begin{aligned}U(\tau,E) &= U^{(0)} - \mu_i^{(0)} E_i - \tfrac{1}{2} a_{ij} E_i E_j - \tfrac{1}{6} b_{ijk} E_i E_j E_k + \ldots \\ &= U^{(0)} - \mu_i^{(0)} E\, l_i^x - \tfrac{1}{2} a_{ij} E^2 l_i^x l_j^x - \tfrac{1}{6} b_{ijk} E^3 l_i^x l_j^x l_k^x + \ldots .\end{aligned} \qquad (11)$$

Here $U^{(0)}$ is the potential energy of the molecule when in the absence of a biasing field, $\mu_i^{(0)}$ is the molecule's permanent dipole moment, a_{ij} is the static polarizability while b_{ijk} is the static first-order hyperpolarizability.

The above approach can be taken because the assumption that at characteristic experimental temperatures the rotational energy levels of molecules are very close and so can be treated classically has been validated.[4] Furthermore the period at which the light wave oscillates is significantly smaller than the time taken for the molecule to rotate.

The biased average polarizability is converted into an isotropic average by Taylor expanding $\bar{\pi}$ in terms of E so that

$$\bar{\pi} = A + B\,E + C\,E^2 + \ldots, \qquad (12)$$

where

$$A = \left(\bar{\pi}\right)_{E=0},\ B = \left(\frac{\partial \bar{\pi}}{\partial E}\right)_{E=0},\ C = \tfrac{1}{2}\left(\frac{\partial^2 \bar{\pi}}{\partial E^2}\right)_{E=0}. \qquad (13).$$

The average differential polarizability is then related to the induced birefringence by

$$n_x - n_y = \frac{2\pi N_A}{(4\pi\varepsilon_0)}\bar{\pi}. \qquad (14)$$

In evaluating $\bar{\pi}$ one needs to determine A, B and C and to do so requires the determination of the isotropic averages of the direction cosines. This makes use of some previously derived results: we have from Barron[5]

$$\left\{\begin{array}{l} \left\langle l_i^x \right\rangle = \left\langle l_i^y \right\rangle = \left\langle l_i^z \right\rangle = 0 \\ \left\langle l_i^x l_j^x \right\rangle = \left\langle l_i^y l_j^y \right\rangle = \left\langle l_i^z l_j^z \right\rangle = \tfrac{1}{3}\delta_{ij} \\ \left\langle l_i^x l_j^x l_k^x \right\rangle = \left\langle l_i^y l_j^y l_k^z \right\rangle = \left\langle l_i^z l_j^z l_k^z \right\rangle = \tfrac{1}{6}\varepsilon_{ijk} \end{array}\right\} \qquad (15)$$

and from Buckingham and Pople[1]

$$\left\{\begin{array}{l}\left\langle l_i^x l_j^x l_k^x l_l^x \right\rangle = \frac{1}{15}\left(\delta_{ij}\delta_{kl} + \delta_{ik}\delta_{jl} + \delta_{il}\delta_{kj}\right) \\ \left\langle l_i^z l_j^z l_k^x l_l^x \right\rangle = \frac{1}{30}\left(4\delta_{ik}\delta_{jl} - \delta_{ij}\delta_{kl} - \delta_{il}\delta_{kj}\right)\end{array}\right\}. \qquad (16).$$

When $E = 0$, A becomes zero because $\langle \pi \rangle = 0$, no birefringence being induced in the medium. In determining B, we set $E = 0$ and equation (10) is differentiated with respect to E, so that

$$B = \left(\frac{\partial \bar{\pi}}{\partial E}\right)_{E=0} = \left\langle \frac{\partial \pi}{\partial E} \right\rangle - \frac{1}{k_B T}\left\langle \pi \frac{\partial U}{\partial E} \right\rangle \qquad (17)$$

where

$$\left\{\begin{array}{l}\left(\frac{\partial \pi}{\partial E}\right)_{E=0} = \beta_{ijk} l_k^x \left(l_i^x l_j^x - l_i^y l_j^y\right) \\ \left(\frac{\partial U}{\partial E}\right) = -\mu_i^{(0)} l_i^x\end{array}\right\}. \qquad (18).$$

By invoking equation (15) the set of equations (18) evaluate to zero, yielding $B = 0$. Hence the leading contribution to the differential polarizability is C, given as[1]

$$C = \frac{1}{2}\left(\frac{\partial^2 \bar{\pi}}{\partial E^2}\right)_{E=0} = \frac{1}{2}\left\langle \frac{\partial^2 \pi}{\partial E^2} \right\rangle - \frac{1}{2k_B T}\left\langle 2\frac{\partial \pi}{\partial E}\frac{\partial U}{\partial E} + \pi \frac{\partial^2 U}{\partial E^2} \right\rangle + \frac{1}{2(k_B T)^2}\left\langle \pi \left(\frac{\partial U}{\partial E}\right)^2 \right\rangle \qquad (19)$$

where

$$\left\{\begin{array}{l}\left(\frac{\partial^2 \pi}{\partial E^2}\right)_{E=0} = \gamma_{ijkl} l_k^x l_l^x \left(l_i^x l_j^x - l_i^y l_j^y\right) \\ \left(\frac{\partial^2 U}{\partial E^2}\right)_{E=0} = -\alpha_{ij} l_i^x l_j^x\end{array}\right\}. \qquad (20).$$

Buckingham and Pople used the isotropic averages in equation (16) to evaluate expressions for equation (20), and hence found the relationship between the differential polarizability and the biasing field as being

$$\bar{\pi} = \left\{ \tfrac{2}{30}\gamma_{iijj} + \frac{2}{15k_BT}\beta_{iij}\mu_j^{(0)} + \frac{1}{15k_BT}\left(\alpha_{ij}a_{ij} - 3\alpha a\right) + \frac{3}{15(k_BT)^2}\left(\alpha_{ij}\mu_i^{(0)}\mu_j^{(0)} - \alpha\left(\mu^{(0)}\right)^2\right)\right\} E^2 \tag{21}$$

where

$$\left.\begin{aligned} \alpha &= \tfrac{1}{3}\left(\alpha_{11} + \alpha_{22} + \alpha_{33}\right) \\ a &= \tfrac{1}{3}\left(a_{11} + a_{22} + a_{33}\right) \end{aligned}\right\}, \tag{22}$$

α being the mean dynamic polarizability and a the mean static polarizability. Using equations (3), (12) and (21) the dilute-gas molar Kerr constant was established as

$${}_mK = A_K = \frac{2\pi N_A}{405(4\pi\varepsilon_0)}\left\{2\gamma_{iijj} + \frac{1}{k_BT}\left[4\beta_{iij}\mu_j^{(0)} + 3\left(\alpha_{ij}a_{ij} - 3\alpha a\right)\right] + \frac{3}{(k_BT)^2}\left(\alpha_{ij}\mu_i^{(0)}\mu_j^{(0)} - \alpha\left(\mu^{(0)}\right)^2\right)\right\}. \tag{23}$$

This is the general form of the Langevin-Born equation, which considers the effect of high field strengths on the polarizability. When the symmetry of the molecule is taken into account the general expression is often greatly simplified. The molecule studied in this work is dimethyl-ether, of C_{2v} symmetry, and is taken to lie in the 1-3 plane of the molecule-fixed axes *O*(1,2,3), where *3* is along the principal molecular axis so that[6]

$$A_K = \frac{N_A}{81\varepsilon_0}\left\{\gamma^K + \frac{1}{k_BT}\left[\tfrac{2}{3}\mu\beta^K + \tfrac{1}{5}\Delta\alpha\Delta a\right] + \tfrac{3}{10}\frac{1}{(k_BT)^2}\mu^2\left(\alpha_{33} - \alpha\right)\right\}. \tag{24}$$

Here the dipole moment is along the *3*-axis so that $\mu = \mu_3^{(0)}$, while the dynamic and static polarizability anisotropies $\Delta\alpha$ and Δa are defined as

$$\Delta\alpha = \frac{1}{\sqrt{2}}\left[(\alpha_{11}-\alpha_{22})^2 + (\alpha_{22}-\alpha_{33})^2 + (\alpha_{33}-\alpha_{11})^2\right]^{1/2} \qquad (25)$$

and

$$\Delta a = \frac{1}{\sqrt{2}}\left[(a_{11}-a_{22})^2 + (a_{22}-a_{33})^2 + (a_{33}-a_{11})^2\right]^{1/2}. \qquad (26).$$

β^K and γ^K, the first and second Kerr hyperpolarizabilities, are given by

$$\left\{\begin{array}{l}\beta^K = \frac{3}{10}\left(3\beta_{i3i} - \beta_{ii3}\right) \\ \gamma^K = \frac{1}{10}\left(3\gamma_{ijij} - \gamma_{iijj}\right)\end{array}\right\}. \qquad (27).$$

The molar Kerr constant for atomic gases such as argon and isotropically polarizable molecules such as methane emerges as

$${}_mK = \frac{4\pi N_A}{81(4\pi\varepsilon_0)}\gamma^K, \qquad (28)$$

and it is seen that it is the temperature-independent term that is proportional to the second hyperpolarizability. Measurement of the Kerr constant for such gases leads directly to γ^K.

For molecules of lower symmetry, two alternative methods exist for analyzing experimental data. The first involves converting equation (24) into a straight-line equation of the form

$$\left[A_K - \frac{N_A}{81\varepsilon_0}\gamma^K\right]T = \frac{N_A}{81\varepsilon_0}\frac{1}{k_B}\left[\tfrac{2}{3}\mu\beta^K + \tfrac{1}{5}\Delta\alpha\Delta a\right] + \frac{N_A}{270\varepsilon_0}\frac{1}{k_B^2 T}\mu^2(\alpha_{33}-\alpha), \qquad (29)$$

which requires an estimate of γ from some other experiment (such as electric-field-induced second-harmonic generation). Plotting the left-hand side of the expression as a function of the inverse temperature T^{-1} allows for the determination of β^K from the

intercept of the graph. The parameters μ, $\Delta\alpha$ and Δa can be obtained from published data.

A second, alternative, method requires expressing the low-density molar Kerr constant in the form of a polynomial function to take the form[7,8]

$$_mK = A_K = P + \frac{Q}{T} + \frac{R}{T^2} \cdots . \qquad (30)$$

A direct comparison of equations (24) and (30) indicates that P, Q and R represent respectively the temperature independent, the inverse and the inverse square absolute temperature dependent terms. By fitting a second-degree polynomial to experimental $A_K(T)$ data as a function of inverse temperature T^{-1}, the coefficients P, Q and R can be extracted and used to determine Kerr hyperpolarizabilities as well as the polarizability anisotropy.

2.3 HIGH-PRESSURE : INTERACTING MOLECULES

As the gas or vapour pressure increases molecular interactions can become significant, and so the theory discussed above needs to be modified. The effects of molecular interactions on the molar Kerr constant are best accounted for by means of a virial expansion

$$_mK = A_K + \frac{B_K}{V_m} + \frac{C_K}{V_m^2} + \cdots , \qquad (31)$$

where A_K, B_K and C_K are the first, second and third Kerr virial coefficients which describe the contributions to the molar Kerr constant arising from isolated molecules, interacting pairs and interacting triplets respectively. B_K is given by

$$B_K = \lim_{V_m \to \infty} \left({}_m K - A_K \right) V_m \ . \qquad (32)$$

It was Buckingham who pioneered the theory of B_K.[3] Couling and Graham have recently extended Buckingham's molecular-tensor theory for B_K to molecules of general symmetry.[10] This theory is summarized here, and will be used to obtain calculated estimates of B_K for dimethly ether against which to compare the measured values obtained in this work. The theory is built upon the approach first used by Buckingham and Pople.[9]

We have already seen that the birefringence induced in a fluid by the presence of a strong static electric field E_x is $n_x - n_y = \frac{2\pi N_A}{(4\pi\varepsilon_0)} \bar{\pi}$ where $\bar{\pi}$ is the average over all configurations of $\pi_{ij}\left(l_i^x l_j^x - l_i^y l_j^y\right)$ of a representative molecule in the presence of the biasing influence E_x. For higher gas densities the contribution of a representative molecule 1 to $\left(n_x - n_y\right)$ is modified by the presence of a neighbouring molecule 2. Couling and Graham[10] have argued that for a pair of interacting molecules in the specific relative configuration τ, molecule 1's contribution to the induced birefringence is a half of the total contribution at a particular instant in time,

$$\tfrac{1}{2}\left\{ \frac{2\pi N_A}{(4\pi\varepsilon_0) V_m} \pi^{(12)}(\tau, E) \right\} \qquad (33)$$

where $\pi^{(12)}$ represents the differential polarizabilty of the interacting pair in molecule-fixed axes and is given by

$$\pi^{(12)}(\tau, E) = \pi_{ij}^{(12)}\left(l_i^x l_j^x - l_i^y l_j^y\right). \qquad (34)$$

At first the pair is taken to be held in a fixed relative configuration τ and is allowed to rotate as a rigid whole while under the influence of the electric field E_i. The biased

orientational average $\overline{\pi^{(12)}(\tau,E)}$ is converted into an isotropic average through Taylor expansion in powers of E. The leading contributing term of the series expansion is proportional to the square of the static electric field and is

$$\overline{\pi^{(12)}(\tau,E)} = \tfrac{1}{2}\left(\frac{\partial^2\overline{\pi^{(12)}(\tau,E)}}{\partial E^2}\right)_{E=0} E^2 \qquad (35)$$

where

$$\tfrac{1}{2}\left(\frac{\partial^2\overline{\pi^{(12)}(\tau,E)}}{\partial E^2}\right)_{E=0} = \tfrac{1}{2}\left\langle\frac{\partial^2\pi^{(12)}}{\partial E^2}\right\rangle - \frac{1}{2k_BT}\left\langle 2\frac{\partial\pi^{(12)}}{\partial E}\frac{\partial U^{(12)}}{\partial E} + \pi^{(12)}\frac{\partial^2U^{(12)}}{\partial E^2}\right\rangle + \frac{1}{2(k_BT)^2}\left\langle\pi^{(12)}\left(\frac{\partial U^{(12)}}{\partial E}\right)^2\right\rangle \qquad (36)$$

and $\partial U^{(12)}(\tau,E)$ is the potential energy of the interacting pair of molecules in the presence of the applied field. Including this pair interaction the molar Kerr constant becomes

$${}_mK = A_K + \int_\tau \frac{2\pi N_A}{27(4\pi\varepsilon_0)}\left\{\tfrac{1}{2}\left(\frac{\partial^2\overline{\pi^{(12)}(\tau,E)}}{\partial E^2}\right)_{E=0} - \left(\frac{\partial^2\overline{\pi}}{\partial E^2}\right)_{E=0}\right\}P(\tau)d\tau \,. \qquad (37).$$

Here $P(\tau)d\tau$ represents the probability of molecule 1 having a neighbouring molecule in the range τ to $\tau + d\tau$ and is related to the intermolecular potential $U_{12}(\tau)$ by

$$P(\tau) = \frac{N_A}{\Omega\, V_m} e^{-(U_{12}(\tau)/k_BT)} \qquad (38)$$

where Ω is the intergral over the orientational coordinates of the neighbouring molecule and is described by $\Omega = V_m^{-1}\int d\tau$. The second Kerr virial coefficient now takes the form[10,12]

$$B_K = \frac{2\pi N_A^2}{27\Omega(4\pi\varepsilon_0)} \int_\tau \left\{ \frac{1}{2} \left(\frac{\partial^2 \overline{\pi^{(12)}(\tau, E)}}{\partial E^2} \right)_{E=0} - \left(\frac{\partial^2 \overline{\pi}}{\partial E^2} \right)_{E=0} \right\} e^{-(U_{12}(\tau)/k_B T)} d\tau . \qquad (39).$$

For interacting pairs of molecules with symmetry lower than linear, B_K is written[10,12]

$$B_K = \frac{N_A^2}{216\pi^2(4\pi\varepsilon_0)} \int_{R=0}^{\infty} \int_{\alpha_1=0}^{2\pi} \int_{\beta_1=0}^{\pi} \int_{\gamma_1=0}^{2\pi} \int_{\alpha_2=0}^{2\pi} \int_{\beta_2=0}^{\pi} \int_{\lambda_{12}=0}^{2\pi} \left\{ \frac{1}{2} \left(\frac{\partial^2 \overline{\pi^{(12)}(\tau, E)}}{\partial E^2} \right)_{E=0} - \left(\frac{\partial^2 \overline{\pi}}{\partial E^2} \right)_{E=0} \right\} \qquad (40)$$
$$\times e^{-(U_{12}(\tau)/k_B T)} R^2 \sin\beta_1 \sin\beta_2 dR d\alpha_1 d\beta_1 d\gamma_1 d\alpha_2 d\beta_2 d\gamma_2 .$$

Here the interaction coordinates are the Euler angles and the intermolecular displacement R.[10,12]

For this interacting pair the dipole moment of molecule 1 is given as

$$\mu_i^{(1)}(\xi_0) = \left(\alpha_{ij}^{(1)} + \beta_{ijk}^{(1)} E_k + \tfrac{1}{2}\gamma_{ijkl}^{(1)} E_k E_l + \cdots\right)\left(\xi_{0j} + F_j^{(1)}\right). \qquad (41)$$

This dipole moment is not induced solely by the oscillating field of the laser beam's incident light wave ξ_{0i} but also by the field $F_i^{(1)}$ due to the oscillating moment of the neighbouring molecule. The corresponding relationship between the dipole moment of molecule 2 and the field resulting from the oscillating moment at the origin of molecule 1 is described by

$$F_i^{(1)} = T_{ij}^{(1)} \mu_j^{(2)} . \qquad (42)$$

Following the same reasoning as above, the dipole moment of molecule 2 is

$$\mu_i^{(2)}(\xi_0) = \left(\alpha_{ij}^{(2)} + \beta_{ijk}^{(2)} E_k + \tfrac{1}{2}\gamma_{ijkl}^{(2)} E_k E_l + \cdots\right)\left(\xi_{0j} + F_j^{(2)}\right). \qquad (43)$$

In turn the electric field due to the oscillating dipole moment of molecule 1 arising at the origin of molecule 2 is

$$F_i^{(2)} = T_{ij}^{(2)} \mu_j^{(1)} . \qquad (44)$$

To obtain the total dipole moment of molecule 1, equations (43) and (44) are substituted into equation (42). The resulting expression is in turn substituted into equation (41) yielding the total oscillating dipole moment induced on molecule 1 by the light-wave field in the presence of molecule 2. This expression is then differentiated with respect to ξ_{0i} to yield the differential polarizability of a general molecule p in the presence of the applied static field and the neighbouring molecule q. These last two expressions are too lengthy to reproduce here, and may be found in references 10 and 13.

In the molecule-fixed frame the expression for the difference between differential polarizabilities (for a specific interaction configuration τ of molecules p and q) is

$$\pi^{(p)}(\tau, E) = \pi_{ij}^{(p)}\left(l_i^x l_j^x - l_i^y l_j^y\right). \qquad (45)$$

Assuming that each of the molecules in the interaction pair maintain their own identities the total dipole moment of the interacting molecules can be written as [9,11]

$$\mu_i^{(12)} = \mu_i^{(1)} + \mu_i^{(2)} \qquad (46)$$

resulting in the differential polarizability for the system, which takes the form

$$\pi_{ij}^{(12)} = \frac{\partial \mu_i^{(12)}}{\partial \xi_{0j}} = \frac{\partial\left(\mu_i^{(1)} + \mu_i^{(2)}\right)}{\partial \xi_{0j}}. \qquad (47)$$

Hence the difference in the differential polarizabilities of the interacting molecules in the presence of an applied field becomes

$$\pi^{(12)}(\tau,E)=\pi_{ij}^{(12)}\left(I_i^x I_j^x - I_i^y I_j^y\right)$$

$$=\left(\pi_{ij}^{(1)}+\pi_{ij}^{(2)}\right)\left(I_i^x I_j^x - I_i^y I_j^y\right) \qquad (48)$$

$$=\pi^{(1)}(\tau,E)+\pi^{(2)}(\tau,E).$$

The potential energy of the interacting pair in the presence of the biasing field is given by[13]

$$U^{(12)}(\tau,E)=U^{(12)}(\tau,0)-\int_0^E \mu_i^{(12)}(\tau,E)I_i^x\,dE\,. \qquad (49)$$

The dipole moment of molecule p in the presence of molecule q and the applied field is

$$\mu_i^{(p)}=\mu_{0i}^{(p)}+a_{ij}^{(p)}\left(E_j+F_j^{(p)}\right) \qquad (50).$$

where $F_j^{(p)}$ is the static field occurring at molecule p when E_i and molecule q are present. Such a field is related to the inducing dipole moment via a T-tensor[14]

$$F_i^{(p)}=T_{ij}\,\mu_j^{(q)}. \qquad (51).$$

Now the total dipole moment for molecule q is

$$\mu_i^{(q)}=\mu_{0i}^{(q)}+a_{ij}^{(q)}\left(E_j+F_j^{(q)}\right) \qquad (52)$$

where

$$F_i^{(q)}=T_{ij}\,\mu_j^{(p)}. \qquad (53).$$

From these equations the total oscillating dipole moment can then be determined.[10] In a similar manner the potential energy for the interacting pair can be obtained:

$$U^{(12)}(\tau,E)=U^{(12)}(\tau,0)+U^{(1)}(\tau,E)+U^{(2)}(\tau,E). \qquad (54).$$

Based on the assumption that the molecules retain their individual identities, equation (36) is written as

$$\begin{aligned}\frac{1}{2}\left(\frac{\partial^2\overline{\pi^{(12)}(\tau,E)}}{\partial E^2}\right)_{E=0} &= \left\langle\frac{\partial^2\pi^{(1)}}{\partial E^2}\right\rangle-\frac{1}{k_BT}\left\{\left\langle 2\frac{\partial\pi^{(1)}}{\partial E}\frac{\partial U^{(1)}}{\partial E}\right\rangle+\left\langle 2\frac{\partial\pi^{(1)}}{\partial E}\frac{\partial U^{(2)}}{\partial E}\right\rangle\right\}\\ &-\frac{1}{k_BT}\left\{\left\langle\pi^{(1)}\frac{\partial^2U^{(1)}}{\partial E^2}\right\rangle+\left\langle\pi^{(1)}\frac{\partial^2U^{(2)}}{\partial E^2}\right\rangle\right\}\\ &+\frac{1}{(k_BT)^2}\left\{\left\langle\pi^{(1)}\left(\frac{\partial U^{(1)}}{\partial E}\right)^2\right\rangle+2\left\langle\pi^{(1)}\frac{\partial U^{(1)}}{\partial E}\frac{\partial U^{(2)}}{\partial E}\right\rangle+\left\langle\pi^{(1)}\left(\frac{\partial U^{(2)}}{\partial E}\right)^2\right\rangle\right\}.\end{aligned} \qquad (55)$$

Using isotropic averages, equation (55) can be simplified to[12]

$$\begin{aligned}\left\{\frac{1}{2}\left(\frac{\partial^2\overline{\pi^{(12)}(\tau,E)}}{\partial E^2}\right)_{E=0}-\left(\frac{\partial^2\bar{\pi}}{\partial E^2}\right)_{E=0}\right\} &= \alpha_2+\alpha_3+\alpha_4+\alpha_5+\cdots\gamma_1\alpha_1+\gamma_1\alpha_2+\cdots+\mu_2\alpha_1\\ &+\mu_2\alpha_2+\mu_2\alpha_3+\cdots+\mu_1\beta_1+\mu_1\beta_1\alpha_1+\cdots.\end{aligned} \qquad (56)$$

The individual terms are identified explicitly in the list below:

$$\alpha_2=\frac{1}{k_BT}\left\{\alpha_{ij}^{(1)}\alpha_{kl}^{(2)}\right\}\left\langle l_i^x l_j^x l_k^x l_l^x-l_i^y l_j^y l_k^x l_l^x\right\rangle \qquad (57)$$

$$\alpha_3=\frac{1}{k_BT}\left\{\alpha_{ij}^{(1)}a_{km}^{(1)}T_{mn}a_{nr}^{(2)}+\alpha_{ij}^{(1)}a_{km}^{(2)}T_{mn}a_{nr}^{(1)}+\alpha_{ij}^{(1)}T_{km}\alpha_{mn}^{(2)}a_{nr}^{(1)}+\alpha_{ij}^{(1)}T_{km}\alpha_{mn}^{(2)}a_{nr}^{(2)}\right\}\times\left\langle l_i^x l_j^x l_k^x l_r^x-l_i^y l_j^y l_k^x l_l^x\right\rangle \qquad (58)$$

$$\alpha_4 = \frac{1}{k_B T}\begin{Bmatrix} \alpha_{ij}^{(1)} a_{kl}^{(1)} T_{lm} a_{mw}^{(2)} T_{wv} a_{vr}^{(1)} + \alpha_{ij}^{(1)} a_{kl}^{(2)} T_{lm} a_{mw}^{(1)} T_{wv} a_{vr}^{(2)} \\ + \alpha_{ij}^{(1)} T_{kl} \alpha_{lm}^{(2)} a_{mw}^{(1)} T_{wv} a_{vr}^{(2)} + \alpha_{ij}^{(1)} T_{kl} \alpha_{lm}^{(2)} a_{mw}^{(2)} T_{wv} a_{vr}^{(1)} \\ + \alpha_{ij}^{(1)} T_{kl} \alpha_{lm}^{(2)} T_{mw} \alpha_{wv}^{(1)} a_{vr}^{(1)} + \alpha_{ij}^{(1)} T_{kl} \alpha_{lm}^{(2)} T_{mw} \alpha_{wv}^{(2)} a_{vr}^{(2)} \end{Bmatrix} \times \left\langle l_i^x l_j^x l_k^x l_r^x - l_i^y l_j^y l_k^x l_l^x \right\rangle \tag{59}$$

$$\alpha_5 = \frac{1}{k_B T}\begin{Bmatrix} \alpha_{ij}^{(1)} a_{kl}^{(1)} T_{lm} a_{mn}^{(2)} T_{nw} a_{wv}^{(1)} T_{vu} a_{ur}^{(2)} \\ + \alpha_{ij}^{(1)} a_{kl}^{(2)} T_{lm} a_{mn}^{(1)} T_{nw} a_{wv}^{(2)} T_{vu} a_{ur}^{(1)} \\ + \alpha_{ij}^{(1)} T_{kl} \alpha_{lm}^{(2)} a_{mn}^{(1)} T_{nw} a_{wv}^{(2)} T_{vu} a_{ur}^{(1)} \\ + \alpha_{ij}^{(1)} T_{kl} \alpha_{lm}^{(2)} a_{mn}^{(2)} T_{nw} a_{wv}^{(1)} T_{vu} a_{ur}^{(2)} \\ + \alpha_{ij}^{(1)} T_{kl} \alpha_{lm}^{(2)} T_{mn} \alpha_{mw}^{(1)} a_{wv}^{(1)} T_{vu} a_{ur}^{(2)} \\ + \alpha_{ij}^{(1)} T_{kl} \alpha_{lm}^{(2)} T_{mn} \alpha_{mw}^{(1)} a_{wv}^{(2)} T_{vu} a_{ur}^{(1)} \\ + \alpha_{ij}^{(1)} T_{kl} \alpha_{lm}^{(2)} T_{mn} \alpha_{mw}^{(1)} T_{wv} \alpha_{vu}^{(2)} a_{ur}^{(1)} \\ + \alpha_{ij}^{(1)} T_{kl} \alpha_{lm}^{(2)} T_{mn} \alpha_{mw}^{(1)} T_{wv} \alpha_{vu}^{(2)} a_{ur}^{(2)} \end{Bmatrix} \times \left\langle l_i^x l_j^x l_k^x l_r^x - l_i^y l_j^y l_k^x l_l^x \right\rangle \tag{60}$$

$$\gamma_1 \alpha_1 = \left\{ \gamma_{ijkl}^{(1)} T_{lw} \alpha_{wr}^{(2)} + \alpha_{iw}^{(1)} T_{wl} \gamma_{ljkr}^{(2)} \right\} \left\langle l_i^x l_j^x l_k^x l_r^x - l_i^y l_j^y l_k^x l_l^x \right\rangle \tag{61}$$

$$\mu_2 \alpha_1 = \frac{1}{(k_B T)^2} \left\{ \alpha_{ik}^{(1)} \mu_{ok}^{(2)} \mu_{or}^{(2)} + 2\alpha_{ij}^{(1)} \mu_{ok}^{(1)} \mu_{or}^{(2)} \right\} \left\langle l_i^x l_j^x l_k^x l_r^x - l_i^y l_j^y l_k^x l_l^x \right\rangle \tag{62}$$

$$\mu_2 \alpha_2 = \frac{1}{(k_B T)^2} \begin{Bmatrix} 2\alpha_{ik}^{(1)} \mu_{ok}^{(1)} a_{lm}^{(1)} T_{mn} \mu_{or}^{(2)} + 2\alpha_{ik}^{(1)} \mu_{ok}^{(2)} a_{lm}^{(2)} T_{mn} \mu_{or}^{(1)} \\ + 2\alpha_{ik}^{(1)} \mu_{ok}^{(1)} a_{lm}^{(2)} T_{mn} \mu_{or}^{(1)} + 2\alpha_{ik}^{(1)} \mu_{ok}^{(2)} a_{lm}^{(1)} T_{mn} \mu_{or}^{(2)} \\ + \alpha_{ij}^{(1)} T_{kl} \alpha_{lm}^{(2)} \mu_{0m}^{(1)} \mu_{or}^{(1)} + \alpha_{ij}^{(1)} T_{kl} \alpha_{lm}^{(2)} \mu_{0m}^{(2)} \mu_{or}^{(2)} \\ + 2\alpha_{ij}^{(1)} T_{kl} \alpha_{lm}^{(2)} \mu_{0m}^{(1)} \mu_{or}^{(2)} \end{Bmatrix} \left\langle l_i^x l_j^x l_k^x l_r^x - l_i^y l_j^y l_k^x l_l^x \right\rangle \tag{63}$$

$$\mu_2\alpha_3 = \frac{1}{k_B T}\begin{Bmatrix} \alpha_{ij}^{(1)}\alpha_{kl}^{(1)}T_{lm}\mu_{0m}^{(2)}a_{nw}^{(1)}T_{wr}\mu_{0n}^{(2)} + \alpha_{ij}^{(1)}\alpha_{kl}^{(2)}T_{lm}\mu_{0m}^{(1)}a_{nw}^{(2)}T_{wr}\mu_{0n}^{(1)} \\ + 2\alpha_{ij}^{(1)}\alpha_{kl}^{(1)}T_{lm}\mu_{0m}^{(2)}a_{nw}^{(1)}T_{wr}\mu_{0n}^{(2)} + 2\alpha_{ik}^{(1)}T_{kl}\alpha_{lm}^{(2)}\mu_{0m}^{(1)}a_{nw}^{(1)}T_{wr}\mu_{0n}^{(1)} \\ + 2\alpha_{ik}^{(1)}T_{kl}\alpha_{lm}^{(2)}\mu_{0m}^{(2)}a_{nw}^{(2)}T_{wr}\mu_{0n}^{(1)} + 2\alpha_{ik}^{(1)}T_{kl}\alpha_{lm}^{(2)}\mu_{0m}^{(1)}a_{nw}^{(2)}T_{wr}\mu_{0n}^{(1)} \\ + 2\alpha_{ik}^{(1)}T_{kl}\alpha_{lm}^{(2)}\mu_{0m}^{(2)}a_{nw}^{(1)}T_{wr}\mu_{0n}^{(2)} + 2\alpha_{ik}^{(1)}\mu_{0k}^{(1)}a_{lm}^{(1)}T_{mn}a_{n}^{(2)}T_{wr}\mu_{0n}^{(1)} \\ + 2\alpha_{ik}^{(1)}\mu_{0k}^{(2)}a_{lm}^{(2)}T_{mn}a_{n}^{(1)}T_{wr}\mu_{0n}^{(2)} + 2\alpha_{ik}^{(1)}\mu_{0k}^{(1)}a_{lm}^{(2)}T_{mn}a_{n}^{(1)}T_{wr}\mu_{0n}^{(2)} \\ + 2\alpha_{ik}^{(1)}\mu_{0k}^{(2)}a_{lm}^{(1)}T_{mn}a_{n}^{(2)}T_{wr}\mu_{0n}^{(1)} + \alpha_{ij}^{(1)}T_{kl}\alpha_{l}^{(2)}T_{mn}\alpha_{n}^{(1)}\mu_{0n}^{(1)}\mu_{0r}^{(1)} \\ + \alpha_{ij}^{(1)}T_{kl}\alpha_{l}^{(2)}T_{mn}\alpha_{n}^{(1)}\mu_{0n}^{(2)}\mu_{0r}^{(2)} + 2\alpha_{ij}^{(1)}T_{kl}\alpha_{l}^{(2)}T_{mn}\alpha_{n}^{(1)}\mu_{0n}^{(1)}\mu_{0r}^{(2)} \end{Bmatrix} \times \left\langle l_i^x l_j^x l_k^x l_r^x - l_i^y l_j^y l_k^x l_l^x \right\rangle \tag{64}$$

$$\mu_2\beta_1 = \frac{1}{k_B T}\left\{\beta_{ijk}^{(1)}\mu_{or}^{(2)}\right\}\left\langle l_i^x l_j^x l_k^x l_r^x - l_i^y l_j^y l_k^x l_l^x \right\rangle . \tag{65}$$

Determining these quantities requires the use of equations (16) to evaluate the individual isotropic averages. Furthermore the intermolecular potential energy is required for the calculation of B_K. In their derivations Couling and Graham[10] used the classical potential

$$U_{12}(\tau) = U_{LJ} + U_{\mu,\mu} + U_{\mu,\theta} + U_{\theta,\theta} + U_{\mu,ind\mu} + U_{\theta,ind\mu} + U_{shape} \tag{66}$$

where U_{LJ} is the Lennard-Jones 6:12 potential, $U_{\mu,\mu}$ is the dipole-dipole, $U_{\mu,\theta}$ the dipole-quadrupole, $U_{\theta,\theta}$ the quadrupole-quadrupole, $U_{\mu,ind\mu}$ the dipole-induced dipole and $U_{\theta,ind\mu}$ the quadrupole-induced dipole interaction energies for the pair of molecules. U_{shape} explains the angular dependence of short-range repulsive forces for molecules of non-spherical shape.[12]

The interaction energies depend on molecular symmetry and hence may be expressed as direction cosines through use of Euler angles. These expressions have been evaluated previously[13,14], while U_{shape} is given by[13]

$$U_{shape} = 4\varepsilon\left(\frac{R_0}{R}\right)^{12}\left\{D_1\left[3\cos^2\beta_1 + 3\cos^2\beta_2 - 2\right] + D_2\left[3\sin^2\beta_1\cos^2\gamma_1 + 3\sin^2\beta_2\cos^2\gamma_1 - 2\right]\right\}. \quad (67)$$

By collating the results from these expressions B_K could be numerically calculated, and then compared against experimental data.

2.4 REFERENCES

1. A. D. Buckingham and J. A. Pople, *Proc. Phys. Soc. A*, 1955, **68**, 905
2. J. Kerr, *Phil. Mag.*, 1875, **50**, 337 & 446
3. A. D. Buckingham, *Proc. Phys. Soc. A*, 1955, **68**, 910
4. P. W. Atkins, *Physical Chemistry*, 6th Edn, Oxford University Press, Oxford, 1998, 596
5. L. D. Barron, *Molecular Light Scattering and Optical Activity*, Cambridge University Press, Cambridge, 1982
6. T. J. Sono, M Sc thesis, University of Natal, 2003
7. I. R. Gentle, D. R. Laver and G. L. D. Ritchie, *J. Phys. Chem.*, 1990, **94**, 3434
8. V. W. Couling, B. W. Halliburton, R. I. Keir and G. L. D. Ritchie, *J. Phys. Chem. A*, 2001, **105**, 4365
9. A. D. Buckingham and J. A. Pople, *Faraday Soc. Disc.*, 1956, **22**, 17
10. V. W. Couling and C. Graham, *Mol. Phys.*, 1998, **93**, 31
11. A. D. Buckingham, P. A. Galwas and Liu Fan-Chen, *J. Mol. Struct*, 1983, **100**, 3
12. V. W. Couling, Ph D thesis, University of Natal, 1995
13. V. W. Couling and C. Graham, *Mol. Phys.*, 1996, **87**, 779
14. A. D. Buckingham, *Adv. Chem. Phys.*, 1967, **12**, 107

CHAPTER 3: EXPERIMENTAL DETAILS

3.1 INTRODUCTION

The Kerr experiment is one that researchers have sought to improve on ever since its birth. In this respect our experimental arrangement shall bear certain similarities to previous work done in the field. It is accepted that the greater the sensitivity of the system, the better the accuracy but the method employed to take measurements is just as significant as the apparatus used. The assembly has been developed over the last few years and was inherited from a previous student Mr TJ Sono. Certain modifications were however made to the setup and these shall be discussed accordingly.

However for the successful completion of any project it is necessary to understand how the different components work and complement each other hence this chapter provides a brief overview of the experiment and apparatus used and shall conclude with certain precursors to measurements of the molar Kerr constant at various temperatures and corresponding pressures. The interlude between the two shall be provided by a detailed look as to the method of measurement employed and exact experimental procedure.

Excessive technical detail is avoided by referencing Sono's thesis where appropriate. Contributions specific to this project include a recalibration of the electrode spacing, recalibrations of the high-voltage power supply, the Faraday cell and the pressure transducer, leak testing, and improvements to the HPBASIC control program. The temperature control of the cell has been thoroughly investigated, yielding some important conclusions.

3.2 BRIEF OVERVIEW

Fig. 1: A Photograph of the Experimental Arrangement

Figure 1 is a photograph of the present experimental setup. One can see the laser, oven (containing the Kerr cell), analyzing system, gas cylinder and electronics. These various components will shortly be discussed in more detail.

A linearly polarized beam of light emerges from the laser and passes through the polarizing prism with its transmission axis set at 45° to the applied electric field. The beam then passes through the Kerr cell which resides in a well-insulated oven. The light emerges from the cell elliptically polarized, and then passes through a quarter-wave plate to convert it back to a linearly-polarized beam, although its axis of polarization will be offset from the initial 45° position of the light incident on the Kerr cell. The beam then passes through a Faraday cell to be rotated back to its initial plane of polarization. By measuring how much the plane of polarization has had to be corrected to be brought back to 45° it is possible to obtain the phase difference induced by the Kerr cell. The light wave is detected by a photodiode, the signal being fed to a lock-in-amplifier which is in turn monitored by a Hewlett Packard (HP) data-acquisition unit controlled by a Personal

Computer (PC). The PC records and analyzes the data via an HP BASIC program which was initially written by Dr Couling and Mr T J Sono,[1] and modified as part of this project during 2003-2004.

The successful operation of the experiment is dependent on a series of electronic devices such as the high-voltage power supply (which applies a voltage across the Kerr electrodes to supply an electric field across the medium under study), a waveform synthesizer (which generates the sinusoidal signal), a phase shifter and frequency doubler (which ensure that the signal supplied to the Faraday cell is of the same frequency as that emanating from the Kerr cell, as well as in anti-phase to it).

We shall now discuss each of the experimental components in turn:

3.3 THE APPARATUS

3.3.1 The Optical Cascade

3.3.1.1 The Optical Bench

The optical bench comprised a 4.25 m by 25 cm concrete slab of height 60 cm on top of a 10 cm cork foundation. The cork is responsible for absorbing vibrations from the building and outer environment so as to minimize spurious contributions to signal noise levels. The stability of the system was increased by joining another concrete slab perpendicular to the initial one such that it forms a T-shape. Magnetic holders hold all optical components on a 9 cm high, 23 cm wide steel bar which rests on anti-vibration pads. The Kerr cell rests in an oven which is attached to the optical bench by means of adjustable bases which are bolted onto the steel bar. The optical bench is supported by a vibration-damped concrete wall.

3.3.1.2 The Laser

Fig 2: A Photograph of the He-Ne Laser

The Melles Griot 25-LHP-928 He-Ne laser shown in the photograph above was the light source for all work reported here. It produces a continuous-wave monochromatic beam of wavelength 632.8 nm. In comparison to most He-Ne lasers it has a relatively high power rating of 35 mW, producing a linearly polarized beam with an extinction ratio of 500:1. The laser is secured using magnetic holders and a system of adjustors allows for fine directional adjustment of the laser beam. A converging lens placed in front of the beam focuses it so that the beam waist is at the centre of the Kerr cell.

3.3.1.3 The Polarizer

The polarizer is a Glan-Thompson prism residing in a divided circle with a resolution of 2' of arc. The transmission axis of the polarizer was set at 45° to vertical (and hence to the applied electric field). This ensures that the parallel and perpendicular components of the light-wave field are equal in magnitude. In a later subsection we discuss the procedure for obtaining the true vertical for the polarizer.

3.3.1.4 The Kerr Cell

The photograph in Figure 3 shows the different components of the Kerr cell. The Kerr cell consists of a bulkhead, an end plate, a gas inlet as well as a viewing porthole, a

flange and an adjustable cell stand. Shown quite clearly in the picture are the bulkhead, the RTD's, the circulating fan, as well as the oven in which the cell resides.

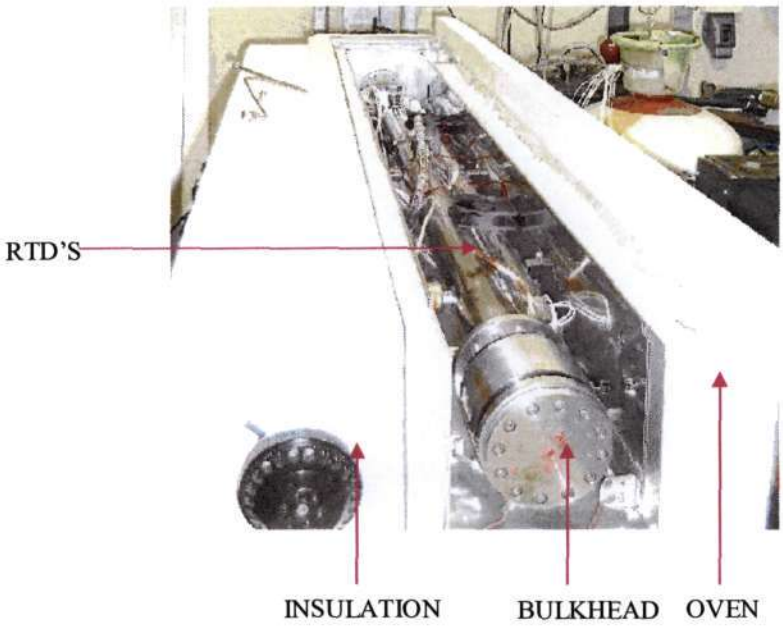

Fig 3: A Photograph Of The Kerr Cell

3.3.1.4.1 Kerr Cell Specifications

The cell is a 316-stainless steel cylinder of length 1.5 m with inner diameter 5.44 cm and wall thickness of 0.38 cm. There are three portholes at evenly-spaced intervals along the cylinder, serving to enable measurement of the separation between electrodes when placed in the cell. There is also an outlet to facilitate connection of the cell to the gas line. At each end of the steel cylinder lies an end plate of diameter 10.5 cm and thickness 1 cm. A flange with a teflon seal was fitted to one of these endplates using Alan bolts. The flange is comprised of a 316-stainless steel disk with holes to allow for bolting onto the cell, as well as a central hole (sealed by a Pockels-glass window sandwiched between teflon seals and held in place by a smaller flange also attached using Alan screws) through which the beam could pass. Pockels glass was used in preference to other forms of glass because it has low residual strain even when under mechanical stress, and so introduces minimal stray birefringence into the experiment.

The windows on the cell are coated with a 0.5 μm layer of quartz so that corrosive gases used in the cell would not damage the glass. Figure 3 also shows a Hastelloy C-276 bulkhead bolted onto the other end of the cell. This allows for the connection of the high-voltage signal to the electrodes.

Teflon was chosen as an appropriate flange seal because it is able to withstand temperatures of the order of 200°C: the current upper limit of our experimental temperature is 220°C. 316-stainless steel was chosen as the material for the cell because it is able to withstand most corrosive gases. Although the dimethyl ether (DME) which has been investigated here is non-corrosive, several corrosive gases are likely to be studied in the future.

3.3.1.4.2 The Electrodes

Fig 4: A Picture of the electrodes while the separation was being determined

Two stainless-steel electrodes, which are close to parallel over their entire length of 1.468 m and width of 3.2 cm, were used to generate the required electric field. The electrodes were polished by hand in the Mechanical Instrument Workshop so that they

could be flat and smooth, any scratches providing points for corona discharge which could cause unwanted breakdowns in the cell. The field has to be uniform over the entire length of the electrodes, hence their flatness. The edges of the electrodes were also rounded so as to avoid corona at the edges.

The electrodes were polished in a dust-free room using 3 μm diamond paste followed by 1 μm diamond suspension. This process took a considerable amount of time, but eventually the electrodes were found to be flat and scratch free. For a complete explanation of the polishing process refer to Sono's thesis.[1]

Having obtained a remarkably flat scratch-free surface the parallelity of the electrodes needed to the checked (a condition essential to obtaining a uniform electric field). The process involved placing fifteen glass-reinforced teflon rings (which do not distort easily under strain) at equal intervals to hold the electrodes in place. Macor blocks of uniform thickness were placed between the electrodes, which were then squeezed onto the blocks. Two springs were placed below each ring to allow for expansion and contraction during heating and cooling of the system. Thirty Macor blocks of dimensions 3.1 by 3 mm were cut using a diamond saw, and were polished to attain uniform thickness of (3.100 ± 0.002) mm. Nickel shim of thickness 0.2 mm was placed between the rings to squeeze the electrodes onto the Macor blocks.

The electrode spacing was measured at 44 evenly-spaced intervals and then Nickel shim was added at places where the readings deviated most from the 3.100 mm of the Macor spacers. Another set of readings was taken and the shimming process repeated until a final spacing of (3.107 ± 0.004) mm was attained.[1]

Presented below are the results for various sets of measurements of the electrode spacing, showing our attempts to attain uniformity. The "tleyane1" data-set shows the readings taken when the first nickel shim was added. The standard deviation is ±0.20% of the mean, which is relatively small. On adding further shim the "ann2" data-set was obtained which shows an even lower standard deviation of ±0.19%. The final two sets of readings

(independently taken by Ann Singh and Dr Couling) were obtained after adding the last of the shim: they agree very well with each other and have a standard deviation of ±0.13%. This procedure was completed during Miss Singh's Honours project, and is reproduced here since it is a crucial result required for the experimental analysis.

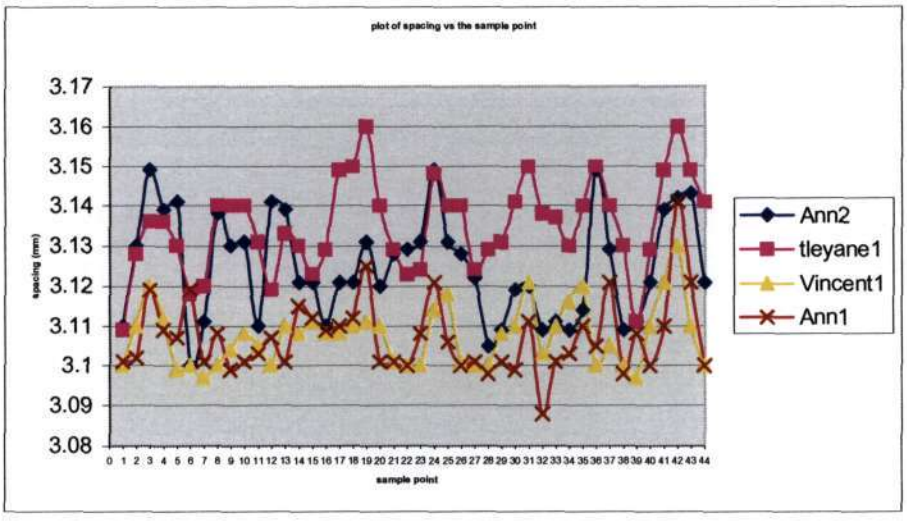

Fig 5: Results Of The Spacing Between The Electrodes

To increase the phase difference induced in the light beam by the Kerr effect, the cell length can be increased. This further reduces the relative significance of end effects due to non-uniformities in the field at the extremities. In general a 1 m path-length has been accepted as being practical. Our cell has a total path-length of 1.4688 m which further increases the sensitivity of the experiment.

3.3.1.4.3 Cleaning The Kerr Cell

Optical experiments generally require that components be absolutely clean. This is because dirt or unwanted particles could possibly interact with the light and produce undesirable results such as shifts in polarization state. For this reason the cell had to be properly cleaned. The Macor blocks were placed in warm soap solution in a sonic bath and then rinsed with trichloroethylene and a 50/50 water/ethanol solution to remove the

organic impurities. The other components of the cell were cleaned with soapy solution and rinsed with petroleum ether, acetone and trichloroethylene.

3.3.1.5 The Quarter-wave Plate

The $\lambda/4$-wave plate is used to convert the elliptically-polarized light emerging from the Kerr cell back to linearly polarized light so that the measurement of the induced phase difference is more direct and is not sensitive to stray retardation.

A primary disadvantage of the $\lambda/4$–plate plate is that the retardance is wavelength dependent, which means that each wavelength requires its own $\lambda/4$–plate. Another disadvantage is that the signal is proportional to 2ω (twice the applied frequency) so that the apparatus becomes more susceptible to mechanical disturbances; at the microradian level the variation of the analyzer angle will be a source of noise and drift during measurements. However these disadvantages can be investigated and improved on and the positive outcome of using a $\lambda/4$-plate outweighs its two disadvantages. Use of a $\lambda/4$-plate reduces the components on the optical bench and so reduces the percentage error in measurements. We have made use of a zero-order $\lambda/4$-plate with a retardance of precisely $\pi/2$ for a beam with wavelength 632.8 nm. A stepper motor was connected to the divided circle of the $\lambda/4$-plate to automatically offset it from its null position of 45^{o} for the fast axis.

3.3.1.6 The Faraday Cell

Figure 6: The Faraday Cell

The Faraday cell is shown above. It is made of a heavy-gauge copper-wire coil with 100 turns as well as a thinner copper-wire coil of 10 000 turns. Both coils surround a toluene-filled glass tube 400 mm long with a 12 mm internal diameter. A 2 cm polystyrene layer separates the tube from the coils so that the toluene is insulated from any heat generated in the cell. Pockels glass (reduces stray birefringence) windows are situated at either end of the glass tube, the seal being provided by a teflon-washer sandwich. The cell is mounted on rods and is supported by two magnetic bases

The Faraday cell forms part of the compensator. It is used to rotate the linearly-polarized light emerging from the $\lambda/4$-plate back to a null position. Recall that the $\lambda/4$-plate converts the elliptically-polarized light back to a linearly-polarized state, but offset by an angle $\theta = \frac{\delta}{2}$ where δ is the induced phase difference. Hence a calibrated Faraday cell can be employed to rotate this signal to the null position and so determine the induced phase difference.

3.3.1.7 Analyzing Prism

Figure 7: The analyzing system based on the design of Imrie[2]

The analyzer prism is a Glan-Taylor prism embedded in a cork support, and held within a rotating device that could facilitate very small, yet accurately known, rotations of the prism. A micrometer with a resolution of 0.001 inches was placed ~1 m from the axis of rotation of the analyzer, permitting fine rotations. The micrometer could be disengaged so that crude rotations could be made. The distance between the prism and the micrometer was found to be 1.0415 m, thereby enabling the calibration of the micrometer mechanism such that:

$$\theta = s \times 0.0243879 \qquad (68)$$

where θ represents the rotation of the prism in degrees and s the distance that the micrometer moves. This relationship is required when calibrating the Faraday cell.

3.3.2 The Gas Line

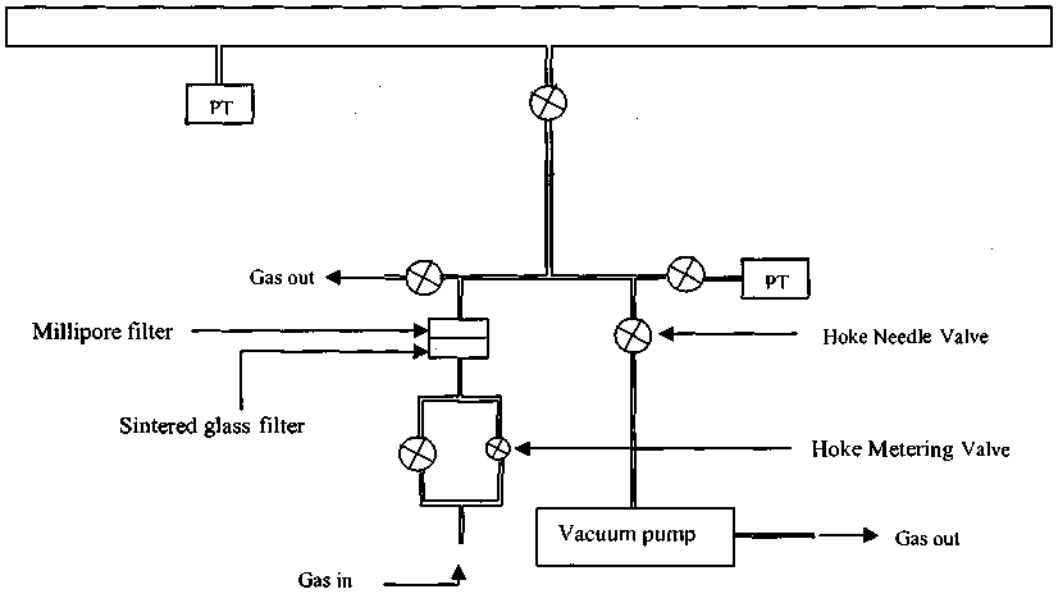

Key : PT = Pressure Transducer

Fig 8: The gas line used in the experiment

The gas line was constructed from $\frac{1}{4}$ – inch Hoke 316-stainless-steel tubing. A sintered-glass filter with porosity 15 to 40 micrometers is used to filter the gas before it reaches to the main section of the gas line. This process ensures that the gas that reaches the cell is free of dust particles. A 0.22 micrometer Millipore filter is used to further filter the gas of even smaller dust particles. A flexible stainless-steel hose connects the cell and the gas line so that they can be moved independently of each other: this facilitates alignment of the cell electrodes so that they lie horizontal. Here again stainless steel was used as the preferred material because of its durability and ability to withstand corrosive materials. Although dimethyl ether is not highly corrosive, the current system will be used to study a wide range of compounds, including some which are corrosive.

A system of inlet and outlet taps to and from the Kerr cell allowed for admitting and removing gas samples. The rate of gas flow was controlled by a fine-metering valve. The system was designed such that the oven did not need to be repeatedly opened: the cell tap had an extension reaching outside the oven (via a small hole) so that gas could be admitted or evacuated while maintaining the oven equilibrium temperature.

3.3.3 The Electronics

3.3.3.1 Waveform Snythesizer

A Phillips PM5190-LF synthesizer was used to obtain a sinusoidal signal of frequency 363 Hz and peak-to-peak voltage 1.41 V (500 mV rms). This signal was divided, one component being attenuated to 50 mV rms before being fed to the high-voltage power supply, while the other component was fed to the Faraday cell. The signal was also fed to the phase sensitive detector as a reference frequency. The Faraday cell was modulated at 2f for reasons that shall become apparent in the discussion on the method of measurement. Due to the very sensitive nature of the experiment it is possible for the mains frequency of 50 Hz or that of its harmonics to interfere with the signal being detected. To avoid such an occurrence 363 Hz was chosen as the reference frequency.

3.3.3.2 Detector

A suitable photodiode detector was used to measure the intensity of the emergent light. It was linked to the phase sensitive detector using a coaxial cable.

3.3.3.3 The Phase Sensitive Detector (PSD)

A Stanford Research Systems Model SR830 DSP Lock-In Amplifier was used as the PSD, to which the signal from the photodiode detector was fed. Both the reference signal produced by the waveform synthesizer and the photodiode signal are fed into the PSD. The PSD then extracts from the photodiode signal the component that oscillates at twice the frequency of the reference signal. A voltage, which is proportional to the intensity of the light that has been modulated at the chosen frequency, is displayed by the PSD. An HP 3478A digital multimeter connected to a Personal Computer via an HP 3421A data-acquisition unit reads the voltage, which is analysed and averaged by the computer.

3.3.3.4 The High-voltage Power Supply

The high-voltage power supply is used to generate an electric field in the cell by applying a voltage via a high-voltage connector to the one electrode while the other is grounded. The power supply/transformer is used to convert 1 V ac to 1 kV ac through a step-up transformer. It makes use of a step up, step down mechanism to monitor its driving signal.

This process involves stepping up the signal by a factor of 1000 using a primary transformer and then stepping it down by a factor of 1000 using a secondary transformer. In the process part of the signal is converted into a dc signal so that 1 V dc corresponds to a 1000 V rms ac signal using a precision rectifier. This allows one to relate the dc voltage output to the ac voltage applied to the cell. An ac voltage is applied because an oscillating

field is required for the effect to be detected by a PSD. The calibration of the high-voltage power supply is essential before commencing the experiment.

3.3.3.5 The Automated System

The errors in the experiment are minimized by having a computer program to control the experiment and analyze data. The driving program is written in HP BASIC requiring all the equipment to be HP (now Agilent) or HP compatible. This automation was made possible through an IEEE interface, which enables communication and interaction between the various pieces of equipment.

These components include the data-acquisition unit, the multimeter and the power supply. The location and function of each of these components shall become transparent in a block diagram (to follow shortly) but it is the data-acquisition unit which serves as the central liaison between the computer and the experiment. It is used to measure the temperature in the cell and oven, the phase sensitive detector output signal, the Faraday-cell signal current and the pressure-transducer voltage, each of which is crucial in determining the measurable property of the Kerr Effect.

The data are collected and processed by the HP BASIC program which also monitors the temperature and pressure changes in the experimental environment. It is an interactive program in that it controls the experiment via the data-acquisition unit. For example the temperature in the cell is controlled by actuating cooling or heating mechanisms using the data-acquisition unit's relays. In addition a stepper motor is controlled to rotate the $\lambda/4$-wave plate to its negative and positive offset positions.

The details of the program are not referred to here as the original authors are Dr Couling and Mr Sono: a complete description of the program appears in Sono's thesis[1], However modifications were made during the year, including changes to decrease the time taken in heating or cooling the system and in analyzing the data produced. The program was found to work exceptionally well for all temperatures and pressures.

Having described the components of the system, it now becomes necessary to look at the method of measurement employed in determining the molar Kerr constant. We begin with a look at the methods used in taking measurements. A Mueller-calculus analysis of the optical cascade is found in Appendix A.

3.4 *METHOD OF MEASUREMENT*

The Kerr cell contains a liquid or gaseous substance between two parallel-plate electrodes. A linearly-polarized light beam is passed through the sample with the plane of polarization typically at 45° to the applied electric field. Initially the components of the oscillating electric field of the light wave parallel and perpendicular to the applied static field are equal in magnitude. However, as the beam travels through the birefringent medium, a phase difference is induced.

A compensator can be used to determine the induced phase difference in the emergent beam. The compensator may be in the form of another liquid Kerr cell or a Faraday cell and a quarter-wave plate. For the purposes of this investigation, a Farday cell and λ/4-plate were employed. The λ/4-plate converts the elliptically-polarized light which emerges from the Kerr cell back into linearly polarized light, which is offset from the initial 45° by half the induced phase difference δ. This is then compensated by an equal-in-magnitude but opposite-in-direction rotation of the plane of polarization induced by the applied magnetic field in the Faraday cell. By measuring the Faraday rotation required to bring the plane of polarization back to 45° the phase difference can be determined.

For a Faraday cell the induced rotation is defined as

$$\theta = VH_z\ell \tag{69}$$

where V is the Verdet constant of the medium of the Faraday cell and ℓ is its path-length. A toluene Faraday cell has been utilized in our experiment, the Verdet constant for toluene being V = 7.825 rad T^{-1} m^{-1} at 295.0 K. H_z is the magnetic field in the direction of propagation of the light beam. The coil current and the magnetic field are related as

$$H_z = \frac{\mu_0 N i}{L} \tag{70}$$

Where μ_0 is the permeability of free space, N is the number of turns in the coil, i is the dc current through the coil and L is the length of the coil. Comparison of these two equations above shows that the induced rotation of the plane of polarization is directly proportional to the coil current, therefore

$$\theta = K_F i \tag{71}$$

where $K_F = \mu_0 NV$ is known as the Faraday-cell calibration constant. The plane of polariation of the light emerging from the λ/4- plate is rotated back to the initial state by varying the Faraday-cell current, in a process known as nulling. Knowledge of the nulling current and the calibration constant K_F allows one to precisely determine the angle of rotation and from this the induced phase difference.

The optical signal is measured by a photodiode, the output from which is fed into a phase sensitive detector (PSD). The PSD yields a reading that is proportional to the intensity of the light oscillating at a certain chosen frequency.

In the event of no voltage being applied across the electrodes, the the laser beam will be extinguished by the analyzer as it has been crossed with the polarizer (i.e. the transmission axis is set at -45°), so that a minimum intensity will reach the photodiode. However, when an electric field is applied to a gas sample, the phase sensitive detector will show a reading. The Faraday-cell current (and hence rotation) needed to null the signal emerging from the cell can be determined by varying the current in the Faraday

cell until a minimum is recorded by the PSD. We shall now discuss this procedure in detail.

It has been determined[2] that by offsetting the fast axis of the λ/4-plate from 45° by a small rotation $-\varepsilon_1$ and varying the Faraday-cell current, one can obtain a straight line plot of the PSD output as a function of the current. Offsetting the λ/4-plate in turn by $+\varepsilon_2$, one obtains a second line with a slope opposite in sign to the first line. These two lines intersect at $\theta_{null} = \frac{\delta}{2}$, hence yielding an accurate reading for the phase difference that is proportional to the square of the applied electric field. Invoking equation (71), where K_F is the Faraday-cell calibration constant and i the current at which the two lines intersect, the precise angle of rotation can be obtained, yielding the phase difference. It is crucial that the signals which drive the Kerr and Faraday cells be exactly in anti-phase so that the rotation of the plane of polarization of the light by the Faraday cell will be to the null position.

The field due to the voltage V which is applied to the electrodes is

$$E_0 = \frac{V_0}{d} \tag{72}$$

where for an alternating voltage

$$V = V_0 \cos \omega t \ . \tag{73}$$

Here V_0 is the amplitude of the alternating voltage, ω the corresponding frequency and t the time. We have

$$E^2 = \frac{V_0^2 \cos^2 \omega t}{d^2} = \frac{V_0^2}{d^2}\left(\frac{1+\cos 2\omega t}{2}\right). \tag{74}$$

From equation (63) it is clear that δ oscillates with twice the frequency of the driving voltage applied to the Kerr electrodes. From this it clear that the Faraday cell must be supplied with an ac signal of 2ω, and that the PSD should lock in to the signal oscillating at this frequency.

Once the phase difference is experimentally measured and the molar Kerr constant determined a graph of ${}_mK_0$ versus V_m^{-1} for each experimental temperature can be plotted so that first and second Kerr virial coefficients, A_K and B_K, can be deduced from the intercept and the slope of the graph respectively, using the relation[8]

$$ {}_mK_0 = A_K + \left[B_K + A_K\left(2A_\varepsilon + \tfrac{1}{2}A_R\right)\right]V_m^{-1} + \vartheta\left(V_m^{-1}\right) \qquad (75) $$

where A_ε and A_R are the low-density molar dielectric polarization and molar refraction respectively. They are

$$ A_\varepsilon = \frac{N_A}{3\varepsilon_0}\left\{a_0 + \frac{\mu_0^2}{3kT}\right\} $$
$$ A_R = \frac{N_A\alpha_0}{3\varepsilon_0} \qquad (76) $$

where N_A is Avogadro's number, ε_0 is the permittivity of free space, and a_0 is the mean static polarizability, μ_0 the permanent dipole moment and α_0 the mean dynamic polarizability of the molecule.

The experimental setup can now be understood with greater ease as the theoretical basis of the experiment has been expounded. Presented below is a block representation of the experiment:

3.5 *AN OVERVIEW OF THE EXPERIMENTAL SET UP IN BLOCK FORM*

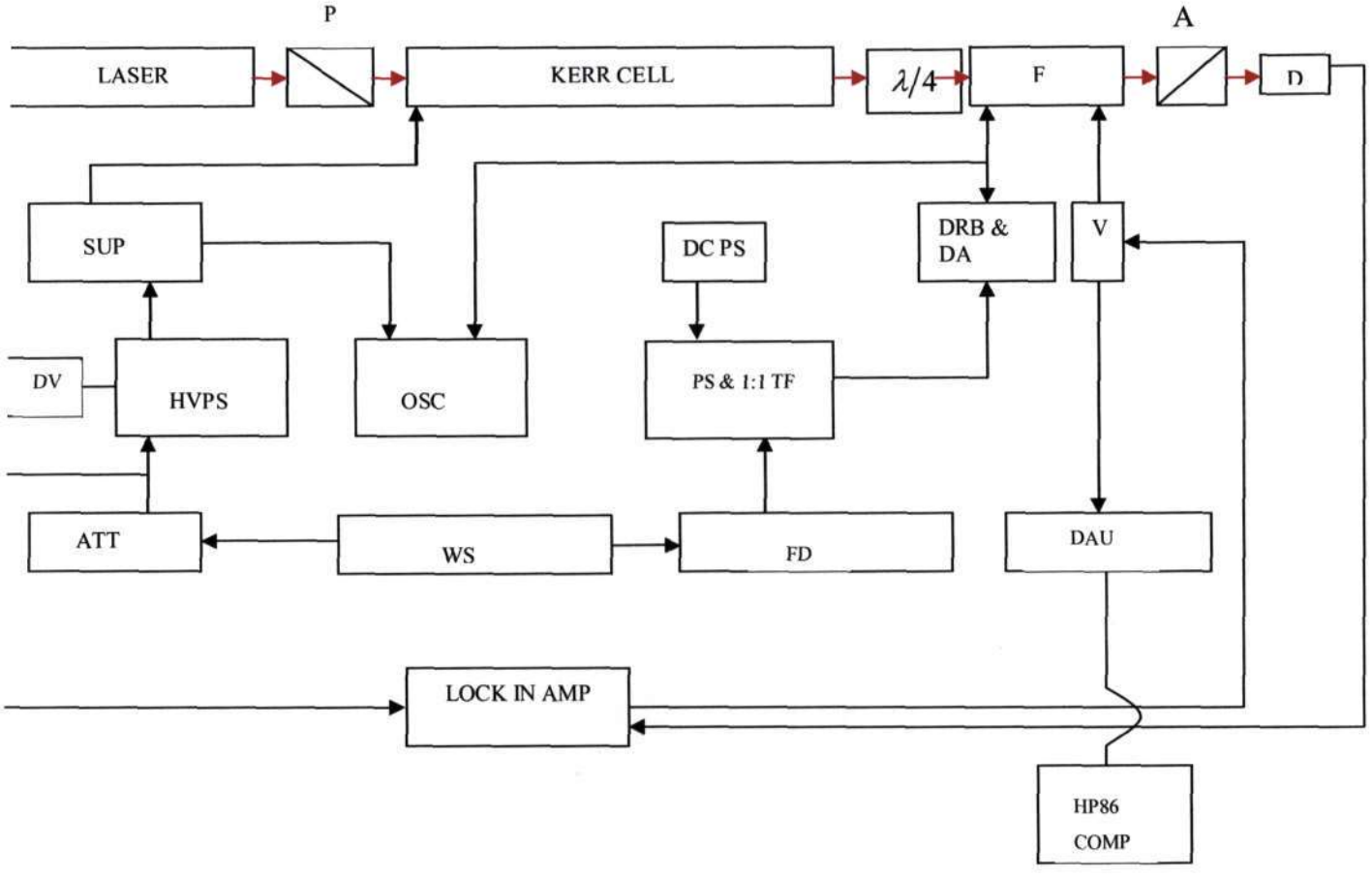

FIG KEY
P = POLARIZER, $\lambda/4$ = QUARTER-WAVE PLATE, FC = FARDAY CELL, A = ANALYZER, D = DETECTOR, SUP = STEP UP TRANSFORMER, DV = DIGITAL VOLTMETER, HVPS = HIGH VOLTAGE POWER SUPPLY, ATT = ATTENUATOR, WS = WAVEFORM SYNTHESISER, OSC = OSCILLOSCOPE, DC PS = DC POWER SUPPLY, PS & 1:1 TF = PHASE SHIFTER AND 1:1 TRANSFORMER, FD = FREQUENCY DOUBLER, DRB & DA = DECADE RESISTANCE BOX AND DIGITAL AMMETER, V = VOLTMETER, DAU = DATA-ACQUISITION UNIT, LOCK IN AMP = LOCK IN

The experimental assembly has already been discussed in great detail. However, the schematic representation in the diagram above ties all the pieces together so what follows is a brief summary of the diagram.

Application of a modulated voltage to the Kerr electrodes subjects the medium to an applied electric field, introducing birefringence in the medium. A linearly-polarized laser beam passes through the polarizer (transmission axis at 45°) and emerges from the cell elliptically polarized with an induced phase difference δ due to the birefringent behaviour of the medium. δ is the quantity that needs to be measured as precisely as possible. The elliptically-polarized wave then passes through the $\lambda/4$-plate, causing it to become linearly polarized but offset from its initial axis of polarization (i.e. +45°) due to the induced phase difference. The calibrated Faraday cell is used to rotate the plane of polarization of the light emergent from the $\lambda/4$-plate back to null (i.e. +45°) so that the detector will record a zero reading. The light that passes through the analyzer falls onto the photodiode detector, and the phase-sensitive detector filters out that portion of the signal oscillating at twice the reference signal. The PSD output is sent to the data-acquisition unit and on to the computer where the results are recorded and analyzed.

The part of the synthesized sinusoidal voltage that passes to the Faraday compensator needs to have its frequency doubled because the signal emerging from the Kerr cell oscillates at twice the frequency of the applied voltage. Once its frequency has been doubled the signal can be sent through to the Faraday cell via a phase shifter which ensures that the signal from the Kerr cell and that going through to the Faraday cell are in anti-phase to each other. The attenuator is required to reduce the synthesized voltage to acceptable limits for the high-voltage controller.

This apparatus was inherited from a previous M Sc student, Mr T J Sono, and credit is due to him for the efficient arrangement and operation of the apparatus. Mr Sono has also written an HP BASIC program to automate the experiment and gather data even when unattended. The program has inbuilt checks and balances so that the experiment will shut down in the eventuality of something having gone wrong. This is an important aspect of the code since it allows compliance with safety requirements, and prevents unwanted damage to the cell or the laboratory should there be a mains failure or a power surge. Another safety measure is that if the temperature of the cell exceeds a pre-desired limit, a

thermal fuse connected in *series* with the oven's heating elements fails, and prevents overheating. These features allow the experiment to run overnight without possibility of catastrophic consequences.

The program also controls the laboratory ambient temperature (via relays to the airconditioner and a fan heater). Once the cell temperature has stabilized, and the cell pressure has equilibrated, measurements can commence. The process of taking measurements at different offsets of the $\lambda/4$-plate, and determining the induced phase difference from these data, followed by calculation of the molar Kerr constant, is all achieved by the computer program.

The tasks that need to be performed manually are the calibrations of the high voltage, the pressure transducer and the Faraday cell. The phase of the Faraday cell needs to be manually set to be in anti-phase to that emerging from the Kerr cell (done before each experimental run). To set these two signals in anti-phase, one switches off the signal to the Faraday cell and feeds the signal from the Kerr cell (with high voltage applied) to the PSD. The phase of this signal is then set to be -180° on the PSD. The high voltage is then switched off, and the Faraday cell is powered up. The phase of the voltage supplying the Faraday cell is then shifted to be 0° on the PSD. The high voltage is reapplied to the Kerr cell and is now in anti-phase with that of the Faraday cell. Measurements can then be taken by the computer. Ten sets of readings are taken for each of the $\lambda/4$-plate offsets.

Having understood these general aspects of the experiment one can now go on to the actual procedures employed. Before commencing measurements various preparatory procedures need to be undertaken. These include the calibration of different pieces of equipment, performing leak tests, checking that the temperature control of the system is effective, aligning the electrodes to be horizontal and finding the true vertical of the polarizer. These aspects are now presented.

3.6 CALIBRATIONS

3.6.1 Finding The True Vertical Of The Polarizer

In our experiment the azimuth angle of the polarizer had to be set at 45° relative to vertical. This requires initially locating the vertical plane of the polarizer. The procedure to determine this true vertical is as follows.

Our laser is approximately linearly polarized in the vertical plane. The intensity of the laser beam emerging from the polarizer is measured using a power meter while the prism is rotated. The angular position for which the power meter indicates a maximum is an approximation of the true vertical.

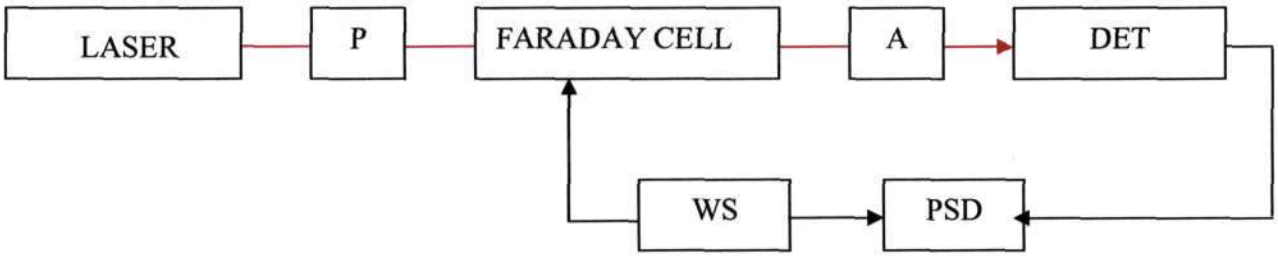

Figure 9: Setup to determine the true vertical of the polarizer

A sinusoidal voltage of frequency 363.0 Hz is fed to the PSD and the Faraday cell. The light emerging from the analyzer falls onto the photodiode detector, the signal from which is fed to the PSD. The micrometer of the analyzing system is rotated until a null is recorded by the PSD. The reading on the micrometer is recorded and the polarizer is then rotated through 180° around its vertical axis. The micrometer is again rotated until the PSD indicates a null, the reading on the micrometer once again being recorded. The difference between the two micrometer values is halved and converted to degrees to ascertain the value through which the polarizer needs to be rotated to attain the true vertical. The process is repeated until the required rotation is found to be less than the limits of resolution of the polarizer's divided circle. Our divided circle has a limit of

resolution on the vernier scale of 2′ of arc. Once true vertical was established the polarizer was set at +45° to the vertical and left there for the duration of the study.

3.6.2 Faraday Cell Calibration

The Faraday cell was calibrated by applying a dc voltage to the 100 turn coil, the dc current ranging from 0 to 100 mA. The induced rotations are easily measured using the PSD, which requires that a small ac voltage be supplied to the 10 000 turn coil to modulate the signal. The ac signal, provided by the waveform synthesizer, enables the PSD to lock on to the modulated signal reaching the photodiode. As the dc current was applied to the 100 turn coil the micrometer connected to the analyzer was rotated until an output of zero was recorded by the PSD, the micrometer reading being recorded for each dc current. This process was repeated for various currents and the data fitted to a straight line graph to find K_F, the Faraday cell constant, from the slope of the graph. Shown below is the Faraday-cell calibration circuit which achieves the process described above.

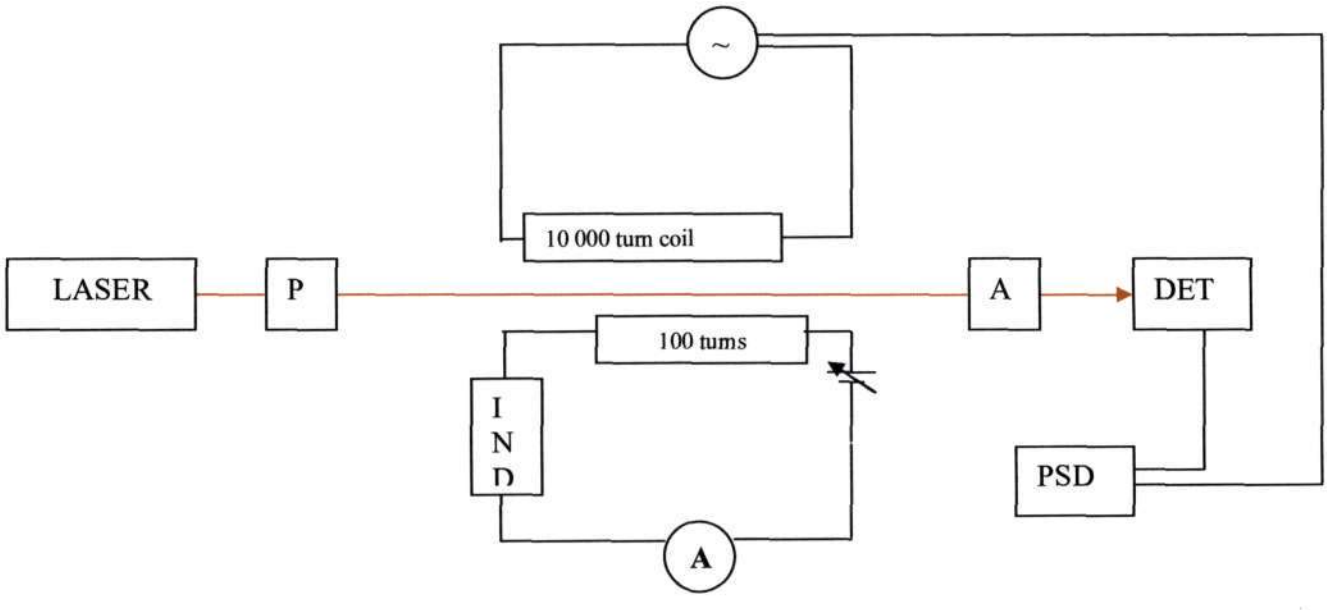

Figure 10: Faraday-cell Calibration Circuit

Table 1 records the micrometer readings (in inches) and the corresponding nulling currents (in mA). The graph that follows shows the plot of micrometer reading as a function of current.

Current (mA)	*Micrometer reading (inches)*		*Current (mA)*	*Micrometer reading (inches)*
1	0.2953		550	0.2224
50	0.2888		600	0.2157
100	0.282		649	0.2093
150	0.2754		700	0.2027
200	0.2689		750	0.1963
250	0.2621		800	0.1895
300	0.2553		850	0.1826
350	0.2487		899	0.1761
400	0.2421		949	0.1698
450	0.2357		999	0.1636
500	0.2291			

Table 1: Calibration Points To Determine The Faraday-cell Calibration Constant K_F

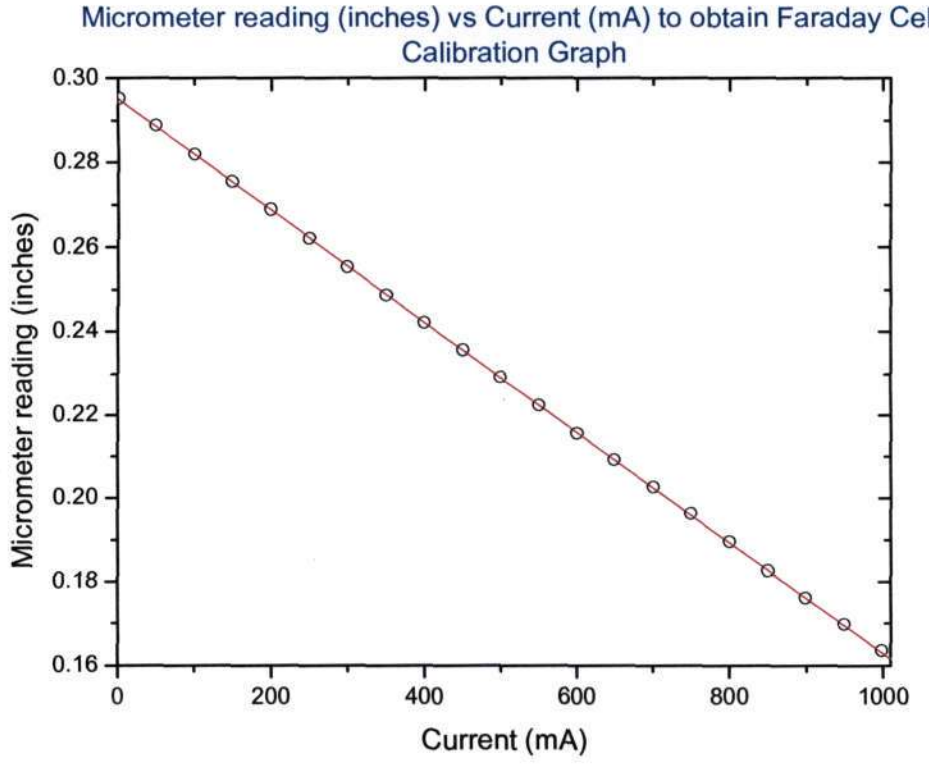

Fig 11: Graph of Faraday Calibration

Results obtained from graph

Parameter	*Value*	*Error*	
INTERCEPT	*0.2952017367*	*8.3019407462 E-5*	
SLOPE	*-1.3221267712 E-4*	*1.4209870724 E-7*	
R	*SD*	*N*	*P*
-0.9999890264	*1.9694924763E-4*	*21*	*<0.0001*

These results indicate a linear regression of 0.99992, which is an indication of a linear calibration. The slope of the graph yielded a value of $K_F = (1.3221 \pm 0.0014)$ H 10^{-4} inch mA^{-1}. Conversion to rad mA^{-1} is achieved via equation (68). Knowing the Faraday nulling current for a particular Kerr measurement, the HP BASIC program uses the Faraday-cell calibration constant to determine the induced phase difference from equation (71) and the relationship $\delta = 2\theta$. This measurement is central to obtaining the molar Kerr constant.

Since the Verdet constant of the toluene in the Faraday cell is temperature dependent it is essential that the laboratory is kept at constant temperature so that K_F does not vary during a run or between calibrations.

3.6.3 High-voltage Calibration

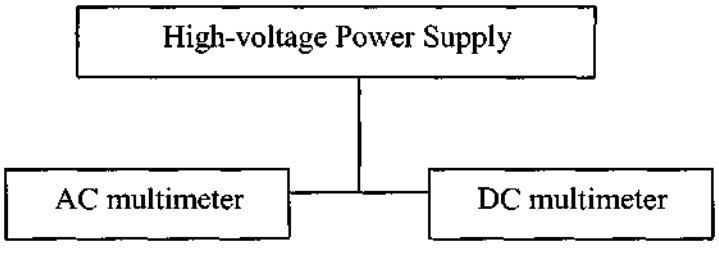

Fig 12: Voltage Calibration Circuit

A high-voltage calibration was performed by varying the output of the high-voltage power supply (up to the meter maximum of 1000 V rms) and reading off the corresponding voltage using a 6½-digit HP multimeter. The dc voltage from the precision

rectifier (used to convert part of the high-voltage transformer's feedback signal into a dc signal such that 1 V dc corresponds to 1000 V rms) was measured using a 5½-digit Fluke multimeter. Once these values were recorded a graph was plotted of the ac versus dc voltages. Table 2 shows the dc and corresponding ac voltages recorded in a typical calibration run, and is followed by the calibration graph.

dc voltage (V)	*ac voltage (V)*		*dc voltage (V)*	*ac voltage (V)*
0.4036	399.72		0.7097	702.76
0.4509	446.59		0.8065	798.55
0.5047	499.85		0.8522	843.69
0.5504	545.11		0.9035	894.44
0.6019	596.1		0.9493	939.65
0.6471	640.8		1.0062	995.95

Table 2: Calibration Points For The High-voltage Calibration

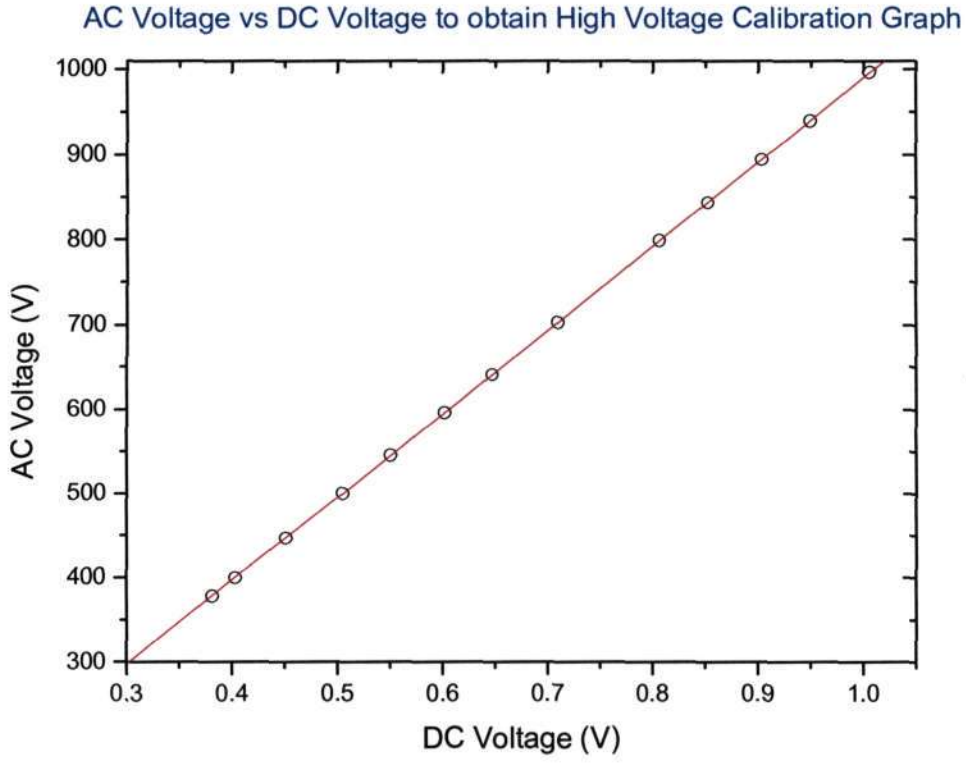

Figure 13: High-voltage Calibration Graph

Results obtained from graph

Parameter	*Value*	*Error*
INTERCEPT	0.4265171969	0.0866656394
SLOPE	989.4972771012	0.1229343584

R	SD	N	P
0.9999999151	0.0909706935	13	<0.0001

The experiment records the dc voltage off the precision rectifier and uses the straight-line equation to determine the ac voltage that had been applied to the electrode of the Kerr cell. Here the program uses $ac\_volts = dc\_volts \times 989.497 + 0.42652$. From the graph the correlation is seen to be close to 1 so that the calibration equation should be adequately linear when extrapolating to voltages higher than 1 kV (the cell typically runs at 3 kV). The excellent regression coefficient offers much assurance as to the linear (one-on-one) relationship of the voltages which is relevant when extrapolating for higher directly immeasurable voltages from low voltages. This high-voltage supply was re-calibrated each time it was worked on by the Electronics Workshop.

3.6.4 Pressure Calibration

As shown in *figure 14*, 10 V is used to power a Honeywell 200PSIA-model SA pressure transducer. Gas is then introduced into the system so that a Budenberg dead-weight pressure tester can be used to calibrate the transducer. When the gas passes through to the dead-weight system it causes the weight stage to be lifted. This is an indication that the outside pressure is higher than that of the dead-weight system. One thus needs to add weights to the stage to balance the pressure of the entire system. Once the weights are added the spindle is rotated, until the weights float and rotate freely. Having achieved a state of equilibrium the sum of the pressure equivalent of the applied weights (given in kPa) is recorded together with the corresponding transducer output voltage as read by a multimeter. Some gas is released from the system via a vacuum pump so that another pressure and voltage can be recorded, and the process repeated. A graph of dead-weight Pressure (kPa) versus transducer voltage (V) is then plotted. One thing to bear in mind

when performing the calibration is that the weight stage already has one non-removable pressure-equivalent weight of 100 kPa; hence in the calibrations the minimum pressure obtainable is 100 kPa. On plotting the graph a straight-line equation is obtained. The BASIC program uses this equation to calculate the true pressure of the Kerr-cell contents from the pressure-transducer output voltage. The graph that is shown below was obtained from the data recorded in table 3.

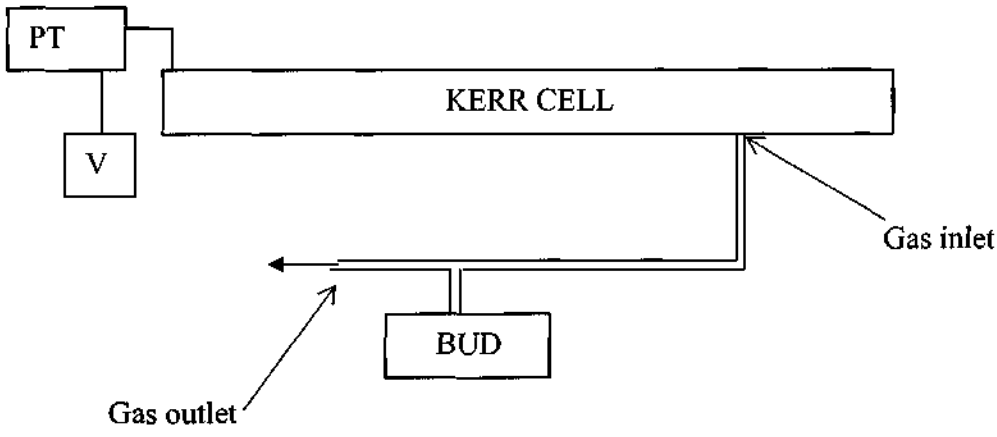

Figure 14: Pressure-gauge Calibration Circuit

Transducer voltage (V)	***Pressure (kPa)***		***Transducer voltage (V)***	***Pressure (kPa)***
0.280095	0		0.7097	702.76
0.614374	94.47223		2.798589	698.47223
0.991601	198.47223		3.145746	794.47223
1.341995	294.47223		3.509493	894.47223
1.716929	398.47223		3.869155	994.47223
2.059949	494.47223		4.244205	1098.47223
2.420103	594.47223		4.589889	1194.47223

Table 3: Calibration Points For The Pressure Transducer Calibration

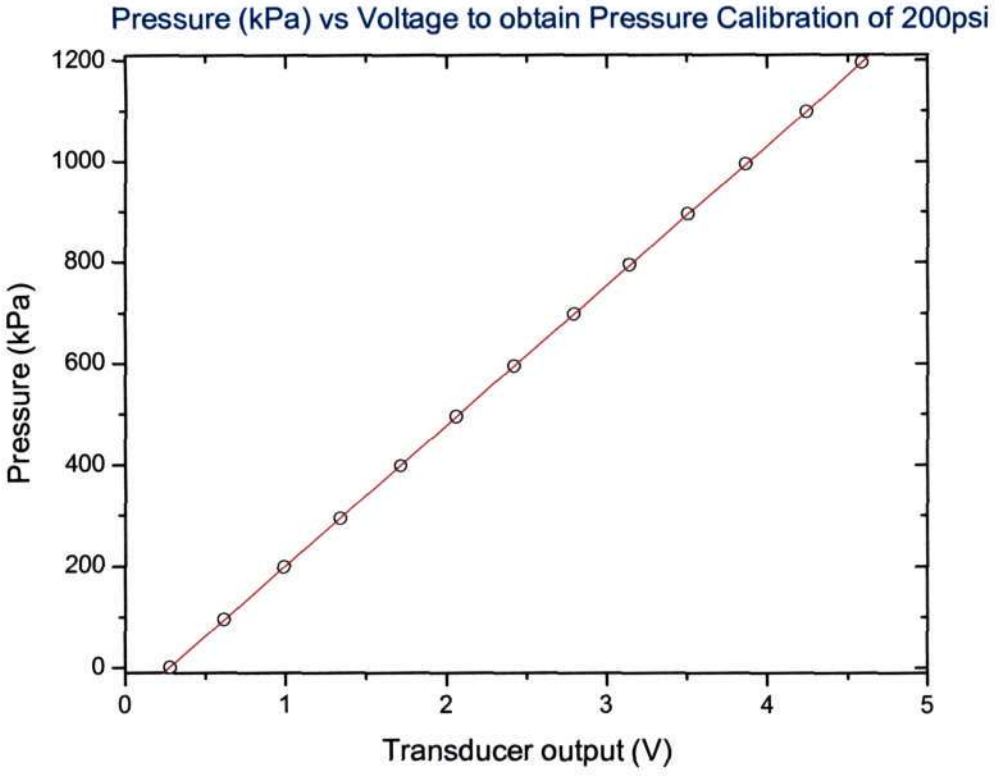

Figure 15: Pressure Transducer Calibration Graph

Results obtained from graph

Parameter	*Value*	*Error*
INTERCEPT	*-76.4751466323*	*0.3619272347*
SLOPE	*276.8605412062*	*0.1302453164*

R	*SD*	*N*	*P*
0.9999987828	*0.6335055033*	*13*	*<0.0001*

The equation used in determining the Pascal equivalent pressure for the system was thus $P = 276.860 \times V - 76.475$.

3.7 *TEMPERATURE CONTROL*

The Kerr effect is both pressure and temperature dependent. In this study, for each experimental temperature measurements have been made over a range of pressure as determined by the dimethyl ether (DME) saturation-vapour-pressure curve.[3] The 200PSIA pressure gauge is used to monitor the pressure in the cell, and simultaneously one needs to use a highly sensitive and accurate means of measuring the temperature in both the oven and the cell as the temperature needs to be constant along the entire cell and oven length.

To accurately measure the temperature at carefully chosen points along the length of the cell and oven, PT100 resistance temperature devices (RTDs) are placed at the different points. A four-wire resistance connection was used to eliminate the resistance of the 4m heat-shielded cables connecting the RTDs to the data-acquisition unit. Comprehensive information on the way in which the RTDs were connected as well as information on the oven design and how it facilitates temperature control is found in Sono's thesis.[1]

PT100 RTDs were chosen because of the following properties: they have a platinum resistance of 100 ohms at 0°, a temperature coefficient of $0.00385^{\circ}C^{-1}$ and a temperature tolerance of $\pm 0.44^{\circ}C$ within $\pm 200^{\circ}C$.

Three RTDs were placed in the oven and two in the cell. They were directly connected to the data-acquisition unit so that the control program could monitor the temperature registered by each RTD.

After careful analysis of the oven it was decided to use a circulating fan at each end of the cell, which would help the air circulate and hence maintain a uniform temperature throughout. The necessity for the fans will become evident in the results chapter where evidence is given to support their need.

High temperatures were achieved in the cell through the use of a 1.5 kW heating element. The coil of the element had been cut in two and was connected in series along the walls of the oven. A thermal fuse with a melting point of 250°C was connected in series with the coil as a precautionary measure in case of inadvertent overheating.

Temperatures below room temperature took a little longer to achieve, and were somewhat more painstaking. Liquid nitrogen was pumped into the oven to lower the temperature. The liquid nitrogen coolant was ejected from a pressurized dewar specifically designed for the experiment, the flow-rate being controlled by a solenoid valve. The dewar was pressurized by applying between 6 to 12 V across a heating coil situated inside the dewar. It was necessary to ensure that the dewar never ran dry since the heating coil could then burn out. A release valve on the dewar ensured that the internal pressure never exceeded safe limits. Figure 16 shows the apparatus used to inject liquid nitrogen into the oven.

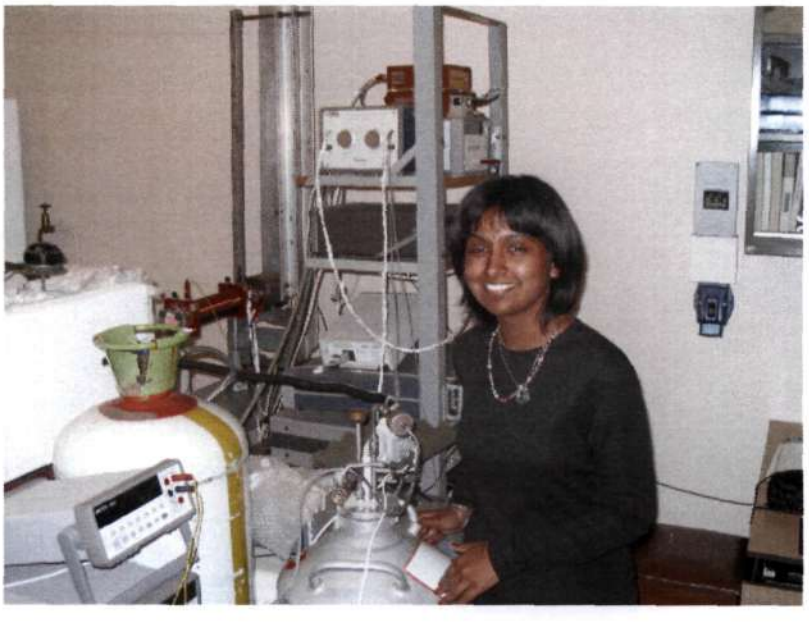

Figure 16: the cooling system

The heating and cooling of the oven is facilitated by a novel switch, which when off does not allow the heater element to be switched on or allow coolant to pass through the solenoid valve. This is a useful safety feature, preventing the cell from overheating or overcooling after a dip in the mains supply.

Cell temperatures below the dew point of ~4°C pose a problem in that at or below this threshold condensation begins to form on the windows of the cell. The solution to this problem was found in connecting a bank of resistors on the flanges surrounding the windows and powering them up so that the temperature at the cell windows would never be below the dew point.

Initially the temperature of the oven and cell was monitored over a day and night to watch for any unforeseen fluctuations. Since no spurious fluctuations were observed, it was believed that the apparatus was ready for use.

The PID algorithm written into the HP BASIC controller program was found to be an effective means of controlling the temperature of the experimental environment, and the uncertainty in temperature was found to be less than ±1°C across the spectrum of temperatures chosen for study. The laboratory itself had to be maintained at some chosen temperature, taken to be 22-23°C, since the Verdet[4] constant of the toluene in the Faraday rotator is temperature dependent.

To maintain a constant room temperature use was made of an air conditioner. The air conditioner output did fluctuate slightly in temperature depending upon the prevailing weather conditions, however drastic changes did not have to be made to its temperature settings. A fan heater was controlled by a relay linked to the data-acquisition unit so that the program could make fine adjustments to the room temperature to compensate for fluctuations caused by the air conditioner. Two desk fans were placed at opposite ends of the laboratory to mix the air and so maintain a uniform temperature throughout. In addition the laboratory windows were insulated with polystyrene sheets. This system sufficed to hold laboratory temperature to (22 ± 1) °C. The room temperature was

monitored using RTDs placed near the laser and the Faraday cell so that the temperature across the assembly could be tracked.

Before experiments could commence the cell had to be checked for leaks. Gas was introduced to the system and allowed to equilibriate for some time while the pressure was monitored and written to a file. The data were plotted to ascertain typical equilibration times. One of the plots is shown below.

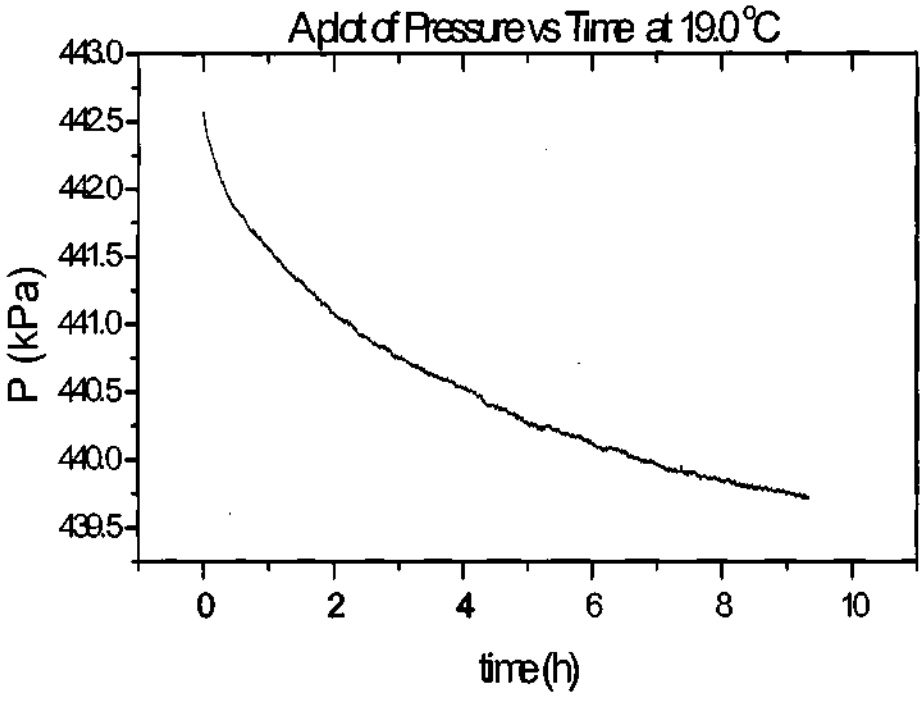

Figure 17: Pressure-monitoring graph

In the graph above, the pressure appears to be taking a long time to stabilize, a plateau not being reached after nine hours. One suspects that a small leak could be in existence. If a leak was suspected the Spectron 300E helium leak detector was used to locate the actual leak points in the apparatus. This was done by first introducing helium to the cell and then placing the sniffer of the leak detector at possible leak sources, and watching the

indicated concentration of helium at that point. Any leaks detected in this manner were sealed up appropriately. During the course of these studies two of the gas-inlet taps had to be replaced due to wear and tear.

Once the leak detector had found all leaks, the pressure was once again monitored over a period of a few hours just to be certain that the system was ready for use. Thereafter measurements commenced.

3.9 REFERENCES

1. T. J. Sono, M Sc thesis, University of Natal, 2003
2. D. A. Imrie, Ph D thesis, University of Natal, 1993
3. W. Braker and A. L. Mossman, *Matheson Gas Data Book*, East Rutherford, New Jersey, 1971, pg 224
4. L. D. Barron, *Molecular Light Scattering and Optical Activity*, Cambridge University Press, Cambridge, 1982

CHAPTER 4: RESULTS AND DISCUSSION

All honest efforts ought to be rewarded with great benefits; in experimental science this sometimes takes a little longer than ordinarily. The results reported here were achieved after a considerable amount of time and careful analysis of the system. Initially it had been envisaged that the project would include a study of the Kerr effect in the fluoromethane series of gases. This would have been attempted after repeating Sono's measurements on dimethyl ether to verify reproducibility of the experiment.[1] However, the initial measurements of dimethyl ether revealed small systematic differences from those of Sono. Fresh calibrations of the high-voltage supply, the pressure transducer and the Faraday cell were then systematically performed to check for consistency. Having achieved this, measurements were again taken and checked with our previous results. Our results were self-consistent: indeed, the lower-temperature results were re-checked after higher-temperature runs to make sure that there was no hysteresis in the system (arising, for example, from slight warping of the electrodes when cycled over 200°C). The systematic differences were found to arise when the oven's circulating fans were switched off. Our investigations of the system have been thorough but time-consuming, and so only dimethyl ether has been investigated here. We are, however, confident that our results for this species are reproducible and that the work can now be published with confidence. The Kerr apparatus can now be used to measure fresh molecular species with confidence.

4.1 SETTING UP A MEASUREMENT

The procedure followed before taking a measurement is now outlined. Initially the analyzer and polariser were checked to be crossed. Although there should not necessarily be a drift in the analyzer setting to obtain null, the highly-sensitive PSD nulling technique saw minute drifts in the null position, these being corrected for before each new measurement. This process involves removing the quarter-wave plate from the optical train and supplying the Faraday cell with a small ripple current for the PSD to lock onto. The micrometer on the analyzing system was then rotated until a null was indicated by

the PSD. The quarter-wave plate was then carefully reintroduced to the system such that its face was at right angles to the incoming beam: even small angles of deviation from the normal saw unwanted alignment errors being introduced into the measured Kerr constants.

The high voltage could then be applied to the electrodes, the phase of the Kerr cell being set to 180° on the PSD. The frequency doubler and phase shifter were then switched on to apply ac current to the Faraday cell, this current being varied until the Kerr signal was nulled. An oscilloscope is used to monitor both the high voltage (suitably attenuated) and the Faraday-cell driving voltage.

Having achieved null, the high voltage was switched off and the phase of the Faraday cell signal set precisely to 0°. The high voltage was again switched on, the null being verified, after which the control program was initialized so that the experimental run could commence. The program allows a few minutes to elapse so that the system can stabilize, after which data-gathering commences.

4.3 RESULTS

The results presented here are consecutively from the lowest temperature of 280 K to the highest temperature of 393 K. Once presented the graphical treatment of the data is discussed and the extracted molecular properties are presented. All results are quoted for a wavelength of $\lambda = 632.8\,nm$.

V_m^{-1} (mol m^{-3})	$10^{27}\ {}_mK_o$ ($C^2m^5J^{-1}mol^{-1}$)	P (kPa)	T (K)
42.775	-12.6845	97.589	280.774
54.396	-12.53673	123.577	281.326
68.266	-12.48808	153.882	281.271
101.793	-12.14127	224.821	280.818
124.405	-11.91596	270.869	280.4625

Table 4: A table of the ${}_mK_0$ values obtained as a function of V_m^{-1} used to determine the first and second Kerr virial coefficients at (280.89 ± 0.43) K

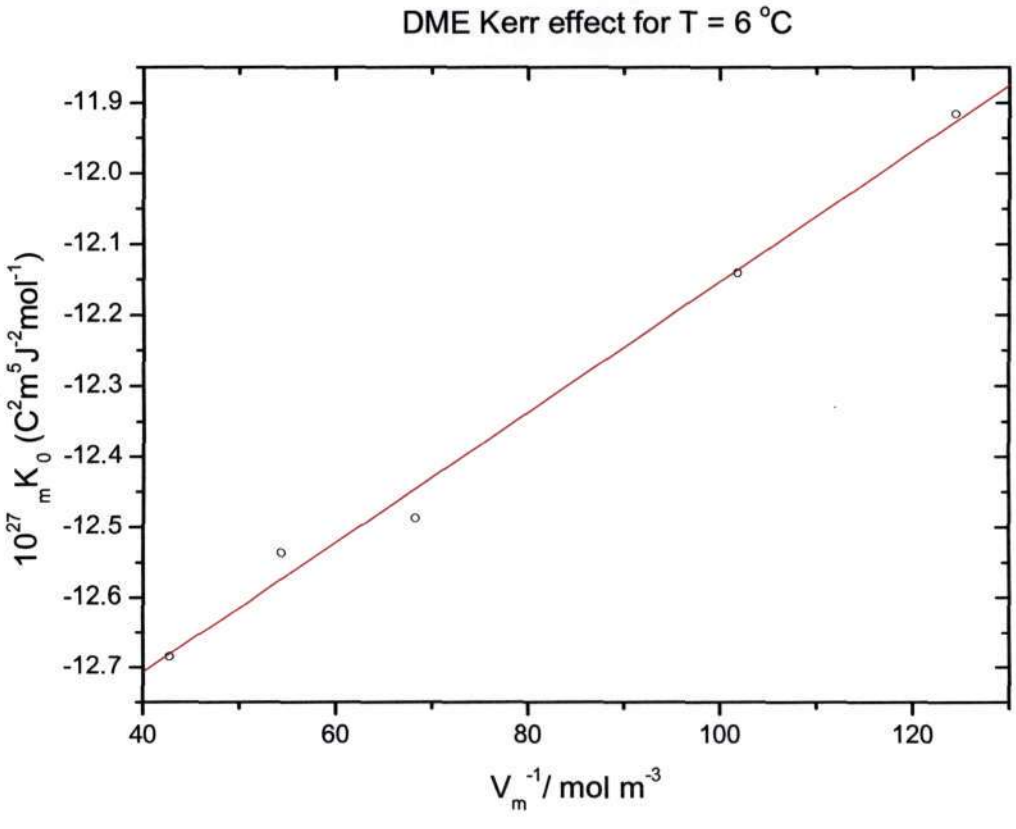

Figure 18: A graph of ${}_mK_0$ vs V_m^{-1} to determine A_K and B_K at (280.89 ± 0.43) K

Parameter	*Value*	*Error*
A_K	-13.111652671	0.035421463
B_K	0.009538638	3.940076115E-4

R	SD	N	P
0.998298129	0.024592611	4	0.001701871

V_m^{-1} (mol m^{-3})	$10^{27}\ {}_mK_o$ ($C^2m^5J^{-1}mol^{-1}$)	P (kPa)	T (K)
34.40878	-10.76388	867.97	307.859
69.56507	-10.50916	172.864	307.902
121.63227	-10.05624		
122.11971	-10.04841	296.495	307.872
149.59918	-9.86762	358.869	307.943
183.29032	-9.64026	432.935	307.891
216.61335	-9.36626	504.105	308.017
235.74446	-9.22227	543.521	307.91
237.01657	-9.21815	546.361	308.01

Table 5: A table of the ${}_mK_0$ values obtained as a function of V_m^{-1} used to determine the first and second Kerr virial coefficients at (307.938 ± 0.079) K

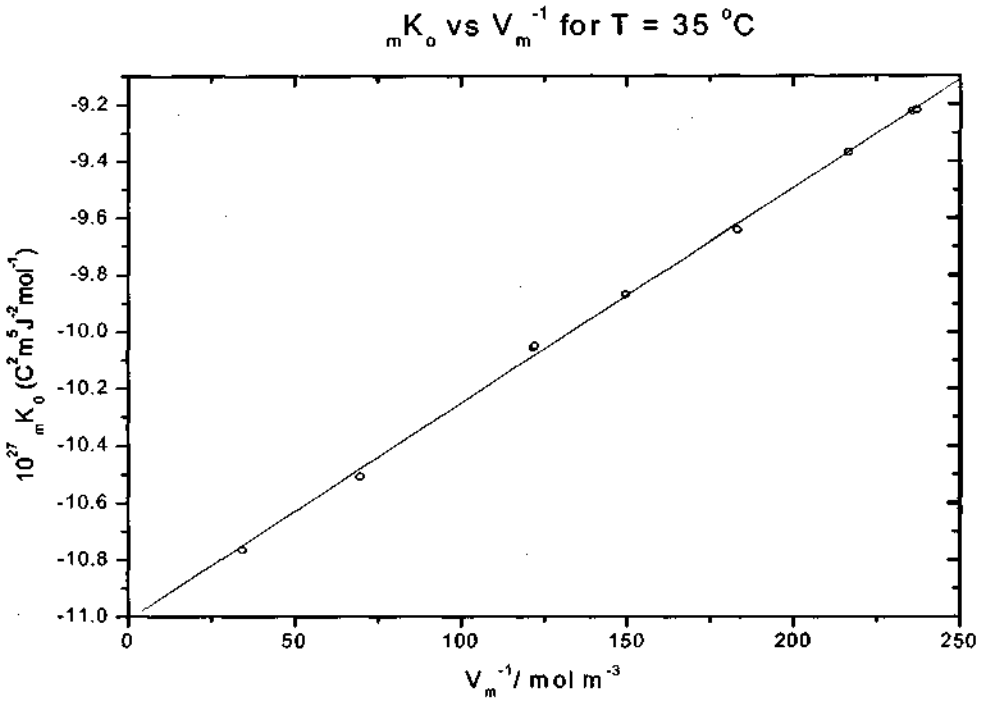

Figure 19: A graph of $_mK_0$ vs V_m^{-1} to determine A_K and B_K at (307.938 ± 0.079) K

Parameter	***Value***	***Error***
A_K	-11.01222183479348	0.01863167419981
B_K	0.00760425787211	0.00011170522712

R	SD	N	P
0.99924558608377	0.02284869963832	9	<0.0001

V_m^{-1} (mol m^{-3})	$10^{27}\ {}_mK_o$ ($C^2m^5J^{-1}mol^{-1}$)	P (kPa)	T (K)
40.90178	-9.09158	111.445	332.591
67.67014	-8.98741	182.459	332.373
86.49549	-8.84952	231.599	332.372
124.15188	-8.65968	327.731	332.322
164.03728	-8.45904	426.815	332.531
187.20476	-8.3854	482.497	332.532
217.08098	-8.21696	553.383	332.523
220.49307	-8.21375	561.165	332.436

Table 6: A table of the ${}_mK_0$ values obtained as a function of V_m^{-1} used to determine the first and second Kerr virial coefficients at (332.46 ± 0.15) K

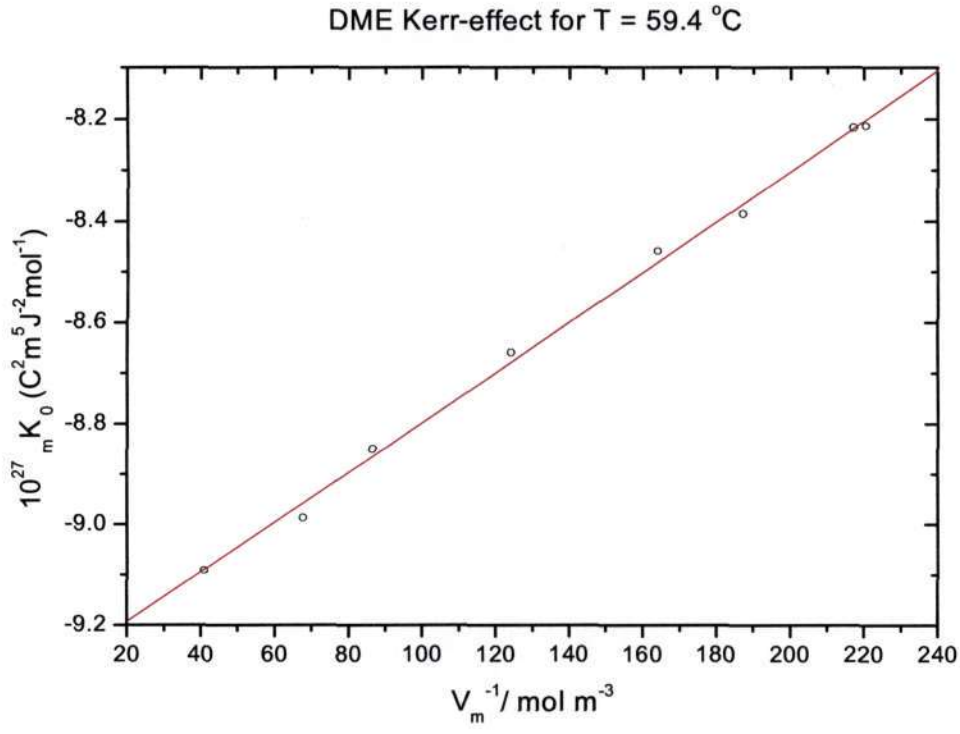

Fig 20: A graph of ${}_mK_0$ vs V_m^{-1} to determine A_K and B_K at (332.46 ± 0.15) K

Parameter	*Value*	*Error*
A_K	-9.29295737430928	0.01688745440649
B_K	0.00494598478483	0.00011050229024

R	SD	N	P
0.99850588480376	0.02018739907412	8	<0.0001

V_m^{-1} (mol m^{-3})	$10^{27}\ {}_mK_o$ ($C^2m^5J^{-1}mol^{-1}$)	P (kPa)	T (K)
45.435	-9.15577	293.723	334.437
84.282	-8.94514	227.355	334.467
109.93	-8.81217	124.409	334.732
145.226	-8.6521	382.985	334.456
231.836	-8.14783	591.719	334.55
261.182	-8.03455	659.177	334.611
284.506	-7.88481	711.385	334.573
396.61	-7.3219	947.970	334.643

Table 7: A table of the ${}_mK_0$ values obtained as a function of V_m^{-1} used to determine the first and second Kerr virial coefficients at (334.58 ± 0.15) K

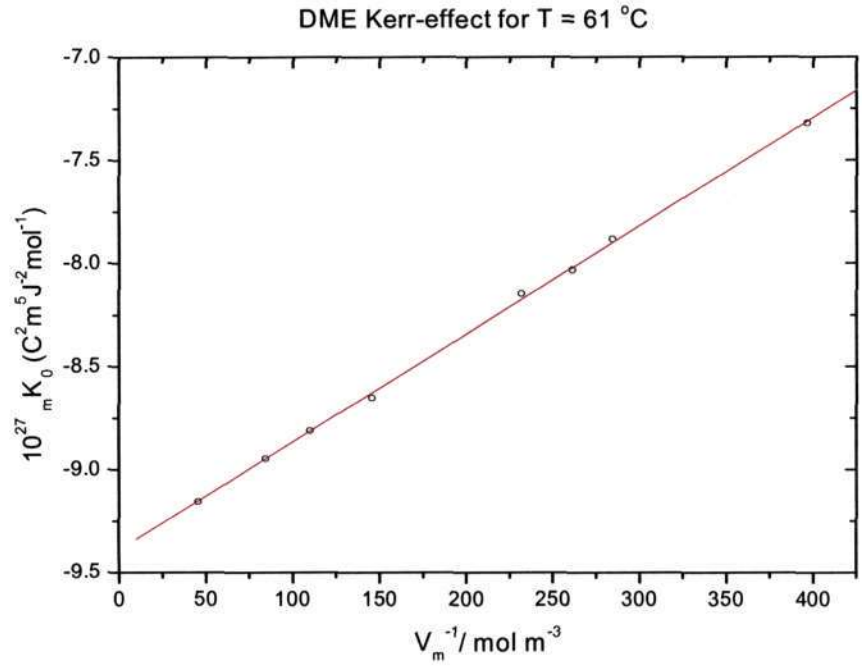

Fig 21: A graph of ${}_mK_0$ vs V_m^{-1} to determine A_K and B_K at (334.58 ± 0.15) K

Parameter	***Value***	***Error***
A_K	-9.39161	0.01232
B_K	0.00525	5.49135E-5

R	SD	N	P
0.99967	0.01726	8	<0.0001

V_m^{-1} (mol m^{-3})	$10^{27}\ {}_mK_o$ ($C^2m^5J^{-1}mol^{-1}$)	P (kPa)	T (K)
30.43	-7.95825	90.572	361.617
79.499	-7.76287	232.800	361.694
117.837	-7.56669	340.609	361.724
150.589	-7.40676	430.249	361.617
189.238	-7.24894	533.398	361.609
219.575	-7.13238	611.972	361.421
237.337	-7.09881	657.152	361.346
303.901	-6.84415	821.500	361.396
365.064	-6.55991	963.589	361.001
435.719	-6.25205	1 121.541	361.623

Table 8: A table of the ${}_mK_0$ values obtained as a function of V_m^{-1} used to determine the first and second Kerr virial coefficients at (361.36 ± 0.36) K

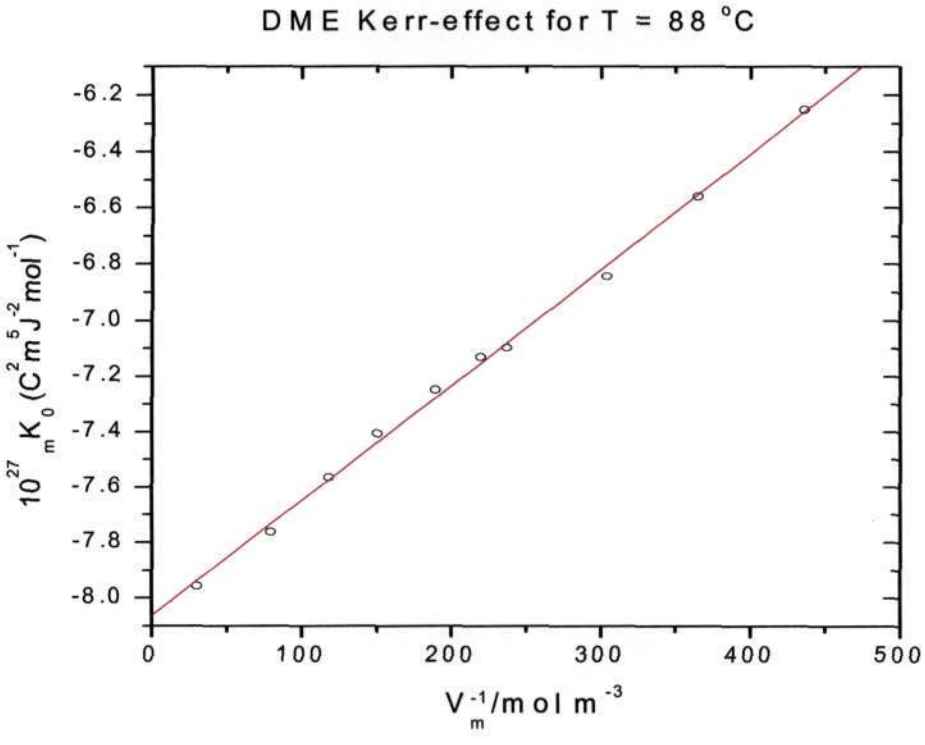

Fig 22: A graph of ${}_mK_0$ vs V_m^{-1} to determine A_K and B_K at (361.36 ± 0.36) K

Parameter	*Value*	*Error*
A_K	-8.06545	0.01726
B_K	0.00414	7.04941E-5

R	SD	N	P
0.99884	0.02696	10	<0.0001

V_m^{-1} (mol m^{-3})	$10^{27}\ {}_mK_o$ ($C^2m^5J^{-1}mol^{-1}$)	P (kPa)	T (K)
354.824	-6.50265	937.584	360.040
253.709	-6.87280	696.116	360.206
210.918	-7.01821	587.781	360.343
201.104	-7.06119	562.422	360.3104
173.158	-7.16018	489.011	360.277
131.399	-7.34009	376.508	360.2705
109.977	-7.37964	317.378	360.181
85.835	-7.55314	249.743	360.157
53.987	-7.62840	158.884	360.392

Table 9: A table of the ${}_mK_0$ values obtained as a function of V_m^{-1} used to determine the first and second Kerr virial coefficients at(360.19 ± 0.15) K

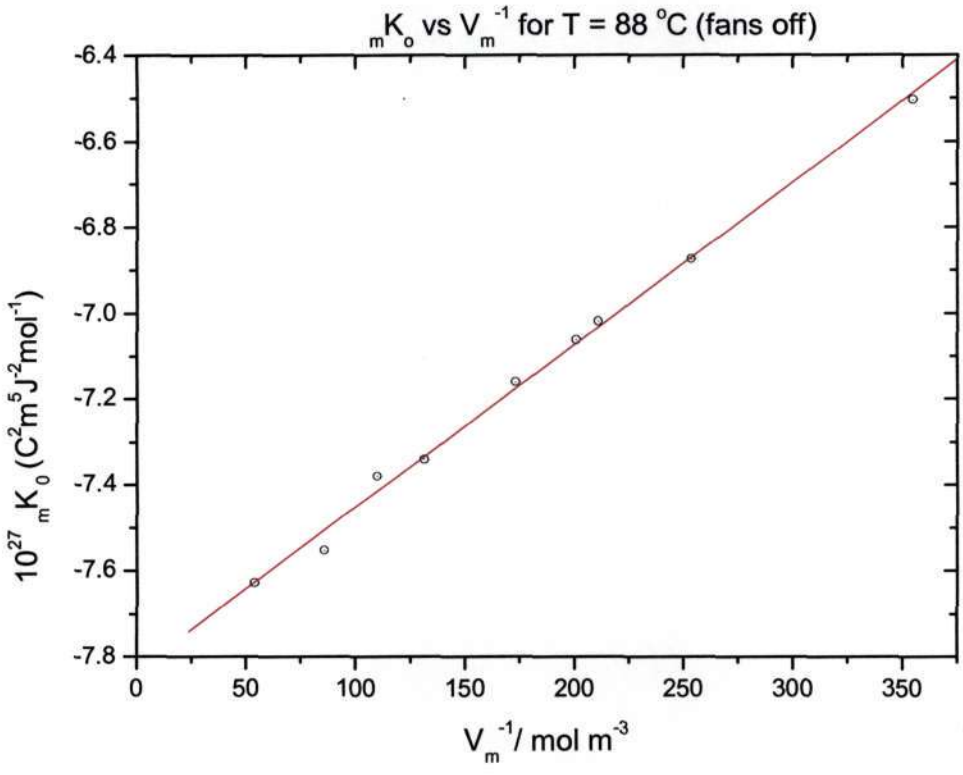

Fig 23: A graph of mKo vs V_m^{-1} to determine A_K and B_K at (360.19 ± 0.15) K

Parameter	***Value***	***Error***
A_K	-7.83163	0.01828
B_K	0.00379	9.3384E-5

R	SD	N	P
0.99788	0.02457	9	<0.0001

V_m^{-1} (mol m^{-3})	$10^{27}\ {}_mK_o$ ($C^2m^5J^{-1}mol^{-1}$)	P (kPa)	T (K)
272.064	-5.96056	804.713	393.814
229.092	-6.07659	689.062	393.811
223.192	-6.11839	672.768	393.7565
223.257	-6.12012	672.987	393.783
202.417	-6.20044	615.079	393.787
188.749	-6.23376	576.568	393.8042
134.554	-6.37437	419.503	393.803
80.437	-6.56306	255.770	393.681
63.827	-6.6182	204.232	393.770
100.553	-6.50937	317.420	393.7315
272.354	-5.94921	805.444	393.792
100.551	-6.52095	317.406	393.719

Table 10: A table of the ${}_mK_0$ values obtained as a function of V_m^{-1} used to determine the first and second Kerr virial coefficients at (393.748 ±0.067) K

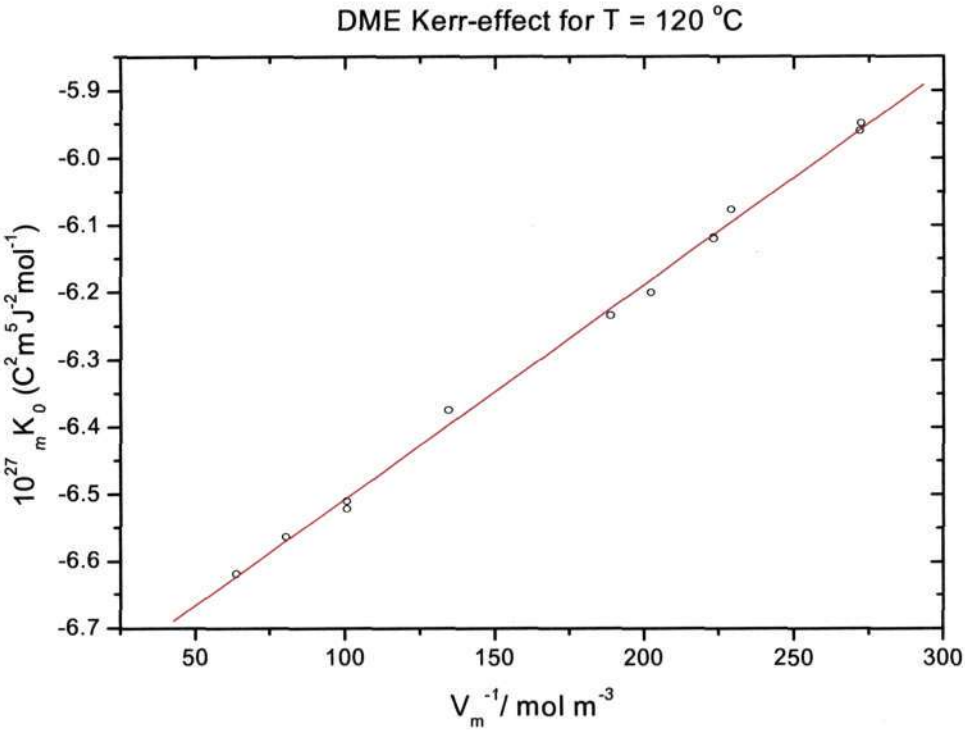

Fig 24: A graph of ${}_mK_0$ vs V_m^{-1} to determine A_K and B_K at (393.748 ± 0.067) K

Parameter	***Value***	***Error***
A_K	-6.82585	0.0102
B_K	0.00319	5.41357E-5

R	SD	N	P
0.99856	0.01342	12	<0.0001

4.3 GRAPHICAL ANALYSIS OF RESULTS

Having obtained the graphs shown above, the first and second virial coefficients can be extracted from the intercept and slope of each graph respectively. Recall equation (75):

$$_mK_0 = A_K + \left[B_K + A_K\left(2A_\varepsilon + \tfrac{1}{2}A_R\right)\right]V_m^{-1} + \vartheta\left(V_M^{-1}\right).$$

Initially the A_K values, extracted from the intercepts, are used to obtain the polarizability and hyperpolarizabilities of the molecule. From chapter 2, it is known that A_K can be used in two different ways to extract these molecular properties. Both methods are now discussed, together with the information yielded by each treatment.

4.3.1 Method A: Linear Treatment of A_K

From Chapter 2 we have:

$$\left[A_K - \frac{N_A}{81\varepsilon_0}\gamma^K\right]T = \frac{N_A}{81\varepsilon_0}\frac{1}{k_B}\left[\tfrac{2}{3}\mu\beta^K + \tfrac{1}{5}\Delta\alpha\Delta a\right] + \frac{N_A}{270\varepsilon_0}\frac{1}{k_B^2T}\mu^2(\alpha_{33} - \alpha)$$

Plotting the left-hand side as a function of the inverse absolute temperature allows one to deduce the polarizability anisotropy$(\alpha_{33} - \alpha)$ from the slope of the graph, and the first Kerr hyperpolarizability tensor β^K from the intercept. γ^K, the second Kerr hyperpolarizability tensor, has to be estimated from some other experiment. Two different values of γ were used in these calculations. The first has a value of $0.393\times10^{-60}\ C^4m^4J^{-3}$ as obtained from second-harmonic generation (SHG) experiments.[2] A precise new SHG γ of $0.737\times10^{-60}\ C^4m^4J^{-3}$ has been measured by Couling and Shelton during 2003 [unpublished data]. These analyses show that using the new corrected value for γ results in better agreement between the experimentally-determined molecular-property values and the theoretically calculated values. Mathematica notebooks were used to facilitate easy calculation of β^K and $(\alpha_{33} - \alpha)$, and

these appear in Appendix C. Having obtained $(\alpha_{33} - \alpha)$, the principal dynamic polarizability tensor components for the molecule were determined using the Mathematica notebook found in Appendix E.

T(K)	$10^{27} A_K$ ($C^2m^5J^{-2}mol^{-1}$)	$10^{24}\left[A_K - \frac{N_A}{81\varepsilon_0}\gamma^K\right]T$	$10^3\ T^{-1}$ (K^{-1})
280.894 ± 0.43	-13.11 ± 0.035	-3.77521	3.56158
307.938 ± 0.079	-11.012 ± 0.019	-3.49263	3.24616
334.58 ± 0.15	-9.392 ± 0.012	-3.25283	2.9901
361.36 ± 0.36	-8.065 ± 0.017	-3.03363	2.76536
393.748 ± 0.067	-6.826 ± 0.010	-2.81765	2.53936

Table 11: A table of the values used to obtain the graph in figure 25 for $\gamma = 0.393 \times 10^{-60}\ C^4m^4J^{-3}$

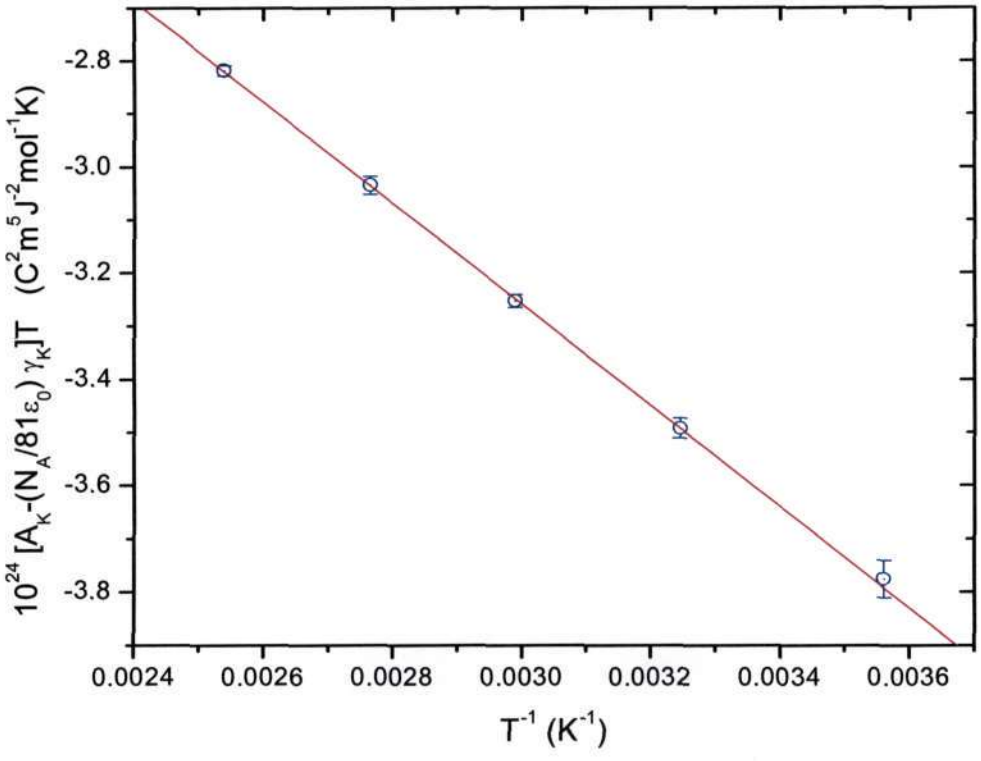

Figure 25 : Linear treatment of Kerr data to determine $(\alpha_{33} - \alpha)$ *and* β^K *from the slope and intercept for* $\gamma = 0.393 \times 10^{-60}\ C^4 m^4 J^{-3}$

Parameter	***Value***	***Error***
intercept	-0.4016080694	0.0641458426
slope	-952.0574265233	22.6407319756

R	SD	N	P
-0.9998844313	0.3691346136	5	<0.0001

	Our experimental values		Previous experimental values [3]	Calculated values [4]
	This work	Sono's thesis[1]		
$10^{40}\alpha_{11}(C^2m^2J^{-1})$	5.301 ± 0.016	5.311 ± 0.016	5.46 ± 0.14	5.28
$10^{40}\alpha_{22}(C^2m^2J^{-1})$	6.697 ± 0.016	6.698 ± 0.012	6.69 ± 0.17	6.68
$10^{40}\alpha_{33}(C^2m^2J^{-1})$	5.433 ± 0.005	5.421 ± 0.005	5.28 ± 0.13	5.47
$10^{40}(\alpha_{33}-\alpha)(C^2m^2J^{-1})$	-0.377 ± 0.005	-0.389 ± 0.005	-.53 ± 0.12	-0.34
$10^{50}(\beta^K)(C^3m^3J^{-2})$	-0.23 ± 0.02	-0.27 ± 0.04	0.3 ± 0.6	

Table 12: A table of the results obtained from the slope and intercept of the linear treatment of Kerr data for $\gamma = 0.393\times10^{-60}\ C^4m^4J^{-3}$

T(K)	A_K values ($C^2m^5J^{-2}mol^{-1}$)	$10^{24}\left[A_K - \frac{N_A}{81\varepsilon_0}\gamma^K\right]T$	$10^3\ T^{-1}$ (K^{-1})
280.89 ± 0.43	-13.11 ± 0.035	-3.85635	3.56158
307.938 ± 0.079	-11.012 ± 0.019	-3.58158	3.24616
334.58 ± 0.15	-9.392 ± 0.012	-3.34947	2.9901
361.36 ± 0.36	-8.065 ± 0.017	-3.13801	2.76536
393.748 ± 0.067	-6.826 ± 0.010	-2.93138	2.53936

Table 13: A table of the values used to obtain the graph in figure 26 for $\gamma = 0.737\times10^{-60}\ C^4m^4J^{-3}$ [5]

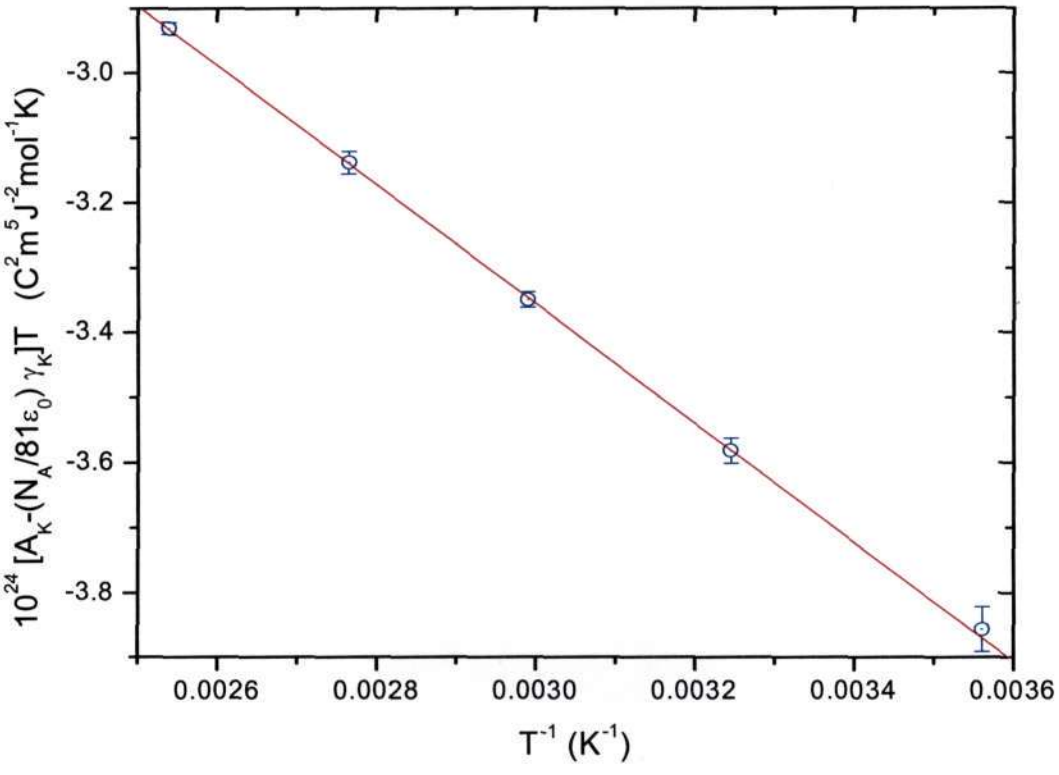

Fig 26 : Linear treatment of Kerr data to determine $(\alpha_{33} - \alpha)$ *and* β^K *from the slope and intercept for* $\gamma^K = 0.737 * 10^{-60}\ C^4 m^4 J^{-3}$

Parameter	***Value***	***Error***
intercept	-0.6028839025	0.0641458426
slope	-917.3580185453	22.6407319756

R	SD	N	P
-0.9999188244	0.2980862905	5	<0.0001

	Our experimental values		Previous experimental values [3]	Calculated values [4]
	This work	Sono's thesis[1]		
$10^{40}\alpha_{11}$ ($C^2m^2J^{-1}$)	5.289 ± 0.016	5.311 ± 0.016	5.46 ± 0.14	5.28
$10^{40}\alpha_{22}$ ($C^2m^2J^{-1}$)	6.695 ± 0.012	6.698 ± 0.012	6.69 ± 0.17	6.68
$10^{40}\alpha_{33}$ ($C^2m^2J^{-1}$)	5.446 ± 0.005	5.421 ± 0.005	5.28 ± 0.13	5.47
$10^{40}(\alpha_{33}-\alpha)$ ($C^2m^2J^{-1}$)	-0.364 ± 0.005	-0.389 ± 0.005	-.53 ± 0.12	-0.34
$10^{50}(\beta^K)$ ($C^3m^3J^{-2}$)	-0.34 ± 0.02	-0.27 ± 0.04	0.3 ± 0.6	

Table 14: A table of the results obtained using the slope and intercept of the linear treatment of Kerr data for $\gamma = 0.737\times10^{-60}\ C^4m^4J^{-3}$

Comparing the results of tables 12 and 14 it can be seen that the experimentally-determined values of the polarizability anisotropy and first Kerr hyperpolarizability tensors have a better agreement with their *ab initio* computed values when the recently-determined value of $\gamma = 0.737\times10^{-60}\ C^4m^4J^{-3}$ is used in the analysis rather than the previous erroneous value of $\gamma = 0.393\times10^{-60}\ C^4m^4J^{-3}$. It is also found that when using $\gamma = 0.393\times10^{-60}\ C^4m^4J^{-3}$ the values obtained in this work are in excellent agreement with those of Sono.[1] This is sound evidence that the current Kerr-effect apparatus is able to consistently reproduce experimental data.

The error bars attributed to the experimentally-deduced A_K values are the statistical uncertainties in the intercepts of the ${}_mK_0$ versus V_m^{-1} plots. The uncertainty at the lowest temperature of 280 K is comparatively large, this being attributable to the relative difficulty in achieving and maintaining lower temperatures. Although injecting liquid-nitrogen coolant is an effective means of lowering the oven temperature, these measurements take longer because the program pauses while the solenoid valve activates to inject coolant. The PID algorithm then takes time to re-establish the equilibrium temperature. Another complication at these lower temperatures is the much lower

saturation vapour pressure of the DME of ~300 kPa, the range of available sample densities becoming much reduced.

Our experimental values for the principal dynamic-polarizability tensor components (obtained using either the Couling and Shelton or the Ward and Miller SHG-value for γ) show a slightly-improved agreement with those calculated by Coonan *et al.*[4] as compared to the earlier values of Sono.[1] To determine the polarizability components the permanent dipole moment of $(CH_3)_2O$ is taken to lie along the 3-axis of the molecule-fixed system of axes (1,2,3), where the COC plane contains the 3- and 2-axis, the 1-axis being at right angles to the COC plane. This is the same arrangement used by Sono.[2] The consistency between Sono's results and our new results confirms that the current apparatus is an effective means of determining the Kerr effect in gases. The results serve to shed light on the relationship between the polarizability components, revealing α_{33} to be larger than α_{11}, which contradicts the earlier experimental findings of Bogaard *et al.*[3]

β^K has been determined to be $-(0.34 \pm 0.02)$ and $-(0.23 \pm 0.02) \times 10^{-50}\, C^3 m^3 J^{-2}$ for $\gamma = 0.737$ and $0.393 \times 10^{-60}\, C^4 m^4 J^{-3}$ respectively. The β^K extracted using the new value for γ compares exceptionally well with the new SHG value of $-0.393 \times 10^{-50}\, C^3 m^3 J^{-2}$ obtained by Couling and Shelton at $\lambda = 633 nm$. This is a considerable improvement on the earlier result of $(0.3 \pm 0.6) \times 10^{-50}\, C^3 m^3 J^{-2}$ obtained by Bogaard *et al.*[3]

4.3.2 Method B: Polynomial Treatment of A_K

As was seen in Chapter 2, the equation for A_K can be recast in a second way. This second treatment of A_K involves fitting a second-degree polynomial to the weighted A_K values and their corresponding inverse temperatures. The polynomial coefficients P, Q and R can then be used to calculate β^K, γ^K and $(\alpha_{33} - \alpha)$ using the equations below. This

method is prone to difficulties since the dominant R coefficient tends to swamp the much-tinier P and Q coefficients. Hence the anisotropy $(\alpha_{33}-\alpha)$ will be quite precisely determined while β^K and γ^K will be altogether imprecise. The notebook used to calculate these values appears in Appendix D.

$$A_K = \frac{N_A}{81\varepsilon_0}\left\{\gamma^K + \frac{1}{k_B T}\left[\tfrac{2}{3}\mu\beta^K + \tfrac{1}{5}\Delta\alpha\Delta a\right] + \frac{3}{10}\frac{1}{(k_B T)^2}\mu^2(\alpha_{33}-\alpha)\right\},$$

$$_m K = A_K = P + \frac{Q}{T} + \frac{R}{T^2}\cdots .$$

The data which are plotted are the weighted A_K values and their corresponding inverse temperatures, which can be seen in tables 11 and 13. The plot follows:

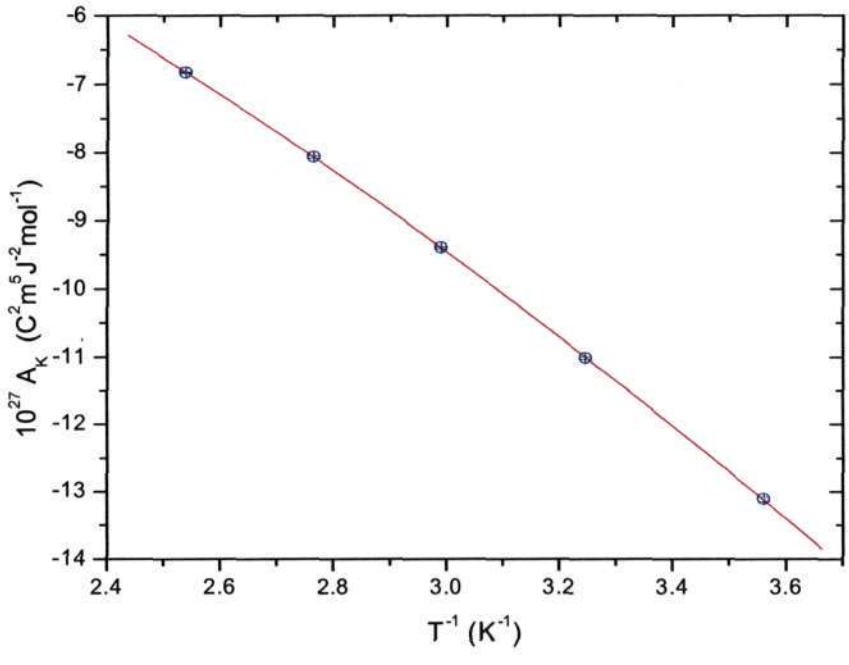

Figure 27: Polynomial fit to weighted A_K values to determine the coefficients P, Q and R used to calculate $(\alpha_{33}-\alpha)$, β^K and γ^K

Y = P + Q*X + R*X^2
Weight given by Data1_C error bars.

Parameter	*Value*	*Error*
P	1.4943427502	0.6285489046
Q	-1.2172531023	0.4345199516
R	-0.8107247663	0.0744858582

R-Square(COD)	SD	N	P
0.9999888679	0.6195345049	5	<0.0001

These values of P, Q and R were then used to calculate the molecular properties shown in table 15.

Parameter	New Values	Previous values[1]
$10^{29} P$	149.4 ± 62.8	9.8 ± 25
$10^{25} Q$	-12.2 ± 4.3	-3.10 ± 1.68
$10^{22} R$	-8.11 ± 0.7	-9.59 ± 0.28
$10^{40}(\alpha_{33} - \alpha)$	-0.32 ± 0.04	-0.38 ± 0.02
$10^{50} \beta^K$	0.82 ± 0.24	0.3 ± 0.1
$10^{60} \gamma^K$	0.18 ± 0.75	-0.12 ± 0.3

Table 15: A table of the results obtained from a polynomial treatment of the Kerr data

As could be expected from the above caveat, the results obtained from the polynomial treatment of the Kerr data differ greatly from those of previous studies. The value for $(\alpha_{33} - \alpha)$ is in reasonable agreement with that from Sono's analysis,[1] however the estimates of the first and second Kerr hyperpolarizability tensors are quite different. This polynomial analysis clearly has limited value, but is included for completeness.

To verify visual consistency of our A_K values with Sono's, they are plotted together below. The plot shows good agreement.

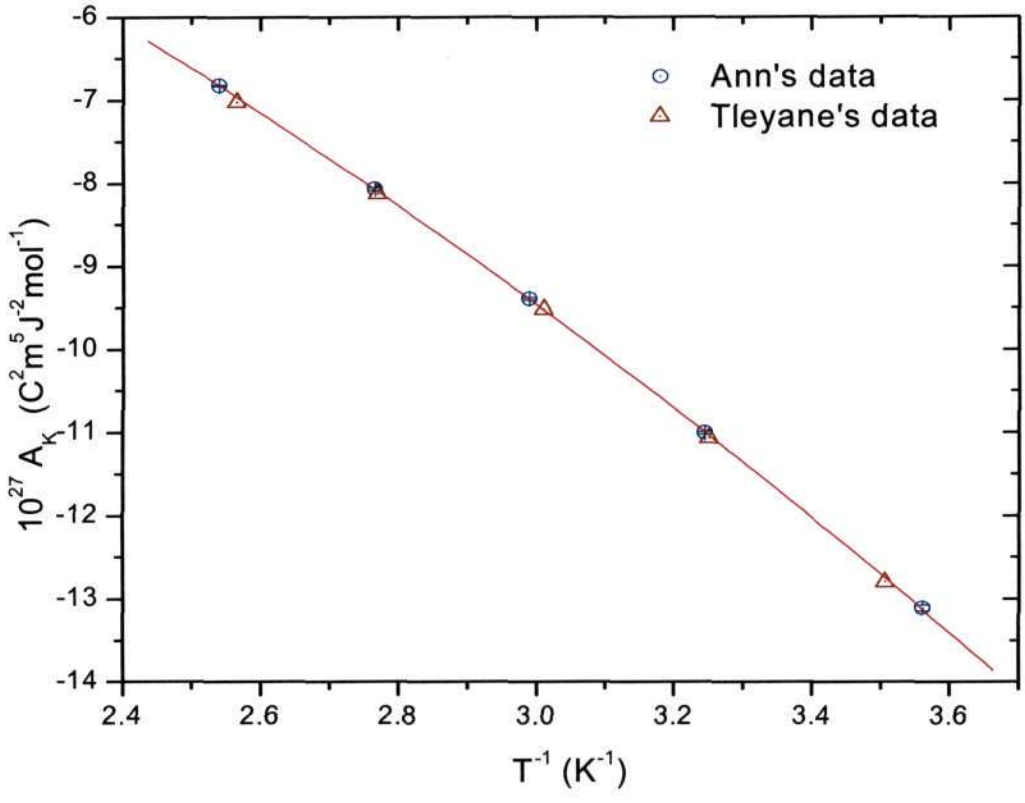

Fig 28 : Polynomial fit to weighted A_K values to show the relationship between the new results and previous findings[1]

The molecular properties of dimethyl ether used in our calculations are found in table 16.

Property	Value
$10^{30}\mu$ (C m)	4.37 ± 0.03 [6]
$10^{40}a$ ($C^2 m^2 J^{-1}$)	6.33 ± 0.33 [7,8]
$10^{40}\alpha$ ($C^2 m^2 J^{-1}$)	5.81 [3]
$10^2 \lvert\kappa^0\rvert$	7.71 [3]
$10^2 \lvert\kappa\rvert$	7.66 ± 0.1 [9]

Table 16: A table of properties used in analyzing the Kerr effect

Furthermore, $\Delta\alpha = 3a\kappa$ and $\Delta a = 3a\kappa^0$. Having completed this analysis we can now proceed to the second Kerr-effect virial coefficients.

4.3.3 Second Kerr-effect virial coefficients

The second Kerr-effect virial coefficients give an indication of the molecular pair-interaction contributions to the molar Kerr constant and are obtained from the slope of the of ${}_mK_0$ versus V_m^{-1} graphs.

T (K)	$10^{30}B_K$ calc ($C^2m^8J^{-2}mol^{-2}$)[10]	T (K)	$10^{30}B_K$ [1] ($C^2m^8J^{-2}mol^{-2}$)	T (K)	$10^{30}B_K$ this work ($C^2m^8J^{-2}mol^{-2}$)
230	35.444	285.109 ± 0.027	11.82 ± 1.03	280.89 ± 0.43	9.54 ± 0.39
270	16.371	307.494 ± 0.017	7.13 ± 0.19	307.938 ± 0.079	7.60 ± 0.11
305	9.740	332.02 ± 0.13	5.54 ± 0.15	334.58 ± 0.15	5.25 ± 0.05
370	4.644	361.049 ± 0.069	4.32 ± 0.08	361.36 ± 0.36	4.14 ± 0.07
420	2.768	389.740 ± 0.013	3.63 ± 0.10	393.748 ± 0.067	3.19 ± 0.05
470	2.131	452.3 ± 1.4	2.09 ± 0.14		
515	1.629				

Table 17: A table of theoretical and experimental B_K values used in obtaining fig 29

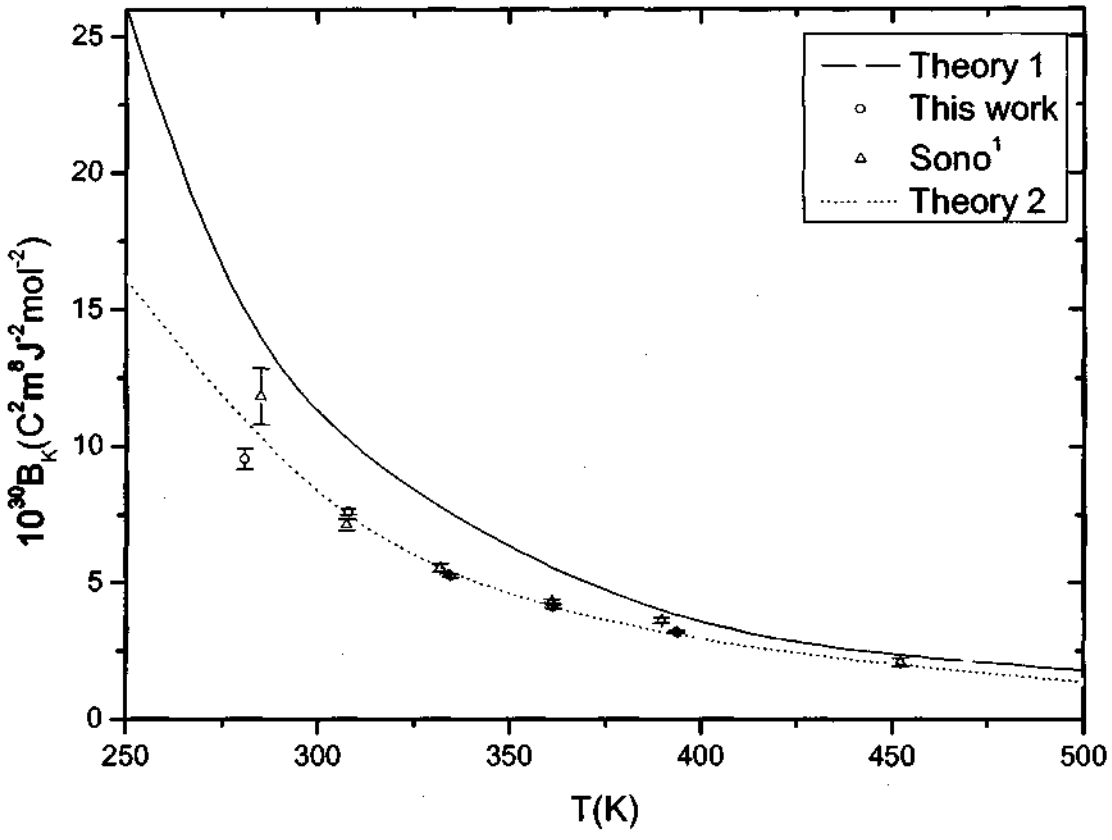

Figure 29: Temperature dependence of B_K for dimethyl ether

The new experimental B_K data are in excellent agreement with the calculated curve (for calculations performed using the second parameter set in Table 18 below, which gives the dotted curve above). The new data are also consistent with the data obtained by Sono,[1] save for the point at 280 K, where there is a sizeable deviation. We have taken care to verify the new results by repeating readings to ensure reproducibility. The new B_K values are also more precise than those of Sono since we have exploited a larger pressure range, and hence have obtained more precise slopes from our ${}_mK_0$ versus V_m^{-1} graphs.

The table below refers to the parameters used in calculating B_K values. The computational procedures are discussed extensively in Sono's thesis.[1]

Parameter	Value	Reference
R_0 (nm)	0.47 [0.48]**	10
ε/k (K)	290.0 [300.0]**	10
D_1	-0.04926 [-0.04443]**	10
D_2	0.29666 [0.29760]**	10
$10^{30}\,\mu_3$ (Cm)	-4.37 ± 0.03	6
$10^{40}\,\alpha_{11}$ ($C^2\,m^2\,J^{-1}$)	5.46	3 *
$10^{40}\,\alpha_{22}$ ($C^2\,m^2\,J^{-1}$)	6.69	3 *
$10^{40}\,\alpha_{33}$ ($C^2\,m^2\,J^{-1}$)	5.28	3 *
$10^{40}\,\alpha$ ($C^2\,m^2\,J^{-1}$)	5.81	3 *
$10^{40}\,a_{11}$ ($C^2\,m^2\,J^{-1}$)	7.278	7,8 +
$10^{40}\,a_{22}$ ($C^2\,m^2\,J^{-1}$)	5.744	7,8 +
$10^{40}\,a_{33}$ ($C^2\,m^2\,J^{-1}$)	5.968	7,8 +
$10^{40}\,a$ ($C^2\,m^2\,J^{-1}$)	6.33	7,8 +
$10^{40}\,\theta_{11}$ ($C\,m^2$)	11.1 ± 2.0	11
$10^{40}\,\theta_{22}$ ($C\,m^2$)	-4.3 ± 2.0	11
$10^{40}\,\theta_{33}$ ($C\,m^2$)	-6.7 ± 1.7	11

Table 18: A table of parameters used in evaluating B_K

** the parameters used to calculate Theory curve 2 in Figure 29 above

* derived from Kerr-effect experimental data

+ a*b initio* MP2 calculated values

4.4 OBSERVATIONS ON TEMPERATURE CONTROL

Many months of work went into investigating the reproducibility of our results, as well as any discrepancies between our results and those of Sono.[1] Any differences were initially thought to arise from calibration changes in the high-voltage supply, the Faraday cell and the pressure transducer; as well as possible hysteresis effects in the electrode spacing after cycling through a range of ±200°C in temperature. Towards this end, the equipment was regularly re-calibrated and the entire experimental set-up and method of measurement reviewed. We carefully examined all other possibilities of influence on the system.

At room temperature we found that our results were reproducible and consistent with Sono's whether or not the oven circulating fans were active. At higher temperatures, however, it was noted that when the fans were off there was a systematic shift in measured A_K values from those of Sono. The fans were switched off because it was thought that they could introduce undesired mechanical noise to the system, and the room-temperature analysis did not seem to support the need for the fans. However, once we reached 393 K, uniform temperature-control in the oven and cell could not be maintained relying on thermal convection alone. Upon switching the circulating fans on it was then found that the new results were once again agreeing with the previous study of Sono,[1] and so it was decided to re-measure the lower temperatures of 334 and 361 K. As is evident from fig 28, the new results did not differ much from Sono's and it was concluded that it is indeed necessary for fans to be used to circulate air in the system and so maintain fine temperature control: thermal convection alone is insufficient to obtain a uniform equilibrium temperature in the cell. Even at the lower temperatures it is necessary to use fans as they help circulate the coolant and the cold air and prevent unwanted local fluctuations in the temperature within the oven and cell.

After analyzing all the results we are able to conclude that the electrodes are not prone to hysteresis effects after cycling over a wide (±200°C) range of temperature. This is based

on our observations that even after heating the system and bringing the temperature down again, fresh measurements agree to within the statistical uncertainty limits of the previous measurements.

The graph below shows the effects of switching the oven fans off:

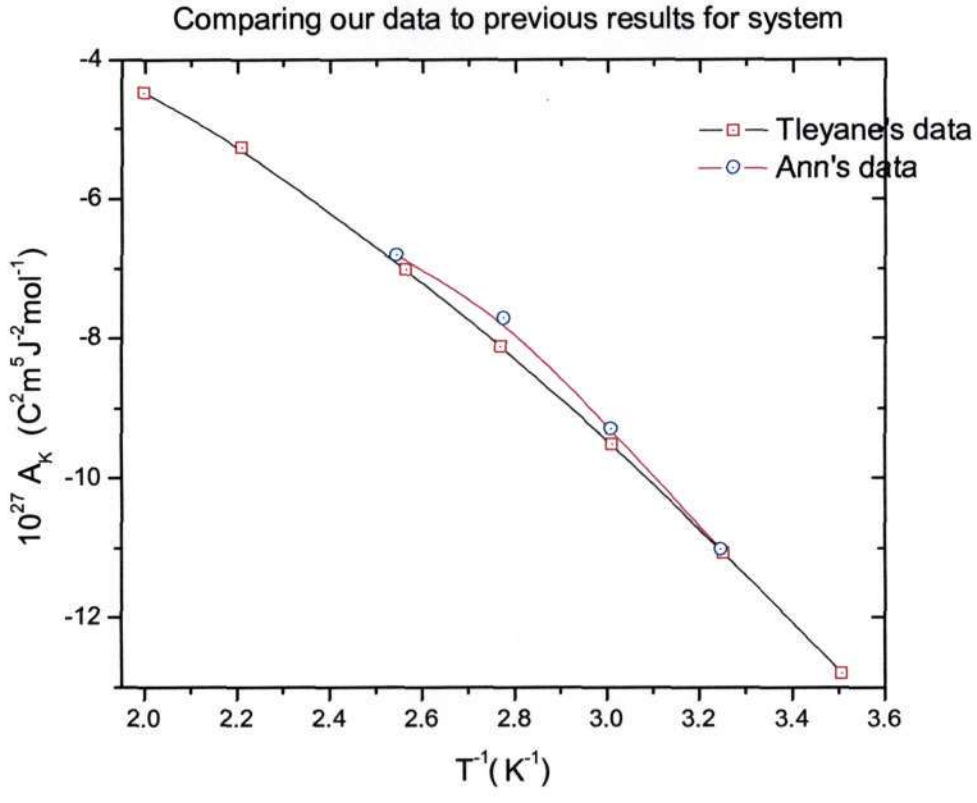

Fig 30 : Polynomial fit to A_K values to show the deviation between the data obtained with the fans off, and previous findings [1]

It becomes evident from the graph above that oven fans are required to establish and maintain thermal equilibrium in the oven and cell. The circular points that do not lie on the curve are the points obtained when the fans were off. It was observed that when the fans were reintroduced to the oven the points once again fell on the original curve.

4.5 CONCLUSION

This investigation of the Kerr effect in dimethyl ether has shown our apparatus to be an effective and accurate means of determining the molar Kerr constant over a wide range of pressure and temperature.

As has been shown in the results section the values obtained for β^K and $(\alpha_{33} - \alpha)$ are in good agreement with the *ab initio* calculated values and the SHG data. The newly-determined values of the dynamic polarizability-tensor components compare most favourably with the calculated values of Coonan *et al.*[4]

What remains to be accomplished is the investigation of the temperature realm below 280 K. The work thus far has shown that it is possible to achieve these temperatures; it is just a means of maintaining the temperatures long enough to gather experimental data, while at the same time ensuring that moisture does not condense and freeze on the windows. During the final months of this project we struggled to obtain measurements at -14°C, but in vain. The problem of water vapour condensing on the windows was solved at 280K by using heating elements around the cell windows. A few modifications to the heater ought to enable lower temperatures to be achieved without ice condensation. Work shall continue in this vain.

Finally, our precise new values of B_K over a range of temperature are in good agreement with the data computed using molecular-tensor theory,[1] with the significant exception evident at 280 K. At this low temperature, there is a low saturation vapour pressure, and the possibility of triplet interactions and perhaps even the formation of dimers is very real. Our molecular-tensor theory applies to freely interacting pairs, and not to dimers, hence the theory is probably no longer appropriate.

4.6 REFERENCES

1. T. J. Sono, M Sc thesis, University of Natal, 2003
2. J. F. Ward and C. K. Miller, *Phys. Rev. A*, 1979, **19**, 826
3. M. P. Bogaard, A. D. Buckingham and G. L. D. Ritchie, *J. Chem. Soc. Faraday Trans. II*, 1981, **77**, 1547
4. M. H. Coonan, I. E. Craven, M. R. Hesling, G. L. D. Ritchie and M. A. Spackman, *J. Phys. Chem.*, 1992, **96**, 7301
5. V. W. Couling, unpublished data
6. U. Blukis, P. H. Kasai and R. J. Meyers, *J. Chem. Phys.*, 1963, **38**, 2753
7. M. A. Spackman, 1999, private communication
8. A. N. Barnes, D. J. Turner and L. E. Sutton, *Trans. Faraday Soc.*, 1971, **67**, 2902
9. M. P. Bogaard, A. D. Buckingham, R. K. Pierens and A. H. White, *J. Chem. Soc. Faraday Trans. I*, 1978, **74**, 3008
10. V. W. Couling and R. V. Nhlebela, *Phys. Chem. Chem. Phys.*, 2001, **3**, 4551
11. R. C. Benson and W. H. Flygare, *J. Chem. Phys.*, 1970, **52**, 5291

APPENDIX A

Mueller Analysis

"This notebook is used to do an error analysis of the optical cascade used in the Kerr effect experiment. The matrices of the different components are initally defined and then the analysis performed."

Case 1

```
Clear [P]
```

```
Array[P, 4]
```

```
{P[1], P[2], P[3], P[4]}
```

```
P[1] = i
```

```
i
```

```
P[2] = 0
```

```
0
```

```
P[3] = i
```

```
i
```

```
P[4] = 0
```

```
0
```

"The matrix for the linear polarizer is defined"

```
Pol = Table[P[j], {j, 1, 4}]
```

```
{i, 0, i, 0}
```

```
MatrixForm[Pol]
```

$$\begin{pmatrix} i \\ 0 \\ i \\ 0 \end{pmatrix}$$

```
Clear [K]

Array[K, {4, 4}]
K[1, 1] = 1
K[1, 2] = 0
K[1, 3] = 0
K[1, 4] = 0
K[2, 1] = 0
K[2, 2] = Cos[δ] + 2 * Sin^2[δ/2]
K[2, 3] = 0
K[2, 4] = 0
K[3, 1] = 0
K[3, 2] = 0
K[3, 3] = Cos[δ]
K[3, 4] = Sin[δ]
K[4, 1] = 0
K[4, 2] = 0
K[4, 3] = -Sin[δ]
K[4, 4] = Cos[δ]

{{K[1, 1], K[1, 2], K[1, 3], K[1, 4]}, {K[2, 1], K[2, 2], K[2, 3], K[2, 4]},
 {K[3, 1], K[3, 2], K[3, 3], K[3, 4]}, {K[4, 1], K[4, 2], K[4, 3], K[4, 4]}}

1

0

0

0

0

2 Sin^2[δ/2] + Cos[δ]

0

0

0

0

Cos[δ]

Sin[δ]

0

0

-Sin[δ]

Cos[δ]
```

"The matrix for the Kerr cell is defined"

```
KC = Table[K[j, m], {j, 1, 4}, {m, 1, 4}]
```

$$\left\{\{1,\ 0,\ 0,\ 0\},\ \left\{0,\ 2\,\text{Sin}^{2\left[\frac{\delta}{2}\right]}+\text{Cos}[\delta],\ 0,\ 0\right\},\ \{0,\ 0,\ \text{Cos}[\delta],\ \text{Sin}[\delta]\},\ \{0,\ 0,\ -\text{Sin}[\delta],\ \text{Cos}[\delta]\}\right\}$$

```
MatrixForm[KC]
```

$$\begin{pmatrix} 1 & 0 & 0 & 0 \\ 0 & 2\,\text{Sin}^{2\left[\frac{\delta}{2}\right]}+\text{Cos}[\delta] & 0 & 0 \\ 0 & 0 & \text{Cos}[\delta] & \text{Sin}[\delta] \\ 0 & 0 & -\text{Sin}[\delta] & \text{Cos}[\delta] \end{pmatrix}$$

```
Clear [Q]

Array[Q, {4, 4}]
Q[1, 1] = 1
Q[1, 2] = 0
Q[1, 3] = 0
Q[1, 4] = 0
Q[2, 1] = 0
Q[2, 2] = 1 - (Cos[2 * ϵ]) ^2 * (Sin[κ] + 1)
Q[2, 3] = -Cos[2 * ϵ] * Sin[2 * ϵ] * (Sin[κ] + 1)
Q[2, 4] = -Cos[2 * ϵ] * Cos[κ]
Q[3, 1] = 0
Q[3, 2] = -Cos[2 * ϵ] * Sin[2 * ϵ] * Sin[κ + 1]
Q[3, 3] = 1 - (Sin[2 * ϵ]) ^2 * (Sin[κ] + 1)
Q[3, 4] = -Sin[2 * ϵ] * Cos[κ]
Q[4, 1] = 0
Q[4, 2] = Cos[2 * ϵ] * Cos[κ]
Q[4, 3] = Sin[2 * ϵ] * Cos[κ]
Q[4, 4] = -Sin[κ]



{{Q[1, 1], Q[1, 2], Q[1, 3], Q[1, 4]}, {Q[2, 1], Q[2, 2], Q[2, 3], Q[2, 4]},
 {Q[3, 1], Q[3, 2], Q[3, 3], Q[3, 4]}, {Q[4, 1], Q[4, 2], Q[4, 3], Q[4, 4]}}

1

0

0

0

0

1 - Cos[2 ϵ]^2 (1 + Sin[κ])

-Cos[2 ϵ] Sin[2 ϵ] (1 + Sin[κ])

-Cos[2 ϵ] Cos[κ]

0

-Cos[2 ϵ] Sin[2 ϵ] Sin[1 + κ]

1 - Sin[2 ϵ]^2 (1 + Sin[κ])

-Cos[κ] Sin[2 ϵ]

0

Cos[2 ϵ] Cos[κ]

Cos[κ] Sin[2 ϵ]

-Sin[κ]
```

"The matrix for the quarter wave plate"

```
QP = Table[Q[j, m], {j, 1, 4}, {m, 1, 4}]
```

```
{{1, 0, 0, 0},
 {0, 1 - Cos[2 ϵ]^2 (1 + Sin[κ]), -Cos[2 ϵ] Sin[2 ϵ] (1 + Sin[κ]), -Cos[2 ϵ] Cos[κ]},
 {0, -Cos[2 ϵ] Sin[2 ϵ] Sin[1 + κ], 1 - Sin[2 ϵ]^2 (1 + Sin[κ]), -Cos[κ] Sin[2 ϵ]},
 {0, Cos[2 ϵ] Cos[κ], Cos[κ] Sin[2 ϵ], -Sin[κ]}}
```

```
MatrixForm[QP]
```

$$\begin{pmatrix} 1 & 0 & 0 & 0 \\ 0 & 1 - \text{Cos}[2\,\epsilon]^2\,(1 + \text{Sin}[\kappa]) & -\text{Cos}[2\,\epsilon]\,\text{Sin}[2\,\epsilon]\,(1 + \text{Sin}[\kappa]) & -\text{Cos}[2\,\epsilon]\,\text{Cos}[\kappa] \\ 0 & -\text{Cos}[2\,\epsilon]\,\text{Sin}[2\,\epsilon]\,\text{Sin}[1 + \kappa] & 1 - \text{Sin}[2\,\epsilon]^2\,(1 + \text{Sin}[\kappa]) & -\text{Cos}[\kappa]\,\text{Sin}[2\,\epsilon] \\ 0 & \text{Cos}[2\,\epsilon]\,\text{Cos}[\kappa] & \text{Cos}[\kappa]\,\text{Sin}[2\,\epsilon] & -\text{Sin}[\kappa] \end{pmatrix}$$

```
Clear [F]

Array[F, {4, 4}]
F[1, 1] = 1
F[1, 2] = 0
F[1, 3] = 0
F[1, 4] = 0
F[2, 1] = 0
F[2, 2] = Cos[2 * θ]
F[2, 3] = Sin[2 * θ]
F[2, 4] = 0
F[3, 1] = 0
F[3, 2] = -Sin[2 * θ]
F[3, 3] = Cos[2 * θ]
F[3, 4] = 0
F[4, 1] = 0
F[4, 2] = 0
F[4, 3] = 0
F[4, 4] = 1
```

```
{{F[1, 1], F[1, 2], F[1, 3], F[1, 4]}, {F[2, 1], F[2, 2], F[2, 3], F[2, 4]},
 {F[3, 1], F[3, 2], F[3, 3], F[3, 4]}, {F[4, 1], F[4, 2], F[4, 3], F[4, 4]}}
```

```
1
```

```
0
```

```
0
```

```
0
```

```
0
```

```
Cos[2 θ]
```

```
Sin[2 θ]
```

```
0
```

```
0
```

```
-Sin[2 θ]
```

```
Cos[2 θ]
```

```
0
```

```
0
```

```
0
```

```
0
```

```
1
```

"The matrix for the Faraday cell is defined"

```
FC = Table[F[j, m], {j, 1, 4}, {m, 1, 4}]
```

```
{{1, 0, 0, 0}, {0, Cos[2 θ], Sin[2 θ], 0}, {0, -Sin[2 θ], Cos[2 θ], 0}, {0, 0, 0, 1}}
```

```
MatrixForm[FC]
```

$$\begin{pmatrix} 1 & 0 & 0 & 0 \\ 0 & \text{Cos}[2\,\theta] & \text{Sin}[2\,\theta] & 0 \\ 0 & -\text{Sin}[2\,\theta] & \text{Cos}[2\,\theta] & 0 \\ 0 & 0 & 0 & 1 \end{pmatrix}$$

```
Clear[A]
```

```
Array[A, {4, 4}]
A[1, 1] = 1
A[1, 2] = Sin[2 * α]
A[1, 3] = -Cos[2 * α]
A[1, 4] = 0
A[2, 1] = Sin[2 * α]
A[2, 2] = Sin[2 * α] ^ 2
A[2, 3] = -Cos[2 * α] * Sin[2 * α]
A[2, 4] = 0
A[3, 1] = -Cos[2 * α]
A[3, 2] = -Cos[2 * α] * Sin[2 * α]
A[3, 3] = Cos[2 * α] ^ 2
A[3, 4] = 0
A[4, 1] = 0
A[4, 2] = 0
A[4, 3] = 0
A[4, 4] = 0
```

```
{{A[1, 1], A[1, 2], A[1, 3], A[1, 4]}, {A[2, 1], A[2, 2], A[2, 3], A[2, 4]},
 {A[3, 1], A[3, 2], A[3, 3], A[3, 4]}, {A[4, 1], A[4, 2], A[4, 3], A[4, 4]}}
```

```
1
```

```
Sin[2 α]
```

```
-Cos[2 α]
```

```
0
```

```
Sin[2 α]
```

```
Sin[2 α]^2
```

```
-Cos[2 α] Sin[2 α]
```

```
0
```

```
-Cos[2 α]
```

```
-Cos[2 α] Sin[2 α]
```

```
Cos[2 α]^2
```

```
0
```

```
0
```

```
0
```

```
0
```

```
0
```

"The matrix for the analyser is defined"

```
AN = Table[A[j, m], {j, 1, 4}, {m, 1, 4}]
```

```
{{1, Sin[2 α], -Cos[2 α], 0}, {Sin[2 α], Sin[2 α]^2, -Cos[2 α] Sin[2 α], 0},
 {-Cos[2 α], -Cos[2 α] Sin[2 α], Cos[2 α]^2, 0}, {0, 0, 0, 0}}
```

```
MatrixForm[AN]
```

$$\begin{pmatrix} 1 & \text{Sin}[2\alpha] & -\text{Cos}[2\alpha] & 0 \\ \text{Sin}[2\alpha] & \text{Sin}[2\alpha]^2 & -\text{Cos}[2\alpha]\,\text{Sin}[2\alpha] & 0 \\ -\text{Cos}[2\alpha] & -\text{Cos}[2\alpha]\,\text{Sin}[2\alpha] & \text{Cos}[2\alpha]^2 & 0 \\ 0 & 0 & 0 & 0 \end{pmatrix}$$

```
Clear[AN2]
```

```
Array[AN2, {4, 4}]
```

```
{{AN2[1, 1], AN2[1, 2], AN2[1, 3], AN2[1, 4]},
 {AN2[2, 1], AN2[2, 2], AN2[2, 3], AN2[2, 4]},
 {AN2[3, 1], AN2[3, 2], AN2[3, 3], AN2[3, 4]},
 {AN2[4, 1], AN2[4, 2], AN2[4, 3], AN2[4, 4]}}
```

"The matrix for the analyser is multiplied by a half"

```
AN2 = Table[A[j, m] * 0.5, {j, 1, 4}, {m, 1, 4}]
```

```
{{0.5, 0.5 Sin[2 α], -0.5 Cos[2 α], 0},
 {0.5 Sin[2 α], 0.5 Sin[2 α]^2, -0.5 Cos[2 α] Sin[2 α], 0},
 {-0.5 Cos[2 α], -0.5 Cos[2 α] Sin[2 α], 0.5 Cos[2 α]^2, 0}, {0, 0, 0, 0}}
```

```
MatrixForm[AN2]
```

$$\begin{pmatrix} 0.5 & 0.5\,\text{Sin}[2\alpha] & -0.5\,\text{Cos}[2\alpha] & 0 \\ 0.5\,\text{Sin}[2\alpha] & 0.5\,\text{Sin}[2\alpha]^2 & -0.5\,\text{Cos}[2\alpha]\,\text{Sin}[2\alpha] & 0 \\ -0.5\,\text{Cos}[2\alpha] & -0.5\,\text{Cos}[2\alpha]\,\text{Sin}[2\alpha] & 0.5\,\text{Cos}[2\alpha]^2 & 0 \\ 0 & 0 & 0 & 0 \end{pmatrix}$$

```
ϵ = 0
```

```
0
```

"The matrix for the quarter wave plate for epsilon set to 0 for the case where analyser is offset by an amount α from -45° and the azimuth of the quarter wave plate is at 45° where epsilon is 0."

```
QP
```

```
{{1, 0, 0, 0}, {0, -Sin[κ], 0, -Cos[κ]}, {0, 0, 1, 0}, {0, Cos[κ], 0, -Sin[κ]}}
```

"The dot product of the five matrices is determined"

AN2.FC.QP.KC.Pol

$$\{0.5\,i + i\,(\text{Cos}[\kappa]\,\text{Sin}[\delta]\,(0.5\,\text{Cos}[2\theta]\,\text{Sin}[2\alpha] + 0.5\,\text{Cos}[2\alpha]\,\text{Sin}[2\theta]) + \text{Cos}[\delta]\,(-0.5\,\text{Cos}[2\alpha]\,\text{Cos}[2\theta] + 0.5\,\text{Sin}[2\alpha]\,\text{Sin}[2\theta])),$$
$$0.5\,i\,\text{Sin}[2\alpha] + i\,(\text{Cos}[\kappa]\,\text{Sin}[\delta]\,(0.5\,\text{Cos}[2\theta]\,\text{Sin}[2\alpha]^2 + 0.5\,\text{Cos}[2\alpha]\,\text{Sin}[2\alpha]\,\text{Sin}[2\theta]) + \text{Cos}[\delta]\,(-0.5\,\text{Cos}[2\alpha]\,\text{Cos}[2\theta]\,\text{Sin}[2\alpha] + 0.5\,\text{Sin}[2\alpha]^2\,\text{Sin}[2\theta])),$$
$$-0.5\,i\,\text{Cos}[2\alpha] + i\,(\text{Cos}[\kappa]\,\text{Sin}[\delta]\,(-0.5\,\text{Cos}[2\alpha]\,\text{Cos}[2\theta]\,\text{Sin}[2\alpha] - 0.5\,\text{Cos}[2\alpha]^2\,\text{Sin}[2\theta]) + \text{Cos}[\delta]\,(0.5\,\text{Cos}[2\alpha]^2\,\text{Cos}[2\theta] - 0.5\,\text{Cos}[2\alpha]\,\text{Sin}[2\alpha]\,\text{Sin}[2\theta])),\ 0\}$$

MatrixForm[%]

$$\begin{pmatrix} 0.5\,i + i\,(\text{Cos}[\kappa]\,\text{Sin}[\delta]\,(0.5\,\text{Cos}[2\theta]\,\text{Sin}[2\alpha] + 0.5\,\text{Cos}[2\alpha]\,\text{Sin}[2\theta]) + \text{Cos} \\ 0.5\,i\,\text{Sin}[2\alpha] + i\,(\text{Cos}[\kappa]\,\text{Sin}[\delta]\,(0.5\,\text{Cos}[2\theta]\,\text{Sin}[2\alpha]^2 + 0.5\,\text{Cos}[2\alpha]\,\text{Sin}[2\alpha]\,\text{Sin}[2\theta]) \\ -0.5\,i\,\text{Cos}[2\alpha] + i\,(\text{Cos}[\kappa]\,\text{Sin}[\delta]\,(-0.5\,\text{Cos}[2\alpha]\,\text{Cos}[2\theta]\,\text{Sin}[2\alpha] - 0.5\,\text{Cos}[2\alpha]^2\,\text{Sin}[2\theta] \\ 0 \end{pmatrix}$$

"The above expression is then simplified by using Taylor series expansion and small angle approximations. The substituitions are shown step by step so that it is easier to follow."

% //. Sin[2 * α] → 2 * α

$$\{0.5\,i + i\,(\text{Cos}[\delta]\,(-0.5\,\text{Cos}[2\alpha]\,\text{Cos}[2\theta] + 1.\,\alpha\,\text{Sin}[2\theta]) + \text{Cos}[\kappa]\,\text{Sin}[\delta]\,(1.\,\alpha\,\text{Cos}[2\theta] + 0.5\,\text{Cos}[2\alpha]\,\text{Sin}[2\theta])),$$
$$1.\,i\,\alpha + i\,(\text{Cos}[\delta]\,(-1.\,\alpha\,\text{Cos}[2\alpha]\,\text{Cos}[2\theta] + 2.\,\alpha^2\,\text{Sin}[2\theta]) + \text{Cos}[\kappa]\,\text{Sin}[\delta]\,(2.\,\alpha^2\,\text{Cos}[2\theta] + 1.\,\alpha\,\text{Cos}[2\alpha]\,\text{Sin}[2\theta])),$$
$$-0.5\,i\,\text{Cos}[2\alpha] + i\,(\text{Cos}[\delta]\,(0.5\,\text{Cos}[2\alpha]^2\,\text{Cos}[2\theta] - 1.\,\alpha\,\text{Cos}[2\alpha]\,\text{Sin}[2\theta]) + \text{Cos}[\kappa]\,\text{Sin}[\delta]\,(-1.\,\alpha\,\text{Cos}[2\alpha]\,\text{Cos}[2\theta] - 0.5\,\text{Cos}[2\alpha]^2\,\text{Sin}[2\theta])),\ 0\}$$

% //. Cos[2 * α] → (1 - ((2 * α)^2) / 2)

$$\{0.5\,i + i\,(\text{Cos}[\delta]\,(-0.5\,(1 - 2\alpha^2)\,\text{Cos}[2\theta] + 1.\,\alpha\,\text{Sin}[2\theta]) + \text{Cos}[\kappa]\,\text{Sin}[\delta]\,(1.\,\alpha\,\text{Cos}[2\theta] + 0.5\,(1 - 2\alpha^2)\,\text{Sin}[2\theta])),$$
$$1.\,i\,\alpha + i\,(\text{Cos}[\delta]\,(-1.\,\alpha\,(1 - 2\alpha^2)\,\text{Cos}[2\theta] + 2.\,\alpha^2\,\text{Sin}[2\theta]) + \text{Cos}[\kappa]\,\text{Sin}[\delta]\,(2.\,\alpha^2\,\text{Cos}[2\theta] + 1.\,\alpha\,(1 - 2\alpha^2)\,\text{Sin}[2\theta])),$$
$$-0.5\,i\,(1 - 2\alpha^2) + i\,(\text{Cos}[\delta]\,(0.5\,(1 - 2\alpha^2)^2\,\text{Cos}[2\theta] - 1.\,\alpha\,(1 - 2\alpha^2)\,\text{Sin}[2\theta]) + \text{Cos}[\kappa]\,\text{Sin}[\delta]\,(-1.\,\alpha\,(1 - 2\alpha^2)\,\text{Cos}[2\theta] - 0.5\,(1 - 2\alpha^2)^2\,\text{Sin}[2\theta])),\ 0\}$$

% //. Sin[δ] → δ

$$\{0.5\,i + i\,(\text{Cos}[\delta]\,(-0.5\,(1 - 2\alpha^2)\,\text{Cos}[2\theta] + 1.\,\alpha\,\text{Sin}[2\theta]) + \delta\,\text{Cos}[\kappa]\,(1.\,\alpha\,\text{Cos}[2\theta] + 0.5\,(1 - 2\alpha^2)\,\text{Sin}[2\theta])),$$
$$1.\,i\,\alpha + i\,(\text{Cos}[\delta]\,(-1.\,\alpha\,(1 - 2\alpha^2)\,\text{Cos}[2\theta] + 2.\,\alpha^2\,\text{Sin}[2\theta]) + \delta\,\text{Cos}[\kappa]\,(2.\,\alpha^2\,\text{Cos}[2\theta] + 1.\,\alpha\,(1 - 2\alpha^2)\,\text{Sin}[2\theta])),$$
$$-0.5\,i\,(1 - 2\alpha^2) + i\,(\text{Cos}[\delta]\,(0.5\,(1 - 2\alpha^2)^2\,\text{Cos}[2\theta] - 1.\,\alpha\,(1 - 2\alpha^2)\,\text{Sin}[2\theta]) + \delta\,\text{Cos}[\kappa]\,(-1.\,\alpha\,(1 - 2\alpha^2)\,\text{Cos}[2\theta] - 0.5\,(1 - 2\alpha^2)^2\,\text{Sin}[2\theta])),\ 0\}$$

%//. Cos[δ]→1-((δ)^2)/2

$$\left\{0.5\,\mathbf{i} + \mathbf{i}\left(\left(1-\frac{\delta^2}{2}\right)\left(-0.5\,(1-2\alpha^2)\,\mathrm{Cos}[2\theta] + 1.\,\alpha\,\mathrm{Sin}[2\theta]\right) + \delta\,\mathrm{Cos}[\kappa]\,\left(1.\,\alpha\,\mathrm{Cos}[2\theta] + 0.5\,(1-2\alpha^2)\,\mathrm{Sin}[2\theta]\right)\right),\right.$$

$$1.\,\mathbf{i}\,\alpha + \mathbf{i}\left(\left(1-\frac{\delta^2}{2}\right)\left(-1.\,\alpha\,(1-2\alpha^2)\,\mathrm{Cos}[2\theta] + 2.\,\alpha^2\,\mathrm{Sin}[2\theta]\right) + \delta\,\mathrm{Cos}[\kappa]\,\left(2.\,\alpha^2\,\mathrm{Cos}[2\theta] + 1.\,\alpha\,(1-2\alpha^2)\,\mathrm{Sin}[2\theta]\right)\right),$$

$$-0.5\,\mathbf{i}\,(1-2\alpha^2) + \mathbf{i}\left(\left(1-\frac{\delta^2}{2}\right)\left(0.5\,(1-2\alpha^2)^2\,\mathrm{Cos}[2\theta] - 1.\,\alpha\,(1-2\alpha^2)\,\mathrm{Sin}[2\theta]\right) + \delta\,\mathrm{Cos}[\kappa]\,\left(-1.\,\alpha\,(1-2\alpha^2)\,\mathrm{Cos}[2\theta] - 0.5\,(1-2\alpha^2)^2\,\mathrm{Sin}[2\theta]\right)\right),\ 0\Big\}$$

%//. Cos[2*θ]→1-((2*θ)^2)/2

$$\left\{0.5\,\mathbf{i} + \mathbf{i}\left(\left(1-\frac{\delta^2}{2}\right)\left(-0.5\,(1-2\alpha^2)\,(1-2\theta^2) + 1.\,\alpha\,\mathrm{Sin}[2\theta]\right) + \delta\,\mathrm{Cos}[\kappa]\,\left(1.\,\alpha\,(1-2\theta^2) + 0.5\,(1-2\alpha^2)\,\mathrm{Sin}[2\theta]\right)\right),\right.$$

$$1.\,\mathbf{i}\,\alpha + \mathbf{i}\left(\left(1-\frac{\delta^2}{2}\right)\left(-1.\,\alpha\,(1-2\alpha^2)\,(1-2\theta^2) + 2.\,\alpha^2\,\mathrm{Sin}[2\theta]\right) + \delta\,\mathrm{Cos}[\kappa]\,\left(2.\,\alpha^2\,(1-2\theta^2) + 1.\,\alpha\,(1-2\alpha^2)\,\mathrm{Sin}[2\theta]\right)\right),$$

$$-0.5\,\mathbf{i}\,(1-2\alpha^2) + \mathbf{i}\left(\left(1-\frac{\delta^2}{2}\right)\left(0.5\,(1-2\alpha^2)^2\,(1-2\theta^2) - 1.\,\alpha\,(1-2\alpha^2)\,\mathrm{Sin}[2\theta]\right) + \delta\,\mathrm{Cos}[\kappa]\,\left(-1.\,\alpha\,(1-2\alpha^2)\,(1-2\theta^2) - 0.5\,(1-2\alpha^2)^2\,\mathrm{Sin}[2\theta]\right)\right),\ 0\Big\}$$

%//. Cos[κ]→1-((κ)^2)/2

$$\left\{0.5\,\mathbf{i} + \mathbf{i}\left(\left(1-\frac{\delta^2}{2}\right)\left(-0.5\,(1-2\alpha^2)\,(1-2\theta^2) + 1.\,\alpha\,\mathrm{Sin}[2\theta]\right) + \delta\left(1-\frac{\kappa^2}{2}\right)\left(1.\,\alpha\,(1-2\theta^2) + 0.5\,(1-2\alpha^2)\,\mathrm{Sin}[2\theta]\right)\right),\right.$$

$$1.\,\mathbf{i}\,\alpha + \mathbf{i}\left(\left(1-\frac{\delta^2}{2}\right)\left(-1.\,\alpha\,(1-2\alpha^2)\,(1-2\theta^2) + 2.\,\alpha^2\,\mathrm{Sin}[2\theta]\right) + \delta\left(1-\frac{\kappa^2}{2}\right)\left(2.\,\alpha^2\,(1-2\theta^2) + 1.\,\alpha\,(1-2\alpha^2)\,\mathrm{Sin}[2\theta]\right)\right),$$

$$-0.5\,\mathbf{i}\,(1-2\alpha^2) + \mathbf{i}\left(\left(1-\frac{\delta^2}{2}\right)\left(0.5\,(1-2\alpha^2)^2\,(1-2\theta^2) - 1.\,\alpha\,(1-2\alpha^2)\,\mathrm{Sin}[2\theta]\right) + \delta\left(1-\frac{\kappa^2}{2}\right)\left(-1.\,\alpha\,(1-2\alpha^2)\,(1-2\theta^2) - 0.5\,(1-2\alpha^2)^2\,\mathrm{Sin}[2\theta]\right)\right),\ 0\Big\}$$

```
%//. Sin[2*θ]→2*θ
```

$$\{0.5\,i + i\left(\left(1-\frac{\delta^2}{2}\right)(2.\,\alpha\theta - 0.5\,(1-2\alpha^2)\,(1-2\theta^2)) + \delta\,(1.\,(1-2\alpha^2)\,\theta + 1.\,\alpha\,(1-2\theta^2))\left(1-\frac{\kappa^2}{2}\right)\right),$$

$$1.\,i\,\alpha + i\left(\left(1-\frac{\delta^2}{2}\right)(4.\,\alpha^2\,\theta - 1.\,\alpha\,(1-2\alpha^2)\,(1-2\theta^2)) + \delta\,(2.\,\alpha\,(1-2\alpha^2)\,\theta + 2.\,\alpha^2\,(1-2\theta^2))\left(1-\frac{\kappa^2}{2}\right)\right),$$

$$-0.5\,i\,(1-2\alpha^2) + i\left(\left(1-\frac{\delta^2}{2}\right)(-2.\,\alpha\,(1-2\alpha^2)\,\theta + 0.5\,(1-2\alpha^2)^2\,(1-2\theta^2)) + \delta\,(-1.\,(1-2\alpha^2)^2\,\theta - 1.\,\alpha\,(1-2\alpha^2)\,(1-2\theta^2))\left(1-\frac{\kappa^2}{2}\right)\right),\ 0\}$$

```
%[[1]]
```

$$0.5\,i + i\left(\left(1-\frac{\delta^2}{2}\right)(2.\,\alpha\theta - 0.5\,(1-2\alpha^2)\,(1-2\theta^2)) + \delta\,(1.\,(1-2\alpha^2)\,\theta + 1.\,\alpha\,(1-2\theta^2))\left(1-\frac{\kappa^2}{2}\right)\right)$$

```
Expand[%]
```

$$0.\,i + 1.\,i\,\alpha^2 + 1.\,i\,\alpha\,\delta + 0.25\,i\,\delta^2 - 0.5\,i\,\alpha^2\,\delta^2 + 2.\,i\,\alpha\,\theta + 1.\,i\,\delta\,\theta - 2.\,i\,\alpha^2\,\delta\,\theta - 1.\,i\,\alpha\,\delta^2\,\theta + 1.\,i\,\theta^2 - 2.\,i\,\alpha^2\,\theta^2 - 2.\,i\,\alpha\,\delta\,\theta^2 - 0.5\,i\,\delta^2\,\theta^2 + 1.\,i\,\alpha^2\,\delta^2\,\theta^2 - 0.5\,i\,\alpha\,\delta\,\kappa^2 - 0.5\,i\,\delta\,\theta\,\kappa^2 + 1.\,i\,\alpha^2\,\delta\,\theta\,\kappa^2 + 1.\,i\,\alpha\,\delta\,\theta^2\,\kappa^2$$

```
FullSimplify[%/(2*i)]
```

$$0. + 0.5\,\theta^2 + \delta^2\,(0.125 - 0.25\,\theta^2) + \delta\,\theta\,(0.5 - 0.25\,\kappa^2) + \alpha^2\,(0.5 - 1.\,\theta^2 + \delta^2\,(-0.25 + 0.5\,\theta^2) + \delta\,\theta\,(-1. + 0.5\,\kappa^2)) + \alpha\,(1.\,\theta + \delta\,(0.5 - 0.5\,\delta\,\theta - 0.25\,\kappa^2 + \theta^2\,(-1. + 0.5\,\kappa^2)))$$

```
MatrixForm[%]
```

$$0. - 0.5\,\theta^2 + \delta^2\,(-0.125 + 0.25\,\theta^2) + \delta\,\theta\,(-0.5 + 0.25\,\kappa^2) + \alpha^2\,(-0.5 + 1.\,\theta^2 + \delta^2\,(0.25 - 0.5\,\theta^2) + \delta\,\theta\,(1. - 0.5\,\kappa^2)) + \alpha\,(-1.\,\theta + \delta\,(-0.5 + 0.5\,\delta\,\theta + 0.25\,\kappa^2 + \theta^2\,(1. - 0.5\,\kappa^2)))$$

```
Expand[%]
```

$$0. + 0.5\,\alpha^2 + 0.5\,\alpha\,\delta + 0.125\,\delta^2 - 0.25\,\alpha^2\,\delta^2 + 1.\,\alpha\,\theta + 0.5\,\delta\,\theta - 1.\,\alpha^2\,\delta\,\theta - 0.5\,\alpha\,\delta^2\,\theta + 0.5\,\theta^2 - 1.\,\alpha^2\,\theta^2 - 1.\,\alpha\,\delta\,\theta^2 - 0.25\,\delta^2\,\theta^2 + 0.5\,\alpha^2\,\delta^2\,\theta^2 - 0.25\,\alpha\,\delta\,\kappa^2 - 0.25\,\delta\,\theta\,\kappa^2 + 0.5\,\alpha^2\,\delta\,\theta\,\kappa^2 + 0.5\,\alpha\,\delta\,\theta^2\,\kappa^2$$

"The terms in δ and θ are extracted since they oscillate at 2ω.
$I_f = I_o/2*\left(4\,\alpha\theta - \alpha\delta\kappa^2 + 2\alpha\delta\right)$ where $\kappa = 1.2° = 0.0209$ rad. $\kappa^2 = 4.39*10^{-4}$. From this $\alpha\delta\kappa^2 << 2\,\alpha\delta$ and the imperfection in the quarter wave plate is taken to be negligible"

Case 2

"For the second case the analyser is set at $\alpha = 0$ and the azimuth of the quarter wave plate is offset from +45° by $+\epsilon$. The steps to obtain the inherent error are the repeated."

α = 0

0

Clear[ϵ]

MatrixForm[AN]

$$\begin{pmatrix} 1 & 0 & -1 & 0 \\ 0 & 0 & 0 & 0 \\ -1 & 0 & 1 & 0 \\ 0 & 0 & 0 & 0 \end{pmatrix}$$

AN.FC.QP.KC.Pol

```
{i + i (-Sin[δ] (Cos[2 θ] Cos[κ] Sin[2 ϵ] - Cos[2 ϵ] Cos[κ] Sin[2 θ]) + Cos[δ]
      (-Cos[2 ϵ] Sin[2 ϵ] Sin[2 θ] (1 + Sin[κ]) - Cos[2 θ] (1 - Sin[2 ϵ]^2 (1 + Sin[κ])))),
 0, -i + i (-Sin[δ] (-Cos[2 θ] Cos[κ] Sin[2 ϵ] + Cos[2 ϵ] Cos[κ] Sin[2 θ]) + Cos[δ]
      (Cos[2 ϵ] Sin[2 ϵ] Sin[2 θ] (1 + Sin[κ]) + Cos[2 θ] (1 - Sin[2 ϵ]^2 (1 + Sin[κ])))), 0}
```

%[[1]]

```
i + i (-Sin[δ] (Cos[2 θ] Cos[κ] Sin[2 ϵ] - Cos[2 ϵ] Cos[κ] Sin[2 θ]) + Cos[δ]
     (-Cos[2 ϵ] Sin[2 ϵ] Sin[2 θ] (1 + Sin[κ]) - Cos[2 θ] (1 - Sin[2 ϵ]^2 (1 + Sin[κ]))))
```

%//. Sin[δ]→δ

```
i + i (-δ (Cos[2 θ] Cos[κ] Sin[2 ϵ] - Cos[2 ϵ] Cos[κ] Sin[2 θ]) + Cos[δ]
     (-Cos[2 ϵ] Sin[2 ϵ] Sin[2 θ] (1 + Sin[κ]) - Cos[2 θ] (1 - Sin[2 ϵ]^2 (1 + Sin[κ]))))
```

%//. Cos[δ]→1-((δ)^2)/2

$$i + i\left(-\delta\,(\text{Cos}[2\theta]\,\text{Cos}[\kappa]\,\text{Sin}[2\epsilon] - \text{Cos}[2\epsilon]\,\text{Cos}[\kappa]\,\text{Sin}[2\theta]) + \left(1 - \frac{\delta^2}{2}\right)\right.$$
$$\left.(-\text{Cos}[2\epsilon]\,\text{Sin}[2\epsilon]\,\text{Sin}[2\theta]\,(1 + \text{Sin}[\kappa]) - \text{Cos}[2\theta]\,(1 - \text{Sin}[2\epsilon]^2\,(1 + \text{Sin}[\kappa])))\right)$$

%//. Cos[κ]→1-((κ)^2)/2

$$i + i\left(-\delta\left(\left(1 - \frac{\kappa^2}{2}\right)\text{Cos}[2\theta]\,\text{Sin}[2\epsilon] - \left(1 - \frac{\kappa^2}{2}\right)\text{Cos}[2\epsilon]\,\text{Sin}[2\theta]\right) + \left(1 - \frac{\delta^2}{2}\right)\right.$$
$$\left.(-\text{Cos}[2\epsilon]\,\text{Sin}[2\epsilon]\,\text{Sin}[2\theta]\,(1 + \text{Sin}[\kappa]) - \text{Cos}[2\theta]\,(1 - \text{Sin}[2\epsilon]^2\,(1 + \text{Sin}[\kappa])))\right)$$

%//. Sin[κ]→κ

$$i + i\left(-\delta\left(\left(1 - \frac{\kappa^2}{2}\right)\text{Cos}[2\theta]\,\text{Sin}[2\epsilon] - \left(1 - \frac{\kappa^2}{2}\right)\text{Cos}[2\epsilon]\,\text{Sin}[2\theta]\right) +\right.$$
$$\left.\left(1 - \frac{\delta^2}{2}\right)(-\text{Cos}[2\theta]\,(1 - (1 + \kappa)\,\text{Sin}[2\epsilon]^2) - (1 + \kappa)\,\text{Cos}[2\epsilon]\,\text{Sin}[2\epsilon]\,\text{Sin}[2\theta])\right)$$

```
%//. Sin[2*ϵ]→2*ϵ
```

$$i + i\left(\left(1 - \frac{\delta^2}{2}\right)\left(-(1 - 4\epsilon^2(1+\kappa))\,\text{Cos}[2\theta] - 2\epsilon(1+\kappa)\,\text{Cos}[2\epsilon]\,\text{Sin}[2\theta]\right) - \delta\left(2\epsilon\left(1 - \frac{\kappa^2}{2}\right)\text{Cos}[2\theta] - \left(1 - \frac{\kappa^2}{2}\right)\text{Cos}[2\epsilon]\,\text{Sin}[2\theta]\right)\right)$$

```
%//. Sin[2*θ]→2*θ
```

$$i + i\left(-\delta\left(-2\theta\left(1 - \frac{\kappa^2}{2}\right)\text{Cos}[2\epsilon] + 2\epsilon\left(1 - \frac{\kappa^2}{2}\right)\text{Cos}[2\theta]\right) + \left(1 - \frac{\delta^2}{2}\right)\left(-4\epsilon\theta(1+\kappa)\,\text{Cos}[2\epsilon] - (1 - 4\epsilon^2(1+\kappa))\,\text{Cos}[2\theta]\right)\right)$$

```
%//. Cos[2*θ]→1-((2*θ)^2)/2
```

$$i + i\left(\left(1 - \frac{\delta^2}{2}\right)\left(-(1 - 2\theta^2)(1 - 4\epsilon^2(1+\kappa)) - 4\epsilon\theta(1+\kappa)\,\text{Cos}[2\epsilon]\right) - \delta\left(2\epsilon(1 - 2\theta^2)\left(1 - \frac{\kappa^2}{2}\right) - 2\theta\left(1 - \frac{\kappa^2}{2}\right)\text{Cos}[2\epsilon]\right)\right)$$

```
%//. Cos[2*ϵ]→1-((2*ϵ)^2)/2
```

$$i + i\left(-\delta\left(-2(1 - 2\epsilon^2)\theta\left(1 - \frac{\kappa^2}{2}\right) + 2\epsilon(1 - 2\theta^2)\left(1 - \frac{\kappa^2}{2}\right)\right) + \left(1 - \frac{\delta^2}{2}\right)\left(-4\epsilon(1 - 2\epsilon^2)\theta(1+\kappa) - (1 - 2\theta^2)(1 - 4\epsilon^2(1+\kappa))\right)\right)$$

```
Expand[%]
```

$$\frac{i\delta^2}{2} - 2i\delta\epsilon + 4i\epsilon^2 - 2i\delta^2\epsilon^2 + 2i\delta\theta - 4i\epsilon\theta + 2i\delta^2\epsilon\theta - 4i\delta\epsilon^2\theta + 8i\epsilon^3\theta - 4i\delta^2\epsilon^3\theta + 2i\theta^2 - i\delta^2\theta^2 + 4i\delta\epsilon\theta^2 - 8i\epsilon^2\theta^2 + 4i\delta^2\epsilon^2\theta^2 + 4i\epsilon^2\kappa - 2i\delta^2\epsilon^2\kappa - 4i\epsilon\theta\kappa + 2i\delta^2\epsilon\theta\kappa + 8i\epsilon^3\theta\kappa - 4i\delta^2\epsilon^3\theta\kappa - 8i\epsilon^2\theta^2\kappa + 4i\delta^2\epsilon^2\theta^2\kappa + i\delta\epsilon\kappa^2 - i\delta\theta\kappa^2 + 2i\delta\epsilon^2\theta\kappa^2 - 2i\delta\epsilon\theta^2\kappa^2$$

"The terms in δ and θ are once again extracted since they oscillate at 2ω.
$I_f = I_o/2*(8\epsilon^2\kappa\theta - 4\epsilon\kappa\theta + 8\epsilon^3\theta - 4\epsilon\theta + \delta\epsilon\kappa^2 - 2\delta\epsilon)$ where $\kappa = 1.2°$ and $\epsilon < 1°$.
For the terms in δ i.e $\delta(\epsilon\kappa^2 - 2\epsilon)$ $\epsilon\kappa^2 < 2\epsilon$ so the term $-2\epsilon\delta$ is retained.
For the terms in θ i.e $\theta(8\epsilon^2\kappa - 4\epsilon\kappa + 8\epsilon^3 - 4\epsilon)$, $8\epsilon^2\kappa << 8\epsilon^3 << 4\epsilon\kappa << 4\epsilon$ so the $-4\epsilon\theta$ term is retained such that $I_f = -I_o/2*(4\epsilon\theta - 2\epsilon)$ which implies the imperfection in the quarter wave plate is still taken to be negligible.

Although both instances introduce minimum imperfection disturbance by the quarter wave plate, the second case is preferred as it is more practical to offset the quarter wave plate by small amounts. it is for this reason that the quarter wave plate is offset by + and - ϵ and plotting a grapg of the psd output as a function of the nulling current to obtain the induced phase difference δ using $\theta_{int} = -\delta/2$ from the intersection of the two graphs for each pair of offsets."

APPENDIX B

Kerr Analysis: Method A

Linear analyis of Kerr data

$$\left[A_K - \frac{N_A}{81\varepsilon_0}\gamma^K\right]T = \frac{N_A}{81\varepsilon_0}\frac{1}{k_B}\left\{\left[\frac{2}{3}\mu\beta^K + \frac{1}{5}\Delta\alpha\Delta a\right] + \frac{N_A}{270\varepsilon_0}\frac{1}{k_B^2 T}\mu^2(\alpha_{33} -$$

"The equation above is thefirst of two ways used to analyse data obtained from the Kerr Effect experiement. Eqns (a) - (d) help to simplify and calculate the values to be plotted. A graph is then plotted of (d) as a linear function of T. The slope and intercept are then used to determine β^K and $(\alpha_{33} - \alpha)$. The uncertainties in these values are determined by using the effective uncertainties in the different quantities when calculating a minimum and maximum value for the properties mentioned. Remember for a maximum value for a term **a-b or a/b** the terms contributing to **a** take on their higher uncertainties and those to **b** their lower uncertainties and vice versa."

$$\mathbf{a} = \frac{\mathbf{N_A}}{\mathbf{81 * \epsilon_o}}$$

$$\frac{N_A}{81\,\epsilon_o}$$

$$\mathbf{b} = \frac{\mathbf{\gamma K\, N_A}}{\mathbf{81\,\epsilon_o}}$$

$$\frac{\gamma K\, N_A}{81\,\epsilon_o}$$

$$\mathbf{c} = \{\mathbf{A_K} - \mathbf{b}\}$$

$$\left\{A_K - \frac{\gamma K\, N_A}{81\,\epsilon_o}\right\}$$

d = c * T

$$\left\{T\left(A_K - \frac{\gamma K N_A}{81 \epsilon_o}\right)\right\}$$

$$\left\{\mathbf{T}\left(\mathbf{A_K} - \frac{\boldsymbol{\gamma} \mathbf{K N_A}}{\mathbf{81}\, \boldsymbol{\epsilon_o}}\right)\right\}$$

"delta alpha is given by (e)"

e = 3 * α * κ

$3\,\alpha\,\kappa$

"delta a is given by (f)"

f = 3 * aa * κκ

$3\,aa\,\kappa\kappa$

g = a * (1 / KB)

$$\frac{N_A}{81\,KB\,\epsilon_o}$$

h = N_A / (270 * ϵ_o)

$$\frac{N_A}{270\,\epsilon_o}$$

i = h * (1 / (KB * KB))

$$\frac{N_A}{270\,KB^2\,\epsilon_o}$$

j = i * μ^2

$$\frac{\mu^2\,N_A}{270\,KB^2\,\epsilon_o}$$

k = g * ((2 / 3) * μ)

$$\frac{2\,\mu\,N_A}{243\,KB\,\epsilon_o}$$

l = ((1 / 5) * f * e)

$$\frac{9}{5}\,aa\,\alpha\,\kappa\,\kappa\kappa$$

m = (int - l) / k

$$\frac{243\,KB\,\left(int - \frac{9}{5}\,aa\,\alpha\,\kappa\,\kappa\kappa\right)\,\epsilon_o}{2\,\mu\,N_A}$$

```
n = slope / j
```

$$\frac{270\ KB^2\ slope\ \epsilon_o}{\mu^2\ N_A}$$

"Constants not having uncertainties are declared "

```
NA = 6.022 * 10^23
KB = 1.3807 * 10^-23
ϵo = 8.8542 * 10^-12
γK = 0.737 * 10^-60
α = 5.81 * 10^-40
κκ = 7.71 * 10^-2
```

6.022×10^{23}

1.3807×10^{-23}

8.8542×10^{-12}

7.37×10^{-61}

5.81×10^{-40}

0.0771

"Constants with known uncertainties are declared
aa is a and $\kappa\kappa$ is κ°"

```
μ=(-4.37+0.03)*10^-30
κ=(7.66+0.1)*10^-2
aa=(6.33+0.33)*10^-40
```

-4.34×10^{-30}

0.0776

6.66×10^{-40}

"Quantities as obtained from the graphs plotted are declared
Ak is from the intercept of the mKo vs Vm graph
T refers to each of the temperatures investigated by the experiment
The slope and intercept are from the the graph of (d) vs T"

```
A_K = -13.11 * 10^-27
T = 280.894
int = -0.6309 * 10^-24
slope = -907.2759 * 10^-21
```

-1.311×10^{-26}

280.894

-6.309×10^{-25}

-9.07276×10^{-19}

"Once the respctive values for the different quantities are declared, the mathematica notebook is recompiled and the respective results obtained. The value of the property quoted is determined by obtaining the average of the the sum and difference of the maximum and minum values."

APPEDIX C

Kerr Analysis: Method B

Polynomial Analysis of Kerr data

$$A_K = \frac{N_A}{81\varepsilon_0}\left\{\gamma^K + \frac{1}{k_B T}\left[\frac{2}{3}\mu\beta^K + \frac{1}{5}\Delta\alpha\Delta a\right] + \frac{3}{10}\frac{1}{(k_B T)^2}\mu^2(\alpha_{33} - \alpha)\right\}$$

"The equation above is the second of the two ways used to analyse data obtained from the Kerr Effect experiement. Eqns (a) - (d) help to simplify and calculate the values to be plotted. A graph is then plotted of (d) as a linear function of T. The slope and intercept are then used to determine . The uncertainties in these values are determined by using the effective uncertainties in the different quantities when calculating a minimum and maximum value for the properties mentioned. Remember for a maximum value for a term **a-b or a/b** the terms contributing to **a** take on their higher uncertainties and those to **b** their lower uncertainties and vice versa."

```
a = NA / (81 * ϵo)
```

$$\frac{N_A}{81\,\epsilon_o}$$

```
b = (1 / (KB))
```

$$\frac{1}{KB}$$

```
c=(1/5)*αα*aa
```

$$\frac{aa\,\alpha\alpha}{5}$$

"delta alpha is given by ($\alpha\alpha$)"

```
αα=3*α*κ
```

$$3\,\alpha\,\kappa$$

"delta a is given by (aa)"

```
aa=3*ac*κκ
```

$$3\,ac\,\kappa\kappa$$

```
d = (2 / 3) * μ
```

$$\frac{2\,\mu}{3}$$

```
e=μ^2* (3/10)
```

$$\frac{3\,\mu^2}{10}$$

"These are the expressions for P, Q and R, not to be compiled"

```
P=a*γK
```

$$\frac{\gamma K\, N_A}{81\, \epsilon_o}$$

```
Q=a*b* ( (d*β)+c)
```

$$\frac{\left(\frac{9}{5}\, ac\, \alpha\, \kappa\, \kappa\kappa + \frac{2\,\beta\,\mu}{3}\right) N_A}{81\, KB\, \epsilon_o}$$

```
R = a * e * (α33 - α) * b * b
```

$$\frac{(-\alpha + \alpha 33)\, \mu^2\, N_A}{270\, KB^2\, \epsilon_o}$$

"These espressions are used to calculate the respective properties to be obtained from the analysis, please note z is the expression for $\alpha 33 - \alpha$"

```
f1 = P / a
```

γK

```
f2 = (Q / (a * b) - c) / d
```

β

```
f3=R/ (a*e*b*b)
```

$-\alpha + \alpha 33$

"Constants not having uncertainties are declared, ***KK*** is K^{O}"

```
NA = 6.022 * 10^23
KB = 1.3807 * 10^-23
ϵo = 8.8542 * 10^-12
α = 5.81 * 10^-40
κκ = 7.71 * 10^-2
```

6.022×10^{23}

1.3807×10^{-23}

8.8542×10^{-12}

5.81×10^{-40}

0.0771

"Constants with known uncertainties are declared, **ac** is *a* "

```
μ=(-4.37+0.03)*10^-30
κ=(7.66-0.1)*10^-2
ac=(6.33-0.33)*10^-40
```

-4.34×10^{-30}

0.0756

$6. \times 10^{-40}$

"Quantities as obtained from the graphs plotted are declared
Ak is from the intercept of the mKo vs Vm graph and it is the weighted Ak values which are plotted as a function of the weighted temperature T. P, Q and R are the coefficients of T for the polynomial expression of Ak."

```
P = (1.494 + 0.629) * 10^-27
Q = (-1.217 - 0.435) * 10^-24
R = (-0.811 - 0.075) * 10^-21
```

2.123×10^{-27}

-1.652×10^{-24}

-8.86×10^{-22}

"Once the respctive values for the different quantities are declared, the mathematica notebook is recompiled and the respective results obtained. The value of the property quoted is determined by obtaining the average of the the sum and difference of the maximum and minum values."

APPENDIX D

Individual Polarizability Tensors Calculation

"This is a methematica booklet used to determine the individual polarizability tensors of a molecules using Kerr experiment data. The uncertainties of the various quantities need to be included in this analysis."

```
k={α33-α==((-0.3636+0.005)*10^-40),α==(1/3)*(α11+α22+α33),κ==(1/(18*α^2))*(((α11-
α22)^2)+((α11-α33)^2)+((α22-α33)^2))}
```

$$\left\{-\alpha + \alpha 33 == -3.586 \times 10^{-41},\ \alpha == \frac{1}{3}(\alpha 11 + \alpha 22 + \alpha 33),\ \kappa == \frac{(\alpha 11 - \alpha 22)^2 + (\alpha 11 - \alpha 33)^2 + (\alpha 22 - \alpha 33)^2}{18\,\alpha^2}\right\}$$

" α_{33}-α is obtained from Kerr data analysis, see Appendix B

"Constants are declared"

```
α=5.81*10^-40
```

$$5.81 \times 10^{-40}$$

```
κ=((7.66+0.1)*10^-2)^2
```

```
0.00602176
```

"One now solves for the individual polarizability tensors"

```
Solve[k,{α11,α22,α33}]
```

$$\{\{\alpha 11 \to 5.2728 \times 10^{-40},\ \alpha 22 \to 6.7058 \times 10^{-40},\ \alpha 33 \to 5.4514 \times 10^{-40}\},\ \{\alpha 11 \to 6.7058 \times 10^{-40},\ \alpha 22 \to 5.2728 \times 10^{-40},\ \alpha 33 \to 5.4514 \times 10^{-40}\}\}$$

APPENDIX E

Determination of Bk

"This notebook is used to calculate the second Kerr virial coefficient which is the contribution of the interacting molecules to the molar Kerr constant at a specific temperature and pressure. The slope of a graph of mKo vs the inverse molar volume is used to calculate Bk as seen by the equation below

$$ {}_m K_0 = A_K + \left[B_K + A_K \left(2A_\varepsilon + \frac{1}{2} A_R \right) \right] V_m^{-1} + \vartheta\left(V_m^{-1}\right) $$

so that

$$ \text{slope} = B_K + A_K \left(2A_\varepsilon + \frac{1}{2} A_R \right) $$

$$ \therefore\ B_K = \text{slope} - A_K \left(2A_\varepsilon + \frac{1}{2} A_R \right) $$

where

$$ A_\varepsilon = \frac{N_A}{3\varepsilon_0} \left\{ a_0 + \frac{\mu_0^2}{3kT} \right\} $$

$$ A_R = \frac{N_A \alpha_0}{3\varepsilon_0} $$

"The two equations for Ae and Ar are defined as is the equation to calculate Bk"

```
Ae=NA/(3*\!\(\(\[Epsilon]\_o\)\))*(a+μ^2/(3*KB*T))
```

$$ \frac{NA \left(a + \frac{\mu^2}{3\,KB\,T} \right)}{3\,\epsilon_o} $$

```
Ar=NA*α/(3*\!\(ϵ\_o\))
```

$$\frac{NA\,\alpha}{3\,\epsilon_o}$$

```
Bk=slope-(Ak*(2*Ae+(0.5)*Ar))
```

$$\text{slope} - Ak\left(\frac{0.166667\,NA\,\alpha}{\epsilon_o} + \frac{2\,NA\left(a + \frac{\mu^2}{3\,KB\,T}\right)}{3\,\epsilon_o}\right)$$

"The individual constants together with their uncertainties are declared, values for Ak and T are dependent on the specific temperature of investigation"

```
NA = 6.0221415*10^23
```

6.02214×10^{23}

```
ϵo = 8.854187817*10^-12
```

8.85419×10^{-12}

```
a = 6.33*10^-40
```

6.33×10^{-40}

```
α = 5.81*10^-40
```

5.81×10^{-40}

```
μ = -4.37*10^-30
```

-4.37×10^{-30}

```
T = 334.4365
```

334.437

```
KB = 1.3806505*10^-23
```

1.38065×10^{-23}

```
Ak = -9.39161*10^-27
```

-9.39161×10^{-27}

```
slope = .00525*10^-27
```

5.25×10^{-30}

"Having input the value of the 'constants' one can recompile the eqn for Bk and so determine the minimum and maximum values for Bk"